SATELLITE RELATIVE MOTION PROPAGATION AND CONTROL IN THE PRESENCE OF J_2 PERTURBATIONS

A Thesis

by

PRASENJIT SENGUPTA

Submitted to the Office of Graduate Studies of
Texas A&M University
in partial fulfillment of the requirements for the degree of

MASTER OF SCIENCE

December 2003

Major Subject: Aerospace Engineering

SATELLITE RELATIVE MOTION PROPAGATION AND CONTROL IN THE PRESENCE OF J_2 PERTURBATIONS

A Thesis

by

PRASENJIT SENGUPTA

Submitted to Texas A&M University
in partial fulfillment of the requirements
for the degree of

MASTER OF SCIENCE

Approved as to style and content by:

Srinivas R. Vadali (Co-Chair of Committee)	Kyle T. Alfriend (Co-Chair of Committee)
Shankar P. Bhattacharyya (Member)	John E. Hurtado (Member)
Walter E. Haisler (Head of Department)	

December 2003

Major Subject: Aerospace Engineering

ABSTRACT

Satellite Relative Motion Propagation and Control

in the Presence of J_2 Perturbations. (December 2003)

Prasenjit Sengupta, B.Tech(H), Indian Institute of Technology, Kharagpur, India

Co–Chairs of Advisory Committee: Dr. Srinivas R. Vadali
Dr. Kyle T. Alfriend

Formation flying is a new satellite mission concept that is concerned with clusters of satellites in neighboring orbits cooperating to perform a specific task. The tasks may be Earth observation or space-based interferometry where a cluster of small satellites is able to fulfill the same requirements as that of a larger, monolithic satellite.

There exist a variety of models for the study of relative motion between two satellites. These include models based upon differential orbital elements, and relative position and velocity coordinates. Extensive work has been done on such models, both in the absence and presence of the J_2 perturbation arising from the aspherical nature of the Earth, which causes variations in the orbital elements that describe the orbit. The approximate relative motion can be obtained analytically by using mean elements. However, the true orbit can only be described by the instantaneous osculating elements.

An analytical method to propagate the relative motion between two satellites in highly elliptic orbits is the main focus of this thesis. The method is kinematically exact and it maintains a high degree of accuracy even in the presence of J_2 perturbations. Mean

orbital elements are used for orbit propagation, and expansions involving the powers of eccentricity are not utilized. The true anomaly of the reference satellite is treated as the independent variable, instead of time. The relative orbit kinematics are obtained by using a projection onto a unit sphere. This procedure allows the relative position variables to be treated as angles depending on the orbital element differences. The effect of adding short-period corrections due to J_2 to the mean elements is also studied.

Finally, the problem of formation reconfiguration is studied. The reconfiguration of a formation may be achieved by using impulsive thrust (velocity increments) or continuous control. This thesis presents a method to obtain the optimal velocity increments through numerical optimization, utilizing the analytical technique developed for relative orbit propagation. A continuous control law is also developed using a candidate Lyapunov function, and the asymptotic stability of the closed-loop system is ascertained.

To my parents

ACKNOWLEDGMENTS

Any record of work is incomplete without an expression of gratitude towards those who made it possible. I would like to thank, at the outset, the co-chairs of my committee Dr. Srinivas Vadali and Dr. Kyle Alfriend. I am grateful to them for their academic guidance and continued support.

I thank my committee members Dr. Shankar Bhattacharyya and Dr. Johnny Hurtado, with whom I have had engaging discussions and who evaluated my research, and Dr. John Junkins for making himself available for the final examination. I greatly value the knowledge they have imparted to me.

I also thank the administrative staff of the Department of Aerospace Engineering for their timely help and continued cooperation with paperwork and other administrative matters. Dr. Dong-Woo Gim and Hui Yan brought additional insight to my research, for which I am grateful.

I value the discussions, both academic and non-academic, with Sai, Puneet and the rest of the folks on the sixth floor of H. R. Bright Building. Sadly, Kishore, who constantly reminded me to look outside the window of my office, is no longer with us. Special gratitude is reserved for Waqar and Dali who have been my traveling companions from the days of Kharagpur.

Nothing would have been possible, of course, without my family, because of whom I am what I am, and am where I am, today.

TABLE OF CONTENTS

CHAPTER Page

CHAPTER Page

LIST OF TABLES

LIST OF FIGURES

FIGURE Page

FIGURE Page

CHAPTER I

INTRODUCTION

1.1 Background

There exists abundant literature on the modeling and analysis of relative motion between satellites in Earth orbits. Some of the earlier works on this subject were motivated by a need to solve the satellite rendezvous problem for near-circular orbits. More recently, there has been a revival of interest on this subject due to the need for deploying swarms of small satellites flying in precise formations which cooperate to form distributed aperture systems for Earth or space observation. Smaller satellites that can accomplish the mission of a single larger satellite are desirable because of the advantages of modularity, simplicity, ease of launch, and graceful degradation. Some of the proposed missions, e.g., LISA (Laser Interferometer Space Antenna), require that the satellites form a circular aperture in the plane perpendicular to the line-of-sight. Such a desired relative orbit may not be achievable without the application of thrust when the satellites themselves are in elliptic orbits about the Earth. Some missions, such as MMS (Magnetospheric Multiscale), require highly elliptic reference orbits. Reconfiguration of the formation will also be required, to perform multiple tasks. It is essential for the success of any mission to choose the required relative orbit geometry that can be maintained with the least amount of fuel in the presence of gravitational and environmental perturbations. This thesis focuses on the mathematical modeling, propagation, and analysis of relative motion in highly elliptic orbits under the influence of a gravitational perturbation due to the oblateness of the Earth.

The journal model is *AIAA Journal of Guidance, Control, and Dynamics.*

1.2 Modeling the Motion of a Single Satellite Including the J_2 Perturbation

The orbit of a satellite is characterized by six quantities known as orbital elements. Alternatively, it can also be characterized by the satellite's position and velocity. Three second-order differential equations are required to describe the motion of a satellite, for a spherical Earth model. The so-called two-body orbit problem admits analytical solutions which are conic sections.

The presence of perturbations complicates the system and exact, closed-form analytical expressions for the position and velocity of a satellite no longer exist. The gravitational potential of a spheroid is conveniently modeled using spherical harmonics. The forces of attraction on a satellite are obtained from the gradient of the potential. Of all the gravitational harmonics that arise dude to oblateness effects, the J_2 perturbation is of the largest magnitude, and is of considerable interest. The effect of the J_2 potential on the orbital elements of the satellite can be studied by using Lagrange's Variation of Parameters or Gauss equations which are valid for arbitrary perturbations. The study of the effect of the J_2 perturbation on orbital elements can be found in Refs. 1, 2. In Ref. 1, to first order in J_2, the gravitational potential is separated into three terms: first-order secular, short-periodic and long-periodic (second-order terms are the contributions of higher harmonics and are beyond the scope of the thesis). If the study of the change of orbital elements is limited to that due to the first-order secular component, it can be shown that three of the six orbital elements can be considered constant and the remaining elements show secular growth. These elements are known as mean elements. If the short-periodic and long-periodic perturbations are also included in the potential then the instantaneous elements, also

known as osculating elements, describe the true orbit. Reference 2 finds short and long period corrections to the mean elements through a perturbation analysis of the Hamiltonian of the system.

Many systems of differential equations exist that model the motion of a single satellite. Gauss' equations[3] relate the change in orbital elements to control and other disturbance accelerations. Kechichian's equations[4] also model satellite motion with coordinates expressed in the local-vertical local-horizontal frame of the satellite. An equivalence between orbital motion and rigid body kinematics is discussed in Ref. 5. The models mentioned are exact and are nonlinear equations of sixth order.

Analytical expressions for the orbital elements have been derived by making approximations to the J_2 potential for low eccentricities.[6] However, these are valid only for very low eccentricities since the theory assumes a precessing, near-circular orbit.

1.3 Modeling Relative Motion Including the J_2 Perturbation

In the study of the relative motion dynamics of two or more satellites, one of the satellites is generally given the designation of the Chief, and the others are designated the Deputies. Consequently, interest arises in the relative motion of the Deputies with respect to the Chief, with a reference frame centered on the Chief. The simplest set of differential equations that model relative motion between a Deputy and Chief satellite are the Hill-Clohessy-Wiltshire (HCW) equations.[7] These are a set of three, second-order, linear differential equations. These equations, while easy to analyze, do not accurately describe the system dynamics, due to the assumptions of a circular reference orbit, linearized differential gravitational attraction, and spherical Earth.

Initial conditions can be found such that the relative motion between the Deputy and the Chief is periodic. The projected circular orbit (PCO) initial conditions are one set of initial conditions among the periodic solution initial conditions, that result in circular relative orbits in the local-horizontal local-vertical plane. However, when the equations of motion of the truth model are integrated numerically with these initial conditions, they result in divergent relative motion. Vaddi et al[8] showed that, by identifying eccentricity and nonlinearity as perturbations, their effects may be studied independently, and corrections may be obtained to the initial conditions for each perturbation. The two corrections may be then combined to produce bounded relative orbit solutions to the nonlinear problem with non-zero eccentricity. While these corrections account for the non-zero eccentricity and second-order nonlinearities, they do not take into account the perturbation due to J_2.

Equations similar to the HCW equations, but with a linearized J_2 field incorporated, have been developed in Ref. 9. The J_2 perturbation, if not accounted for properly, can lead to unbounded relative motion. This drift can be virtually eliminated for small orbit element differences using the concept of J_2-invariant relative orbits.[10] However, J_2-invariant relative orbits may not be attractive for many missions due to the large relative orbit sizes obtained. Hence, a rate-matching constraint has been developed[11] to keep the along-track motion bounded. The out-of-plane motion is controlled by application of thrust, as required.

Analytical expressions for propagating relative motion under the influence of J_2 have been developed by several authors. Gim and Alfriend[12] provide a state transition matrix for the solution of the linearized relative motion problem using curvilinear coordinates. Schaub[13] presents analytical expressions for propagating the linearized

orbital element differences using the true anomaly as the independent variable. His approach does not require the solution of Kepler's equation at each specified value of the true anomaly. Time-explicit solutions have been developed by Sabol et al.[14] using eccentricity expansions. This approach is valid for small eccentricities. A kinematically exact description using the unit sphere approach[15] has also been developed. In this approach, the relative motion problem is studied by projecting the motion of the satellites onto a unit sphere. The projection is achieved by normalizing the position vector of each satellite with respect to its radius. This approach uncouples the translation and attitude kinematics of satellite relative motion, in a manner similar to that given by Junkins and Turner,[5] and allows one to study the relative motion using spherical trigonometry. The original unit sphere approach also uses eccentricity expansions[3] for the radial distance and argument of latitude in order to obtain time-explicit expressions. These eccentricity expansions are not uniformly convergent for high eccentricities. Even for moderate eccentricities, the number of terms required for convergence cannot be determined *a priori*. In such cases it becomes necessary to solve Kepler's equation for each satellite in the formation at every solution point. In this thesis, the true anomaly of the Chief is used as the independent variable, rather than time. It will be shown that even for high eccentricity relative orbits and large relative orbit radii, the unit sphere approach gives accurate results. Kepler's equation has to be solved, but only for the Deputies.

1.4 Formation Reconfiguration

The formation has to be controlled for establishment of the relative orbit, orbit reconfiguration, or orbit maintenance, in the presence of J_2 and drag perturbations. Gauss' equations can be used to find the changes in orbital elements arising due to velocity

increments (impulsive thrust assumption). The analysis in this thesis assumes that the Chief is uncontrolled and impulses are used to control a Deputy. The modified unit sphere model can be used to propagate the orbits of the satellites during the coasting phases. Through a numerical optimization scheme, the optimal magnitude and directions of the impulses, as well as the optimal times (true anomaly) of thrust application can be evaluated. To maintain computational accuracy for highly eccentric reference orbits, it is better to optimize the values of true anomaly of the Chief at points of thrust applications, instead of the time instants of thrust application. By using the kinematic model for relative motion,[16] the reconfiguration problem is analyzed through the propagation of relative Euler parameters corresponding to the true and desired frames of reference of the Deputy.

Reconfiguration can also be performed by using continuous control. Reference 17 presents two Lyapunov-based control laws, one based on orbital elements, and another based on ECI coordinates. The controller using ECI coordinates is shown to be globally and asymptotically stabilizing. However, the stability of the orbital element-based control cannot be proven rigorously. This thesis uses a Lyapunov function based on the kinematic description of satellite motion. The stability of the control law cannot be proven by using Lyapunov's Stability Theory. Therefore, LaSalle's Invariance Principle needs is used to conclude global, asymptotic stability. Lyapunov's Stability Theory and LaSalle's Theorems are explained briefly in the appendices. The control law derived can be used for reconfigurations where the eccentricity of the Chief's orbit may be high or low.

1.5 Organization of the Thesis

This chapter serves as an introduction to the content of the thesis. In Chapter II, the basic concepts of orbital motion are introduced. The potential due to J_2 is presented and the modifications to the different systems of equations that model orbital motion of a satellite are developed. The equivalent kinematic model is also presented.

Chapter III develops the system models for relative motion. The HCW equations are derived, starting from the nonlinear model, in the absence of J_2. Special periodic solutions of these equations are examined and the initial conditions for projected circular orbits are presented. The geometric method for relative motion, and the elemental differences required to establish projected circular orbits are shown. These elemental differences are obtained from the circular projection requirements and the orbit rate-matching condition. Simulations are performed using these models and their errors are compared with those from the unit sphere model for relative motion.

Chapter IV discusses modeling of relative motion when the eccentricity of the orbit of the Chief is very high. The failure of eccentricity expansions is discussed. A modified method that uses the true anomaly of the Chief as the independent variable is presented. The validity of this model for different high-eccentricity cases as well as large formations is verified through numerical simulations.

In Chapter V, the reconfiguration problem is discussed. The first section deals with reconfiguration through the application of velocity impulses by the use of Gauss' equations. Numerical optimization is performed to study the reconfiguration for low-eccentricity as well as high-eccentricity reference orbits. The reconfiguration problem

is also studied through the kinematic approach. The last section deals with reconfiguration with continuous control. A candidate Lyapunov function is used and the control law is derived from it. The global, asymptotic stability of this control law is proven. Numerical simulations for different cases are used to compare the different approaches to the reconfiguration problem. Finally, the thesis is summarized in the last chapter, and a few concluding remarks on future work are presented.

CHAPTER II

MOTION OF A SATELLITE PERTURBED BY J_2

2.1 Introduction

In this chapter various frames of reference and models that are used to describe the motion of a satellite in orbit around the Earth are illustrated. The origin of the J_2 perturbation arising due to the aspherical nature of the Earth is established. Various systems of equations that model the motion of a satellite in orbit about the Earth are presented.

2.2 Frames of Reference

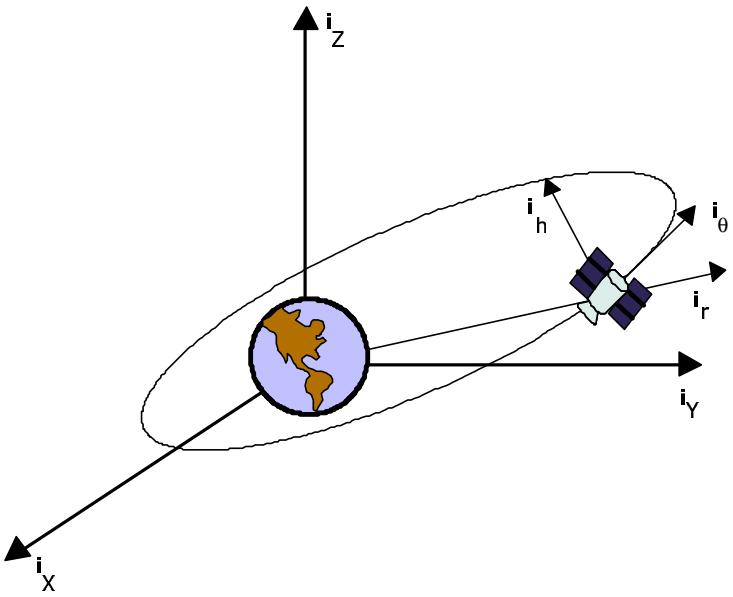

Fig. 2.1 The ECI and LVLH Frames

2.2.1 The Earth-Centered Inertial Frame

The first frame considered is the Earth-Centered Inertial (ECI) frame. The three directions in the frame are denoted by X, Y, and Z, which lie along the unit vectors $\mathbf{i}_X$, $\mathbf{i}_Y$, and $\mathbf{i}_Z$, respectively. The plane determined by $\mathbf{i}_X$ and $\mathbf{i}_Y$ coincides with the equatorial plane and the $\mathbf{i}_Z$ vector passes through the North Pole.

2.2.2 The Local-Horizontal Local-Vertical Frame

The second frame that is used as frequently as the ECI frame is the Local-Horizontal Local-Vertical (LVLH) frame. This frame is denoted by the radial, circumferential, and normal (r-θ-h) directions and the respective unit vectors, $\mathbf{i}_r$, $\mathbf{i}_\theta$, and $\mathbf{i}_h$. Since the orbital plane is defined by the position and velocity vectors, the orbit normal is given by their cross product. That is, $\mathbf{i}_h = (\mathbf{i}_r \times \mathbf{v})/|\mathbf{v}|$. The third unit vector, $\mathbf{i}_\theta$, is perpendicular to both the radial vector and orbit normal. Therefore, $\mathbf{i}_\theta = \mathbf{i}_h \times \mathbf{i}_r$. For circular orbits the velocity vector, the tangential vector at that point, and the circumferential vector coincide. The radial, circumferential and normal directions are also known as 'in-track', 'along-track', and 'cross-track', respectively.

In the description above, a subscript N associated with a vector usually denotes a vector in the ECI frame. A subscript B denotes a vector in the body-fixed frame of the satellite. The LVLH frame of the satellite is also the body-fixed frame of the satellite. Both of the frames are shown in Fig. 2.1.

2.3 Description of Satellite Motion

Different sets of quantities can be used to describe the motion of a satellite in its orbit around the Earth. Since the motion has three degrees of freedom, six quantities will

be required to describe its motion completely - three each, for position and velocity.

2.3.1 Inertial Coordinates

The most obvious set that describes satellite motion is the ECI frame. The position of the satellite in this frame is given by $\mathbf{r}^N = x\mathbf{i}_X + y\mathbf{i}_Y + z\mathbf{i}_Z$, and the velocity is given by $\mathbf{v}^N = \dot{x}\mathbf{i}_X + \dot{y}\mathbf{i}_Y + \dot{z}\mathbf{i}_Z$. The angular momentum vector is obtained by taking the vector product of position and velocity: $\mathbf{h}^N = \mathbf{r}^N \times \mathbf{v}^N$.

2.3.2 Orbital Elements

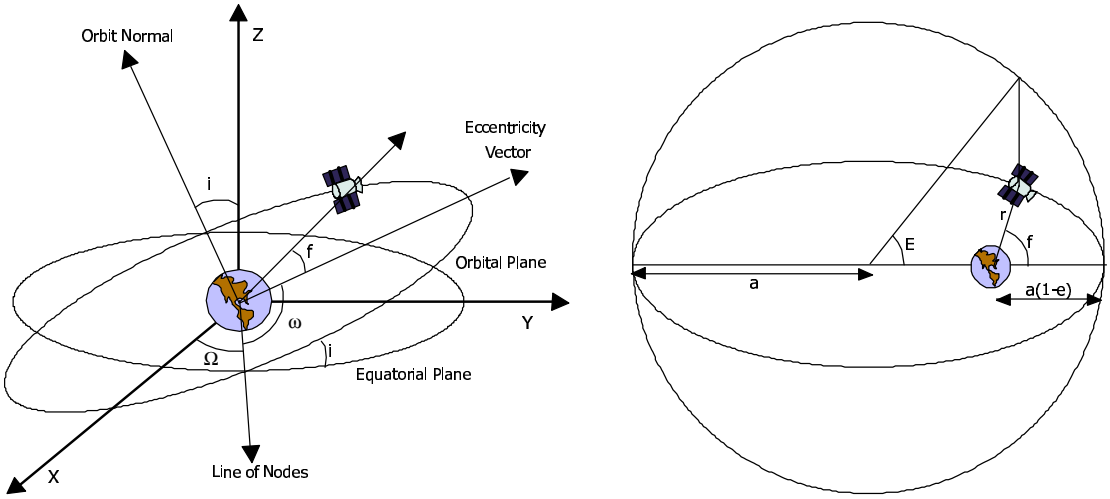

(a) Orbital Angles (b) Elements in Orbital Plane

Fig. 2.2 Orbital Element Description

The most common description of satellite motion is in terms of the orbital elements developed by Kepler,[3] shown in Figs. 2.2a and 2.2b. These elements are: semimajor axis a, eccentricity e, inclination i, longitude of ascending node (right ascension) Ω, argument of perigee ω, and mean anomaly M. Instead of mean anomaly, the true

anomaly f or eccentric anomaly E are also used. The elements M and E are related through Kepler's equation:

$$M = E - e \sin E \tag{2.1}$$

By inspection, M is available directly from E, but to obtain E from M, Eq. (2.1) has to be solved iteratively. The argument of latitude, $\theta = \omega + f$, is another quantity of use. The radial distance r is given by

$$r = \frac{p}{1 + e \cos f} = a(1 - e \cos E) \tag{2.2}$$

where p is the *semi-latus rectum* (orbit parameter), given by $p = a(1 - e^2)$.

Instead of solving Eq. (2.1) iteratively, for low eccentricities, very often a series solution is used. The series is formed by increasing powers of e and harmonics of M. The following expressions are obtained using series expansions:[3]

$$\begin{aligned} f &= M + \left(2e - \frac{1}{4}e^3 + \frac{5}{96}e^5\right)\sin M + \left(\frac{5}{4}e^2 - \frac{11}{24}e^4 + \frac{17}{192}e^6\right)\sin 2M \\ &\quad + \left(\frac{13}{12}e^3 - \frac{43}{64}e^5\right)\sin 3M + \left(\frac{103}{96}e^4 - \frac{451}{480}e^6\right)\sin 4M \\ &\quad + \frac{1097}{960}e^5 \sin 5M + \frac{1223}{960}e^6 \sin 6M + O(e^7) \end{aligned} \tag{2.3a}$$

$$\begin{aligned} E &= M + \left(e - \frac{1}{8}e^3 + \frac{1}{192}e^5\right)\sin M + \left(\frac{1}{2}e^2 - \frac{1}{6}e^4 + \frac{1}{48}e^6\right)\sin 2M \\ &\quad + \left(\frac{3}{8}e^3 - \frac{27}{128}e^5\right)\sin 3M + \left(\frac{1}{3}e^4 - \frac{4}{15}e^6\right)\sin 4M \\ &\quad + \frac{125}{384}e^5 \sin 5M + \frac{27}{80}e^6 \sin 6M + O(e^7) \end{aligned} \tag{2.3b}$$

$$
\begin{aligned}
r &= a\Bigg[1+\frac{1}{2}e^2-\left(e-\frac{3}{8}e^3+\frac{5}{192}e^5\right)\cos M-\left(\frac{1}{2}e^2-\frac{1}{3}e^4+\frac{1}{16}e^6\right)\cos 2M \\
&\quad -\left(\frac{3}{8}e^3-\frac{45}{128}e^5\right)\cos 3M-\left(\frac{1}{3}e^4-\frac{2}{5}e^6\right)\cos 4M \\
&\quad -\frac{125}{384}e^5\cos 5M-\frac{27}{80}e^6\cos 6M+O(e^7)\Bigg] \qquad (2.3c)
\end{aligned}
$$

2.3.3 Nonsingular Classical Elements

The orbital elements discussed above are not free from singularities. In particular, for near-zero eccentricities (circular orbits), ω and f cannot be determined independently and only their sum θ is defined. For near-zero inclinations (equatorial orbits), the Euler angle description involves a singularity - Ω and ω cannot be determined independently. There exist element sets that do not show one or both of the singularities. To account for singularities induced by circular orbits, non-singular classical orbital elements (NSCOE) are used. Three of the NSCOE are the same as the classical element set: a, i and Ω. The three new quantities that are introduced in this set are:

$$
\begin{aligned}
q_1 &= e\cos\omega \\
q_2 &= e\sin\omega \\
\theta &= \omega+f \text{ or } \psi=\omega+M
\end{aligned}
$$

For very low eccentricities, $\theta \approx \psi$.

2.3.4 LVLH Coordinates

The third characterization of motion of a satellite is through the use of LVLH coordinates. It can be seen from Fig. 2.2a that the angles Ω, i, and θ, form a 3-1-3 Euler angle set that characterize the orientation of the LVLH frame with respect to the ECI

frame. The direction cosine matrix that transforms a vector in the ECI frame to one in the LVLH frame is given by[18]

$$\mathbf{C} = \begin{bmatrix} \cos\theta\cos\Omega - \sin\theta\cos i\sin\Omega & \cos\theta\sin\Omega + \sin\theta\cos i\cos\Omega & \sin\theta\sin i \\ -\sin\theta\cos\Omega - \cos\theta\cos i\sin\Omega & -\sin\theta\sin\Omega + \cos\theta\cos i\cos\Omega & \cos\theta\sin i \\ \sin i\sin\Omega & -\sin i\cos\Omega & \cos i \end{bmatrix} \tag{2.4}$$

The characterization of the motion of the LVLH frame is completed by specifying the angular velocity vector of the satellite. Since the LVLH frame is also a body frame of the satellite, the angular velocity of the satellite is also the angular velocity of the frame. The inertial and LVLH angular velocities are given by[18]

$$\boldsymbol{\omega}_{inertial} = \begin{Bmatrix} \dot{\theta}\sin\Omega\sin i + \dot{i}\cos\Omega \\ -\dot{\theta}\cos\Omega\sin i + \dot{i}\sin\Omega \\ \dot{\Omega} + \dot{\theta}\cos i \end{Bmatrix} \tag{2.5a}$$

$$\boldsymbol{\omega}_{LVLH} = \begin{Bmatrix} \dot{\Omega}\sin\theta\sin i + \dot{i}\cos\theta \\ \dot{\Omega}\cos\theta\sin i - \dot{i}\sin\theta \\ \dot{\Omega}\cos i + \dot{\theta} \end{Bmatrix} \tag{2.5b}$$

The equations of motion using the different descriptions will be presented in detail in the next chapter.

2.4 The J_2 Perturbation

2.4.1 The Gravitational Potential

The aspherical nature of the Earth, arising from the equatorial bulge shown in Fig. 2.3a, leads to a gravitational attraction on a body that is no longer directed towards the center of mass of the Earth. From Newton's law of gravitation, the gravitational acceleration vector, $d\mathbf{a}$, due to the infinitesimal mass dm of the body of

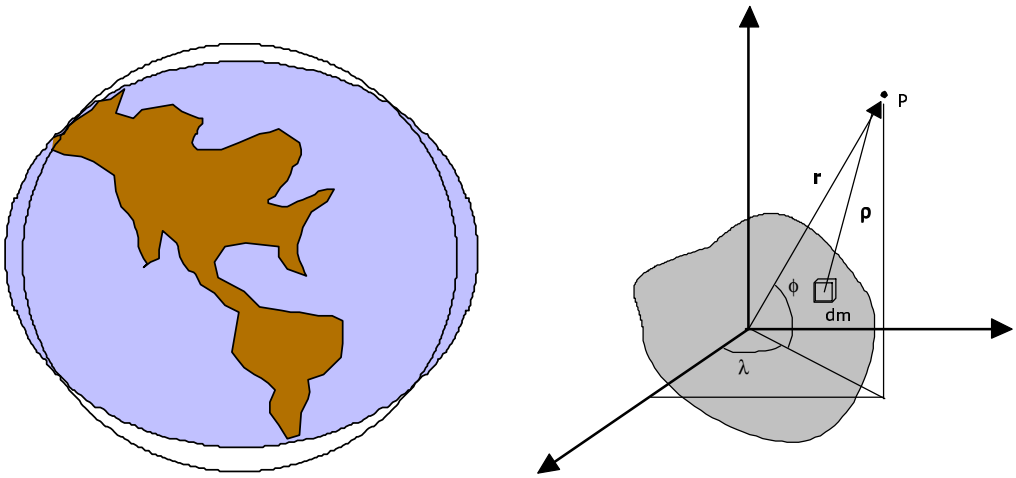

(a) Equatorial Bulge

(b) Potential of an Arbitrarily Shaped Body

Fig. 2.3 Origin of the J_2 Perturbation

arbitrary shape in Fig. 2.3b is given by

$$d\mathbf{a} = -Gdm\frac{\boldsymbol{\rho}}{\rho^3}$$

where $G = 6.672 \times 10^{-11}\text{kg}^{-1}\text{m}^3\text{s}^{-2}$ is the universal gravitation constant. If Φ is a potential function, the acceleration in its field is given by

$$\frac{d^2\mathbf{r}}{dt^2} = -\boldsymbol{\nabla}\Phi = -\frac{\partial\Phi}{\partial x}\mathbf{i}_X + \frac{\partial\Phi}{\partial y}\mathbf{i}_Y + \frac{\partial\Phi}{\partial z}\mathbf{i}_Z$$

The potential due to an elemental mass dm, is therefore given by

$$d\Phi = -\frac{Gdm}{\rho} \tag{2.6}$$

In spherical coordinates, the point P in Fig. 2.3b has the coordinates (r, ϕ, λ) where r is the radial distance, ϕ is the geocentric latitude, and λ is the longitude. For a body with rotational symmetry, the gravitational potential is obtained by integrating

Eq. (2.6) over the entire volume of the body, to obtain

$$\Phi(r,\phi) = -\frac{\mu}{r}\left[1 + \sum_{k=2}^{\infty} J_k \left(\frac{R_e}{r}\right)^k P_k\left(\sin\phi\right)\right] \tag{2.7}$$

where $\mu = GM_e$, and P_k is the kth Legendre polynomial (M_e is the mass of the Earth). Since the mass distribution is the same with respect to the axis of rotation, the potential does not depend on the longitude.

The thesis concentrates on the effects of the second zonal harmonic J_2 since it is the most dominant among the harmonics. The second zonal harmonic for the Earth has the following value:

$$J_2 = 1.082629 \times 10^{-3}$$

The other harmonics are of the order of 10^{-6} or less.

Limiting the series in Eq. (2.7) to $k = 2$, and from $P_2(\nu) = (3\nu^2 - 1)/2$, the gravitational potential of the Earth due to oblateness effects is

$$\Phi(r,\phi)_{J_2} = -\frac{\mu J_2 R_e^2}{2r^3}\left(3\sin\phi^2 - 1\right) \tag{2.8}$$

From spherical trigonometry, $\sin\phi = \sin i \sin\theta = \sin i \sin(\omega + f)$. In terms of Cartesian coordinates, $\sin\phi = z/r$. Hence,

$$\Phi_{J_2} = \frac{\mu J_2 R_e^2}{2r^3}\left(1 - 3\sin^2 i \sin^2\theta\right) \tag{2.9a}$$

$$= \frac{\mu J_2 R_e^2}{2r^3}\left(1 - \frac{3z^2}{r^2}\right) \tag{2.9b}$$

2.4.2 Perturbation Accelerations due to J_2

The accelerations acting on a satellite due to the J_2 perturbation can be derived from the potential functions in the desired coordinate system from Eqs. (2.9). The accelerations in the inertial frame of reference, using Cartesian coordinates, are

$$\begin{aligned} \mathbf{a}_{J_2} &= -\left[\frac{\partial \Phi_{J_2}}{\partial x}\mathbf{i}_X + \frac{\partial \Phi_{J_2}}{\partial y}\mathbf{i}_Y + \frac{\partial \Phi_{J_2}}{\partial z}\mathbf{i}_Z\right] \\ &= -\frac{3}{2}\frac{\mu J_2 R_e^2}{r^4}\left\{\begin{array}{c} \left(1-3\frac{z^2}{r^2}\right)\frac{x}{r} \\ \left(1-3\frac{z^2}{r^2}\right)\frac{y}{r} \\ \left(3-3\frac{z^2}{r^2}\right)\frac{z}{r} \end{array}\right\} \end{aligned} \tag{2.10}$$

The acceleration in spherical coordinates with (r,ϕ,λ), is given by

$$\begin{aligned} \mathbf{a}_{J_2} &= -\left[\frac{\partial \Phi_{J_2}}{\partial r}\mathbf{i}_r + \frac{1}{r}\frac{\partial \Phi_{J_2}}{\partial \phi}\mathbf{i}_\phi + \frac{1}{r\cos\phi}\frac{\partial \Phi_{J_2}}{\partial \lambda}\mathbf{i}_\lambda\right] \\ &= -\frac{3}{2}\frac{\mu J_2 R_e^2}{r^4}\left\{\begin{array}{c} 1-3\sin^2\phi \\ 2\sin\phi\cos\phi \\ 0 \end{array}\right\} \end{aligned} \tag{2.11}$$

However, the spherical coordinate expression is seldom used. Of greater use is the expression for the acceleration due to J_2 terms in the LVLH frame, in terms of the orbital angles and radial distance. The perturbing acceleration due to J_2 can also be written as

$$\mathbf{a}_{J_2} = \frac{1}{2}\mu J_2 R_e^2\left[\frac{3}{r^4} - \frac{15\left(\mathbf{r}\cdot\mathbf{n}\right)^2}{r^6}\right]\frac{\mathbf{r}}{r}$$

Then, in the LVLH frame, the perturbation acceleration is given by

$$\mathbf{a}_{J_2} = -\frac{3}{2}\frac{J_2\mu R_e^2}{r^4}\left\{\begin{array}{c} 1-3\sin^2 i\sin^2\theta \\ 2\sin^2 i\sin\theta\cos\theta \\ 2\sin i\cos i\sin\theta \end{array}\right\} \tag{2.12}$$

2.4.3 Mean and Osculating Elements

From Lagrange's variation of parameters, the differential equations for the orbital elements due to a potential[3] are given by

$$\frac{da}{dt} = \frac{2}{na}\frac{\partial \Phi}{\partial M} \tag{2.13a}$$

$$\frac{de}{dt} = \frac{\eta^2}{na^2 e}\frac{\partial \Phi}{\partial M} - \frac{\eta}{na^2 e}\frac{\partial \Phi}{\partial \omega} \tag{2.13b}$$

$$\frac{di}{dt} = \frac{\cos i}{na^2 \eta \sin i}\frac{\partial \Phi}{\partial \omega} \tag{2.13c}$$

$$\frac{d\Omega}{dt} = \frac{\cos i}{na^2 \eta \sin i}\frac{\partial \Phi}{\partial i} \tag{2.13d}$$

$$\frac{d\omega}{dt} = -\frac{\cos i}{na^2 \eta \sin i}\frac{\partial \Phi}{\partial i} + \frac{\eta}{na^2 e}\frac{\partial \Phi}{\partial e} \tag{2.13e}$$

$$\frac{dM}{dt} = n - \frac{\eta^2}{na^2 e}\frac{\partial \Phi}{\partial e} - \frac{2}{na}\frac{\partial R}{\partial a} \tag{2.13f}$$

where $\eta = \sqrt{1-e^2}$ and $n = \sqrt{\mu/a^3}$ is the orbital rate. In the absence of the J_2 perturbation, five orbital elements remain constant, and M is a linear function of time. It can be seen from Eq. (2.13), that if the J_2 potential is included, all the elements change over time. The resulting elements are known as the *osculating elements*.

The use of *mean elements* for orbit propagation has been studied extensively. Kozai[1] obtained expressions for the components that contribute to the first-order secular, short-periodic and long-periodic parts of the potential function. Second-order secular terms are also obtained if J_4 and higher-order harmonics are included. The first-order secular components are obtained by averaging the short-period terms out of Φ_{J_2}. The short-period terms are those that include harmonics of the true anomaly f. The effect of these terms is noticeable over one orbit. The long-period terms include harmonics of the argument of perigee ω only. The effect of the harmonic terms typically is felt over a large number of orbits only; over one orbit the long-periodic variations appear

similar to secular growth terms.

The secular component of the potential, $\bar{\Phi}$, is obtained as shown below:

$$\begin{aligned} \bar{\Phi} &= \frac{1}{2\pi}\int_0^{2\pi} \Phi_{J_2} dM \\ &= \frac{3}{2} J_2 R_e^2 n^2 \frac{1}{\eta^3}\left(\frac{1}{3} - \frac{1}{2}\sin^2 i\right) \end{aligned} \tag{2.14}$$

The following results are obtained from Eqs. (2.13),

$$\dot{a} = \dot{e} = \dot{i} = 0$$

$$\dot{\Omega} = -\frac{3}{2} n J_2 \left(\frac{R_e}{p}\right)^2 \cos i \tag{2.15a}$$

$$\dot{\omega} = \frac{3}{4} n J_2 \left(\frac{R_e}{p}\right)^2 (5\cos^2 i - 1) \tag{2.15b}$$

$$\dot{M} = n\left[1 + \frac{3}{4}\sqrt{1-e^2} J_2 \left(\frac{R_e}{p}\right)^2 (3\cos^2 i - 1)\right] \tag{2.15c}$$

Thus, given an initial set of mean orbital elements, the mean elements can be obtained at any time by using the rates calculated by Eqs. (2.15).

The short-periodic part of the J_2 potential can be included in Eqs. (2.13) to obtain corrections, by regarding a, e, i, and ω as constants in. The short-period corrections can be found in Ref. 1. These corrections involve periodic functions of f, $\omega + f$, $3\omega + 2f$, etc., and give approximate formulae for the osculating elements.

An alternative treatment to the problem of orbital element variations due to the J_2 perturbation is available in Brouwer,[2] through the use of Delaunay variables. The

use of Delaunay variables requires the following conversions:

$$\left.\begin{array}{ll} L = (\mu a)^{\frac{1}{2}} & l = M \\ G = L\,(1-e^2)^{\frac{1}{2}} & g = \omega \\ H = G\cos i & h = \Omega \end{array}\right\} \tag{2.16}$$

In the Delaunay description, (L, G, H) are the momenta of the system. The Delaunay variables are obtained from a canonical transformation, hence the Hamiltonian F of the system formed by these variables yields straight-forward equations of motion:

$$\dot{l} = \frac{\partial F}{\partial L} \quad \dot{g} = \frac{\partial F}{\partial G} \quad \dot{h} = \frac{\partial F}{\partial H} \tag{2.17a}$$

$$\dot{L} = -\frac{\partial F}{\partial l} \quad \dot{G} = -\frac{\partial F}{\partial g} \quad \dot{H} = -\frac{\partial F}{\partial h} \tag{2.17b}$$

By a perturbation analysis of the Hamiltonian, F can be written as the sum of the Hamiltonian of the unperturbed system and a quantity depending on a small parameter. In the present case, the small parameter is J_2. Brouwer's theory can be used to find the short-periodic as well as long-periodic corrections to obtain osculating elements from mean elements.

The short-period corrections obtained from Kozai and Brouwer are the same.[19] While the corrections from the former are in terms of harmonics of ω and f, in the latter, they are in terms of l and g. It should be noted that Ω and h do not appear anywhere in the formulation. This is a reflection of the fact that the potential due to J_2 in Eq. (2.7) does not depend on the longitude λ.

The theory developed[1,2] is correct up to the first order in J_2; that is, J_2^2 and higher powers have been ignored. The long-period corrections include terms like $J_2 \sin g$, $J_2 \cos g$, etc. Since for short periods of time (a few orbits), $\sin g \approx \sin \dot{g}t \approx \dot{g}t$,

and $\dot{g} \sim O(J_2)$, the resulting terms are of order J_2^2 and are therefore negligible when compared to the short-periodic variations. The greatest contribution in the conversion from mean to osculating elements is therefore from the short-period corrections.

2.5 The Inertial Model for Orbit Propagation

The most obvious equations that describe satellite motion are obtained in the ECI frame. The motion described in ECI coordinates is governed by six first-order non-linear differential equations:[3]

$$\ddot{\mathbf{r}} = -\boldsymbol{\nabla}\Phi \tag{2.18}$$

where Φ is the gravitational potential function and Φ_r is its gradient.

The angular momentum is given by $\mathbf{h} = \mathbf{r} \times \mathbf{v}$. The rate of change of angular momentum is given by

$$\begin{aligned}
\frac{d\mathbf{h}}{dt} &= \mathbf{r} \times \ddot{\mathbf{r}} \\
&= -\mathbf{r} \times \frac{\mu}{r^3}\mathbf{r} - \mathbf{r} \times \frac{1}{2}\mu J_2 R_e^2 \left[\frac{6z}{r^5}\mathbf{i}_Z + \left(\frac{3}{r^5} - \frac{15z^2}{r^7}\right)\mathbf{r}\right] \\
&= \mathbf{r} \times \frac{3\mu J_2 R_e^2}{r^5}\mathbf{i}_Z = -\frac{3\mu J_2 R_e^2}{r^5}\left\{yz\mathbf{i}_X - xz\mathbf{i}_Y\right\}
\end{aligned} \tag{2.19}$$

Thus, the Z-component of angular momentum is always a constant, irrespective of the presence of J_2. This is yet another consequence of the symmetry of the Earth, about its axis of rotation.

2.6 Gauss' Equations

Gauss' equations[3] relate a general disturbance acceleration vector to the corresponding changes in orbital elements. The disturbance can be a control acceleration vector,

or that due to other forces. Gauss' equations are more general than Lagrange's Variation of Parameters equations. A complete derivation of Gauss' equations is presented in Ref. 3. Gauss' equations are given by

$$\frac{d\mathbf{e}}{dt} = \mathbf{f}(\mathbf{e},\mathbf{u}) = \mathbf{G}(\mathbf{e})\mathbf{u} \tag{2.20}$$

where $\mathbf{e} = \{a \quad e \quad i \quad \Omega \quad \omega \quad M\}^T$ and $\mathbf{G}$ is a 6×3 matrix, written as follows

$$\mathbf{G} = \begin{bmatrix} \frac{2a^2}{h}e\sin f & \frac{2a^2}{h}\frac{p}{r} & 0 \\ \frac{p\sin f}{h} & \frac{(p+r)\cos f + re}{h} & 0 \\ 0 & 0 & \frac{r\cos\theta}{h} \\ 0 & 0 & \frac{r\sin\theta}{h\sin i} \\ -\frac{p\cos f}{he} & \frac{(p+r)\sin f}{he} & -\frac{r\sin\theta\cos i}{h\sin i} \\ \frac{\eta}{he}(p\cos f - 2re) & -\frac{\eta}{he}(p+r)\sin f & 0 \end{bmatrix} \tag{2.21}$$

with $h = \sqrt{\mu p}$, $\eta = \sqrt{1-e^2}$, $r = p/(1+e\cos f)$ and $p = a(1-e^2)$. The disturbance acceleration is $\mathbf{u} = \{u_r \quad u_\theta \quad u_h\}^T$. The variation in the orbital elements due to the J_2 perturbation can also be obtained by using the accelerations due to J_2, given by Eq. (2.12).

2.7 Kechichian's Equations

Equations to model the motion of a satellite using the LVLH frame of reference have been developed by Kechichian.[4] These nonlinear equations are exact and include the effects of perturbations due to drag as well as J_2. In the absence of drag and control,

Kechichian's equations are:

$$\begin{aligned}
\ddot{r} &= \dot{\theta}^2 + r\left(c_\theta^2 + c_i^2 s_\theta^2\right)\dot{\Omega}^2 + 2rc_i\dot{\theta}\dot{\Omega} - 2rs_i s_\theta c_\theta \dot{i}\dot{\Omega} + rs_\theta^2 \dot{i}^2 \\
&\quad -\frac{\mu}{r^2} - \frac{3\mu J_2 R_e^2}{2r^4}\left(1 - 3s_i^2 s_\theta^2\right) \qquad (2.22a) \\
\ddot{\theta} &= -\frac{2\dot{r}}{r}\left(c_i\dot{\Omega} + \dot{\theta}\right) - c_i\ddot{\Omega} - s_i^2 s_\theta c_\theta \dot{\Omega}^2 + 2s_i s_\theta^2 \dot{i}\dot{\Omega} \\
&\quad + s_\theta c_\theta\left(\dot{i}^2 - \frac{3\mu J_2 R_e^2}{r^5} s_i^2\right) \qquad (2.22b) \\
\dot{i} &= -\frac{3\mu J_2 R_e^2 s_i c_i s_\theta c_\theta}{hr^3} \qquad (2.22c) \\
\dot{\Omega} &= -\frac{3\mu J_2 R_e^2 c_i s_\theta^2}{hr^3} \qquad (2.22d)
\end{aligned}$$

where,

$$\begin{aligned}
h &= \frac{r^3\dot{\theta} + \left(r^6\dot{\theta}^2 - 12r\mu J_2 R_e^2 s_\theta^2 c_i^2\right)^{\frac{1}{2}}}{2r} \\
\dot{h} &= -\frac{3\mu J_2 R_e^2}{r^3} s_i^2 s_\theta c_\theta \\
\ddot{\Omega} &= -3\mu J_2 R_e^2\left[-\frac{\dot{h}c_i s_\theta^2}{h^2 r^3} - \frac{\dot{r}c_i s_\theta^2}{hr^4} - \frac{s_i s_\theta^2 \dot{i}}{hr^3} + \frac{2c_i s_\theta c_\theta \dot{\theta}}{hr^3}\right]
\end{aligned}$$

The sines and cosines in Eqs. (2.22) are denoted by s and c, respectively, with their subscripts denoting the argument of the function.

Any of the above models may be used as a "truth" model. The thesis will use the ECI model as the truth model and the simulation of subsequent analytical models developed, will be compared with this model.

2.8 Kinematic Analogy to Orbital Motion

An analogy has been drawn between rigid body dynamics and orbital mechanics in Ref. 5. If the position vector of the satellite in its own LVLH frame is $\mathbf{r}^B$, where the

superscript B indicates the body-fixed frame, then,

$$\mathbf{r}^B = r\mathbf{i}_r \tag{2.23}$$

The velocity of the satellite is then given by

$$\begin{aligned} \mathbf{v}^N &= \dot{\mathbf{r}} + \boldsymbol{\omega}^B \times \mathbf{r}^B \quad \left(\boldsymbol{\omega}^B \equiv \boldsymbol{\omega}_{LVLH}\right) \\ &= \dot{r}\mathbf{i}_r + r\omega_h^B \mathbf{i}_\theta - r\omega_\theta^B \mathbf{i}_h \end{aligned} \tag{2.24}$$

Consequently, the inertial acceleration in the LVLH frame is given by

$$\mathbf{a} = \left\{ \begin{array}{c} \ddot{r} - \left(\omega_h^{B2} + \omega_\theta^{B2}\right) r \\ \dot{\omega}_h^B r + 2\omega_h^B \dot{r} + \omega_r^B \omega_\theta^B r \\ -\dot{\omega}_\theta^B r - 2\omega_\theta^B \dot{r} + \omega_r^B \omega_h^B r \end{array} \right\} \tag{2.25}$$

It can be shown that a kinematic constraint exists[5] such that

$$\omega^B = \dot{\Omega}\cos\theta\sin i - \dot{i}\sin\theta = 0 \tag{2.26}$$

This constraint can be independently derived from Gauss' equations (2.20) for $\dot{i}$ and $\dot{\Omega}$.

Reference 20 studies the linearization error associated with different characterizations of the kinematic equivalent of orbital motion. The Euler parameter (EP) set is a redundant set that has less a linearization error than the 3-1-3 Euler angle set. The EPs are also a regularized set and do not have any singularities as do the 3-1-3 Euler angle set. The orientation of any frame with respect to another can be achieved by an Euler principal axis rotation through an angle ϕ about a unit vector $\boldsymbol{l} = \{l_1 \quad l_2 \quad l_3\}^T$. Since the direction cosine matrix $\mathbf{C}$ transforms a vector from the reference frame to the new frame, the Euler axis remains untransformed. Thus, $\mathbf{C}\boldsymbol{l} = \boldsymbol{l}$. Therefore, $\boldsymbol{l}$ is also the eigenaxis of $\mathbf{C}$, corresponding to an eigenvalue of 1. The EPs corresponding

to this transformation are given by

$$\beta_0 = \cos\frac{\phi}{2}, \quad \beta_i = l_i \sin\frac{\phi}{2}, \quad i = 1\ldots 3 \tag{2.27}$$

The direction cosine matrix can be expressed in terms of the EPs:[18]

$$\mathbf{C} = \begin{bmatrix} \beta_0^2+\beta_1^2-\beta_2^2-\beta_3^2 & 2(\beta_1\beta_2+\beta_0\beta_3) & 2(\beta_1\beta_3-\beta_0\beta_2) \\ (\beta_1\beta_2+\beta_0\beta_3) & \beta_0^2-\beta_1^2+\beta_2^2-\beta_3^2 & 2(\beta_2\beta_3+\beta_0\beta_1) \\ 2(\beta_1\beta_3+\beta_0\beta_2) & 2(\beta_2\beta_3-\beta_0\beta_1) & \beta_0^2-\beta_1^2-\beta_2^2+\beta_3^2 \end{bmatrix} \tag{2.28}$$

The EPs can be found from the 3-1-3 Euler angle rotation by the following relations:

$$\begin{aligned} \beta_0 &= \cos\left(\frac{i}{2}\right)\cos\left(\frac{\Omega+\theta}{2}\right) & \beta_1 &= \sin\left(\frac{i}{2}\right)\cos\left(\frac{\Omega-\theta}{2}\right) \\ \beta_2 &= \sin\left(\frac{i}{2}\right)\sin\left(\frac{\Omega-\theta}{2}\right) & \beta_3 &= \cos\left(\frac{i}{2}\right)\sin\left(\frac{\Omega+\theta}{2}\right) \end{aligned} \tag{2.29}$$

For the complete characterization orbit, the nine states $\begin{Bmatrix} r & \dot{r} & \boldsymbol{\omega}^T & \boldsymbol{\beta}^T \end{Bmatrix}^T$ are required. However, other descriptions of the orbit require only six elements. The nine states also have three constraints. One constraint has already been shown in Eq. (2.26). By setting $\omega_h^B = \dot{\omega}_h^B = 0$ in the h-component of $\mathbf{a}$ in Eq. (2.25), another constraint is obtained for ω_r^B:

$$\omega_r^B = \frac{u_h}{r\omega_h^B} \tag{2.30}$$

If the external force in the orbit normal direction is zero, then $\omega_r^B = 0$. Finally, the third constraint is on the redundancy of the Euler parameter set: $\boldsymbol{\beta}^T\boldsymbol{\beta} = 1$. There are thus, seven differential equations of motion, one each for r and $\dot{r}$, four for the EPs, and one for ω_h^B.

2.9 Summary

The frames of reference and quantities to describe the motion of a satellite that are used in the thesis have been presented in this section. An introduction to the basis of the J_2 perturbation has been provided, followed by the relevant theories of Kozai and Brouwer. While the short-period corrections from both Kozai and Brouwer are identical, only one of the theories should be used and they should not be mixed. Of the two approaches, Brouwer's theory is mathematically more reliable since the corrections are obtained from a perturbation analysis of the Hamiltonian, while Kozai's corrections are obtained from an analysis that depends on the time-average of some elements. In this thesis, Brouwer's theory will be used to obtain osculating elements from mean elements.

CHAPTER III

MODELING RELATIVE MOTION INCLUDING THE J_2 PERTURBATION

3.1 Introduction

In the previous chapter, the different models used to study the motion of a single satellite that included the J_2 perturbation, were presented briefly. Since the relative motion under the effect of perturbations is of interest in this thesis, the various models for relative motion will be developed in this chapter. Of special interest are relative orbits that are circular, when projected on the θ-h plane. The initial conditions for the projected circular orbit from the Hill-Clohessy-Wiltshire equations and the geometric method are discussed. With respect to the latter, two different conditions are explored. The first one may lead to large and impractical formations, while the latter causes drift in the cross-track motion that has to be corrected using thrust. Two new approaches to propagating relative motion dynamics: the unit sphere model and the kinematic approach are presented. The errors in relative motion from different models are studied.

3.2 Truth Models for Relative Motion

Let the position and velocity vectors of the Chief satellite be $\mathbf{r}_C$ and $\mathbf{v}_C$, and those of the Deputy be $\mathbf{r}_D$ and $\mathbf{v}_D$, respectively. The inertial relative position and velocity are then defined as

$$\delta\mathbf{r} = \mathbf{r}_D - \mathbf{r}_C \tag{3.1a}$$

$$\delta\mathbf{v} = \mathbf{v}_D - \mathbf{v}_C \tag{3.1b}$$

The relative position can be transformed into the LVLH frame of the Chief by using the direction cosine matrix, $\mathbf{C}$. The columns of $\mathbf{C}$ can be expressed in terms of the position and velocity vectors by

$$\mathbf{C} = \begin{bmatrix} \dfrac{\mathbf{r}_C}{r_C} & \dfrac{\mathbf{h}_C \times \mathbf{r}_C}{|\mathbf{h}_C \times \mathbf{r}_C|} & \dfrac{\mathbf{h}_C}{h_C} \end{bmatrix} \tag{3.2}$$

Then, the relative position (x, y, z) in the LVLH frame of the Chief[21] is given by

$$x = \frac{\delta \mathbf{r}^T \mathbf{r}_C}{r_C} \tag{3.3a}$$

$$y = \frac{\delta \mathbf{r}^T (\mathbf{h}_C \times \mathbf{r}_C)}{|\mathbf{h}_C \times \mathbf{r}_C|} \tag{3.3b}$$

$$z = \frac{\delta \mathbf{r}^T \mathbf{h}_C}{h_C} \tag{3.3c}$$

where $\mathbf{h}_C = \mathbf{r}_C \times \mathbf{v}_C$ is the angular momentum vector of the Chief. The relative velocities in the LVLH frame are:

$$\dot{x} = \frac{\delta \mathbf{v}^T \mathbf{r}_C + \delta \mathbf{r}^T \mathbf{v}_C}{r_C} - \frac{(\delta \mathbf{r}^T \mathbf{r}_C)(\mathbf{r}_C^T \mathbf{v}_C)}{r_C^3} \tag{3.4a}$$

$$\dot{y} = \frac{\delta \mathbf{v}^T (\mathbf{h}_C \times \mathbf{r}_C) + \delta \mathbf{r}^T (\dot{\mathbf{h}}_C \times \mathbf{r}_C + \mathbf{h}_C \times \mathbf{v}_C)}{|\mathbf{h}_C \times \mathbf{r}_C|} - \frac{\delta \mathbf{r}^T (\mathbf{h}_C \times \mathbf{r}_C)(\mathbf{h}_C \times \mathbf{r}_C)^T (\dot{\mathbf{h}}_C \times \mathbf{r}_C + \mathbf{h}_C \times \mathbf{v}_C)}{|\mathbf{h}_C \times \mathbf{r}_C|^3} \tag{3.4b}$$

$$\dot{z} = \frac{\delta \mathbf{v}^T \mathbf{h}_C + \delta \mathbf{r}^T \dot{\mathbf{h}}_C}{h_C} - \frac{\delta \mathbf{r}^T \mathbf{h}_C (\mathbf{h}_C^T \dot{\mathbf{h}}_C)}{h_C^3} \tag{3.4c}$$

Equations (3.3) and (3.4) can be used to transform the inertial position and velocity of the Chief and Deputy into the relative position in the Chief's LVLH frame. To obtain the inertial position and velocity of satellites, two sets of six first-order equations shown in Eq. (2.18) need to be solved. This ECI model will be referred to as the truth model and will be used as a basis for comparison. Further, Gauss' equations or Kechichian's equations can also be used to find the relative position and velocity. In such cases, the direction cosine matrix will have to be obtained from the 3-1-3 Euler

angles of the Deputy and Chief. The position and velocity of the Deputy will have to be transformed into the ECI frame using the transpose of its direction cosine matrix, and back into the LVLH frame of the Chief.

3.3 Hill-Clohessy-Wiltshire Model for Relative Motion

The Hill-Clohessy-Wiltshire (HCW) equations[7] are the simplest equations that model relative motion.

3.3.1 Equations of Motion

Let the position of the Chief (reference) in its LVLH frame by $\mathbf{r}_C = \{r \quad 0 \quad 0\}^T$. If the relative position of the Deputy in the Chief's LVLH is $\delta\mathbf{r} = \{x \quad y \quad z\}^T$, the position of the Deputy is

$$\mathbf{r}_D = \begin{Bmatrix} r+x \\ y \\ z \end{Bmatrix} \tag{3.5}$$

In the absence of J_2 perturbations, the angular velocity of the Chief's LVLH frame is $\dot{\theta}\mathbf{i}_h$. Then, from Eq. (2.24), the velocity of the Deputy is

$$\dot{\mathbf{r}}_D = \dot{\mathbf{r}}_C + \begin{Bmatrix} \dot{x} \\ \dot{y} \\ \dot{z} \end{Bmatrix} + \dot{\theta}\mathbf{i}_h \times \begin{Bmatrix} x \\ y \\ z \end{Bmatrix} = \dot{\mathbf{r}}_C + \begin{Bmatrix} \dot{x} - y\dot{\theta} \\ \dot{y} + x\dot{\theta} \\ 0 \end{Bmatrix} \tag{3.6}$$

Similarly, from Eq. (2.25),

$$\ddot{\mathbf{r}}_D - \ddot{\mathbf{r}}_C = \begin{Bmatrix} \ddot{x} - 2\dot{y}\dot{\theta} - x\dot{\theta}^2 - y\ddot{\theta} \\ \ddot{y} + 2\dot{x}\dot{\theta} - y\dot{\theta}^2 - x\ddot{\theta} \\ 0 \end{Bmatrix} \tag{3.7}$$

In the absence of control, the equations of motion of the two satellites can be written as

$$\ddot{\mathbf{r}}_C = \mathbf{g}_C = \left\{ -\frac{\mu}{r^2} \quad 0 \quad 0 \right\}^T \tag{3.8a}$$

$$\ddot{\mathbf{r}}_D = \mathbf{g}_D = \left\{ -\frac{\mu}{r_D^2} \quad 0 \quad 0 \right\}^T \tag{3.8b}$$

where, $r_D = [(r+x)^2 + y^2 + z^2]^{\frac{1}{2}}$, $\ddot{\mathbf{r}}C$ and $\ddot{\mathbf{r}}_D$ are the inertial accelerations of Chief and Deputy, respectively, and $\mathbf{g}_C$ and $\mathbf{g}_D$ are the respective gravitational attractions.

From Eqs. (3.7) and (3.8), a tenth-order nonlinear system that includes eccentricity effects is obtained:

$$\ddot{x} - 2\dot{y}\dot{\theta} - x\dot{\theta}^2 - y\ddot{\theta} = -\frac{\mu(r+x)}{[(r+x)^2 + y^2 + z^2]^{\frac{3}{2}}} + \frac{\mu}{r^2} \tag{3.9a}$$

$$\ddot{y} + 2\dot{x}\dot{\theta} - y\dot{\theta}^2 + x\ddot{\theta} = -\frac{\mu y}{[(r+x)^2 + y^2 + z^2]^{\frac{3}{2}}} \tag{3.9b}$$

$$\ddot{z} = -\frac{\mu z}{[(r+x)^2 + y^2 + z^2]^{\frac{3}{2}}} \tag{3.9c}$$

$$\ddot{r} = r\dot{\theta}^2 - \frac{\mu}{r^2} \tag{3.9d}$$

$$\ddot{\theta} = -2\frac{\dot{r}}{r}\dot{\theta} \tag{3.9e}$$

By linearizing the differential gravity field, the gravitational attraction on the Deputy can be written as

$$\mathbf{g}_D = \mathbf{g}_C + \frac{\partial \mathbf{g}}{\partial \delta \mathbf{r}} \delta \mathbf{r} + O(|\delta \mathbf{r}|^2)$$

The above result, when substituted in Eqs. (3.9), results in the following linearized equations for relative motion:

$$\ddot{x} - 2\dot{y}\dot{\theta} - x\dot{\theta}^2 - y\ddot{\theta} - 2\frac{\mu}{r^3}x = 0 \tag{3.10a}$$

$$\ddot{y} + 2\dot{x}\dot{\theta} - y\dot{\theta}^2 + x\ddot{\theta} + \frac{\mu}{r^3}y = 0 \tag{3.10b}$$

$$\ddot{z} + \frac{\mu}{r^3}z = 0 \tag{3.10c}$$

$$\ddot{r} = r\dot{\theta}^2 - \frac{\mu}{r^2} \tag{3.10d}$$

$$\ddot{\theta} = -2\frac{\dot{r}}{r}\dot{\theta} \tag{3.10e}$$

By using Eqs. (2.3), Melton[22] truncated the series for r and θ to $O(e^2)$ and reduced the order of Eqs. (3.10) to six. Reference 22 also obtains a state transition matrix for the relative motion problem between elliptical orbits.

If it is further assumed that the Chief's orbit is circular, then $\dot{\theta} = n_C = \sqrt{\mu/a_C^3}$, $\ddot{\theta} = 0$, and $r = a_C$. Under these assumptions, the HCW equations are obtained as given below:

$$\ddot{x} - 2n_C\dot{y} - 3n_C^2 x = 0 \tag{3.11a}$$

$$\ddot{y} + 2n_C\dot{x} = 0 \tag{3.11b}$$

$$\ddot{z} + n_C^2 z = 0 \tag{3.11c}$$

Equations (3.11) are a set of sixth-order, linear constant coefficient ordinary differential equations. The HCW equations admit bounded periodic solutions known as HCW solutions that are suitable for formation flying, given by

$$x = \frac{c_1}{2}\sin(n_C t + \alpha_0) \tag{3.12a}$$

$$y = c_1\cos(n_C t + \alpha_0) + c_3 \tag{3.12b}$$

$$z = c_2\sin(n_C t + \beta_0) \tag{3.12c}$$

$$\dot{x} = \frac{c_1}{2}n_C\cos(n_C t + \alpha_0) \tag{3.12d}$$

$$\dot{y} = -c_1 n_C\sin(n_C t + \alpha_0) \tag{3.12e}$$

$$\dot{z} = c_2 n_C \cos(n_C t + \beta_0) \tag{3.12f}$$

The constants $c_{1...3}$, α_0 and β_0 are determined by the initial conditions. HCW initial conditions refer to those conditions for which there is no secular growth in y, i.e.,

$$\dot{y}_0 + 2n_C x_0 = 0 \tag{3.13}$$

3.3.2 HCW Conditions for a Projected Circular Orbit

Projected Circular Orbits (PCO) are those that are circles in the θ-h plane. They are obtained by choosing $c_1 = c_2 = \rho$, $c_3 = 0$ and $\alpha_0 = \beta_0$. As a result,

$$\begin{aligned} x &= \frac{\rho}{2}\sin(n_C t + \alpha_0) \\ y &= \rho\cos(n_C t + \alpha_0) \\ z &= \rho\sin(n_C t + \alpha_0) \end{aligned}$$

ρ is the relative orbit radius and α_0 is the initial phase angle. ρ and α_0 are shown with respect to the LVLH frame of the Chief in Fig. 3.1.

Since the HCW equations have been derived under the assumptions of a circular reference orbit, linearized differential gravity field and no perturbations, they break down when any of the these assumptions are violated. This has been addressed in Ref. 8. By performing a perturbation analysis on a model with second-order nonlinearities included, corrections to the initial conditions of the HCW equations can be developed that reduce the error due to linearization. Further analysis on Melton's state transition matrix[22] yields a correction to the initial conditions that yield near-circular relative orbits.

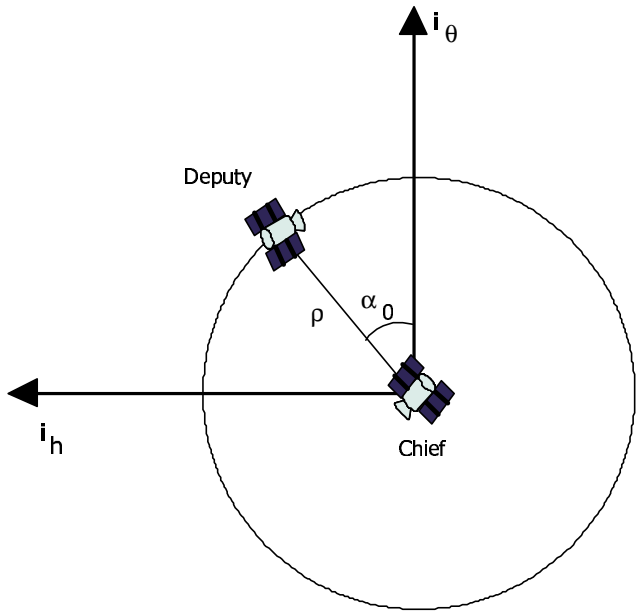

Fig. 3.1 Relative Radius and Initial Phase Angle

3.4 Geometric Approach to Formation Flying

3.4.1 Equations of Motion

Let the orbital elements of the Chief and Deputy be $\mathbf{e}_C$ and $\mathbf{e}_D$, respectively. The differences between the elements of the Deputy and the Chief are then given by $\delta\mathbf{e} = \mathbf{e}_D - \mathbf{e}_C = \{\delta a \quad \delta e \quad \delta i \quad \delta\Omega \quad \delta\omega \quad \delta M\}^T$. If the radial distance of the Chief (reference) is r, the position of the Deputy in the LVLH frame of the Chief can be written as

$$\mathbf{r}_D = \begin{Bmatrix} r + \delta r \\ 0 \\ 0 \end{Bmatrix} \tag{3.14}$$

Let $\mathbf{C}_C$ and $\mathbf{C}_D$ be the direction cosine matrices that transform a vector in the inertial frame into the respective LVLH frames of the Chief and Deputy. Then the relative

position is also given by $\delta\mathbf{r} = \mathbf{C}_C\mathbf{C}_D^T\mathbf{r}_D - \mathbf{r}_C$. The direction cosine matrix of the Deputy can be written as:

$$\mathbf{C}_D = \mathbf{C}_C + \delta\mathbf{C} \tag{3.15}$$

Then, the relative position is

$$\begin{Bmatrix} x \\ y \\ z \end{Bmatrix} = \begin{Bmatrix} \delta r \\ 0 \\ 0 \end{Bmatrix} + r\mathbf{C}_C \begin{Bmatrix} \delta C_{11} \\ \delta C_{21} \\ \delta C_{31} \end{Bmatrix} \tag{3.16}$$

From the expression for $\mathbf{C}$ in Eq. (2.4), the relative position is given by[23]

$$x \approx \delta r \tag{3.17a}$$

$$y \approx r(\delta\theta + \delta\Omega\cos i_C) \tag{3.17b}$$

$$z \approx r(\delta i \sin\theta_C - \delta\Omega\cos\theta_C \sin i_C) \tag{3.17c}$$

Reference 12 develops a state transition matrix by obtaining a linearized relation between the relative position and the orbital element differences. A nonsingular element set is used, and the relative position vector is written as

$$\delta\mathbf{r} = \mathbf{A}\delta\mathbf{e}$$

Given the relative position $\delta\mathbf{r}$, the orbital element differences can be found by $\delta\mathbf{e} = \mathbf{A}^{-1}\delta\mathbf{r}$. The accuracy of the method is improved by using a curvilinear coordinate system affixed on the Chief, rather than the usual rectilinear LVLH frame. A transformation matrix in nonsingular elements is developed that is more accurate than Brouwer's theory, especially at low eccentricities.

3.4.2 Initial Conditions for Bounded, Circular Projection Relative Orbits

The PCO requirement results in the following parametric form for y and z:

$$y = \rho\cos(\theta_C + \alpha_0) \qquad z = \rho\sin(\theta_C + \alpha_0) \tag{3.18}$$

ρ and α_0 are defined in Fig. 3.1. If the reference orbit is of low eccentricity, then $r \approx a$, and from Eq. (2.3a),

$$\begin{aligned} f &= M + 2e\sin M + O(e^2) \\ \Rightarrow \delta f &= \delta M + 2\delta e\sin M + 2e\left[\sin(M+\delta M) - \sin M\right] \\ &= \delta M + 2\delta e\sin M + 2e\left[\sin M\cos\delta M + \cos M\sin\delta M - \sin M\right] \end{aligned} \tag{3.19}$$

For small formations, $\delta M \ll M$, and

$$\delta f = \delta M + 2\delta e\sin M + 2e\cos M\delta M \tag{3.20}$$

$$\begin{aligned} \Rightarrow y &= r(\delta\theta + \delta\Omega\cos i_C) \\ &\approx a_C(\delta\omega + \delta M + \delta\Omega\cos i_C) + 2a_C\delta e\sin M_C + 2a_C e_C\delta M\cos M_C \end{aligned} \tag{3.21}$$

Similarly,

$$z \approx a_C(\delta i\sin\theta_C - \delta\Omega\sin i_C\cos\theta_C) \tag{3.22}$$

In the absence of J_2 perturbations, δi, $\delta\Omega$ and $\delta\omega$ are constants. But,

$$\delta M = \delta M_0 + \delta n t = \delta M_0 + \left(\sqrt{\frac{\mu}{a_D^3}} - \sqrt{\frac{\mu}{a_C^3}}\right)t$$

If $\delta M \neq$ constant then from Eq. (3.21), the Deputy will show secular drift in the along-track direction. $\delta M =$ constant only if the mean rates are equal, that is, if $\delta a = a_D - a_C = 0$.

From Eq. (3.18), the desired parameterization of y can be written as

$$\begin{aligned} y &= \rho\cos(\theta_C + \alpha_0) \\ &\approx \rho\cos(\omega_C + M_C + 2e_C\sin M_C + \alpha_0) \\ &= \rho\cos(\omega_C + M_C + \alpha_0)\cos(2e_C\sin M_C) \\ &\quad -\rho\sin(\omega_C + M_C + \alpha_0)\sin(2e_C\sin M_C) \end{aligned} \tag{3.23}$$

For small eccentricities, $\cos(2e\sin M) \approx 1$ and $\sin(2e\sin M) \approx 2e\sin M$. Substituting in Eq. (3.23),

$$y = \rho\cos(\omega_C + \alpha_0)\cos M_C - \rho\left[\sin(\omega_C + \alpha_0) + 2e_C\sin(\omega_C + M_C + \alpha_0)\right]\sin M_C \tag{3.24}$$

By a term-by-term comparison of Eqs. (3.21) and (3.24),

$$\begin{aligned} &\delta\omega + \delta M + \delta\Omega\cos i_C = 0 \\ &\delta M = \frac{\rho}{2a_Ce_C}\cos(\omega_C + \alpha_0) \\ &\delta e = -\frac{\rho}{2a_C}\left[\sin(\omega_C + \alpha_0) + 2e_C\sin(M_{C_0} + \omega + \alpha_0)\right] \end{aligned}$$

This is only true if δM is small. If δM is not small, then from Eq. (3.19), Eq. (3.21) needs to be modified, and by comparing the coefficients of $\cos M_C$

$$\begin{aligned} 2e_C\sin\delta M &= \frac{\rho}{a_C}\cos(\omega_C + \alpha_0) \\ \Rightarrow \delta M &= \sin^{-1}\left[\frac{\rho}{2a_Ce_C}\cos(\omega_C + \alpha_0)\right] \end{aligned}$$

Thus, δM can be assumed small if $\rho/(2a_Ce_C)\cos(\omega_C + \alpha_0) \ll 1$. This is also a condition for the validity of the above analysis.

The value of δM obtained from either the small angle assumption, or the arc-sine,

can be used to find δe by comparing the coefficients of $\sin M_C$:

$$2\delta e + 2e_C(\cos\delta M - 1) = -\frac{\rho}{\alpha_0}\left[\sin(\omega_C + \alpha_0) + 2e_C\sin(M_C + \omega_C + \alpha_0)\right]$$

The desired parameterization of z from Eq. (3.18) results in

$$z = \rho\sin\theta_C\cos\alpha_0 + \rho\cos\theta_C\sin\alpha_0 \tag{3.25}$$

By comparing the coefficients of $\sin\theta_C$ and $\cos\theta_C$ in Eqs. (3.22) and (3.25),

$$\begin{aligned}\delta i &= \frac{\rho}{a_C}\cos\alpha_0 \\ \delta\Omega &= -\frac{\rho}{a_C}\frac{\sin\alpha_0}{\sin i}\end{aligned}$$

Since $\delta\Omega$ has been determined, $\delta\omega = -\delta M - \delta\Omega\cos i_C$. The orbital element differences for a PCO of relative radius ρ and phase angle α_0 in the absence of J_2 perturbations are summarized in Table 3.1.

Table 3.1 Initial Orbital Element Differences for a Relative Orbit of Radius ρ and Phase Angle α_0 in the Absence of J_2

δa	0
δe	$-\frac{\rho}{2a_C}\left[\sin(\omega_C + \alpha_0) + 2e_C\sin(M_{C_0} + \omega_C + \alpha_0)\right]$
δi	$\frac{\rho}{a_C}\cos\alpha_0$
$\delta\Omega$	- $\frac{\rho}{a_C}\frac{\sin\alpha_0}{\sin i_C}$
$\delta\omega$	$-\frac{\rho}{2a_Ce_C}\cos(\omega_C + \alpha_0) + \frac{\rho}{a_C}\frac{\cos i_C\sin\alpha_0}{\sin i_C}$
δM	$\frac{\rho}{2a_Ce_C}\cos(\omega_C + \alpha_0)$

For low-eccentricity Chief orbits or for small relative orbit radii, $\rho e_C \ll a_C$, and the second term of δe can be ignored. For very low eccentricities, though the sum of $\delta\omega$ and δM is defined, they are undefined individually.

In the presence of J_2 perturbations, the relative motion using mean elements can be analyzed, since the short-periodic variations are oscillatory in nature and the mean elements account for the drifts in the elements. From Eqs. (3.21) and (3.22),

$$y\Big|_{mean} = a_C(\delta\omega + \delta M + \delta\Omega\cos i_C + 2\delta e\sin M_C + 2e_C\delta M\cos M_C)\Big|_{mean} \quad (3.26a)$$

$$z\Big|_{mean} = a_C(\delta i\sin\theta_C - \delta\Omega\sin i_C\cos\theta_C)\Big|_{mean} \quad (3.26b)$$

Since $\delta\dot{\Omega}$, $\delta\dot{\omega}$, and $\delta\dot{M}$ are no longer zero, the relative motion is not bounded. Schaub and Alfriend,[10] as described below, have presented an analytical method to establish J_2-invariant orbits. A normalized Delauney element description is considered. To prevent the Deputy from drifting away from the Chief, it is necessary to have all three relative rates, $\delta\dot{l} = \delta\dot{g} = \delta\dot{h} = 0$. This is only possible if $\delta L = \delta G = \delta H = 0$, which constrains the possible values for the semimajor axis, eccentricity, and inclination of the Deputy with respect to those of the Chief. By relaxing the constraint, and only requiring that the the mean drift rate between the radius vectors be zero, the following conditions for J_2 invariance are obtained:

$$\dot{h}_D = \dot{h}_C \Rightarrow \delta\dot{\Omega} = 0 \quad (3.27a)$$

$$\dot{\theta}_D = \dot{\theta}_C \Rightarrow \dot{l}_D + \dot{g}_D = \dot{l}_C + \dot{g}_C \Rightarrow \delta\dot{\omega} + \dot{\delta}M = 0 \quad (3.27b)$$

However, it is shown in Ref. 10 that δM depends on $\tan i_C$. As the inclination of the reference orbit increases, the required difference in mean anomalies grows very large. This results in relative orbits of very large radii, and for near-polar orbits, the

analysis fails. From Eqs. (3.26), secular drift in y and z exist unless

$$\delta\dot{\omega} + \delta\dot{M} + \delta\dot{\Omega}\cos i_C\Big|_{mean} = 0 \tag{3.28a}$$

$$\delta\dot{\Omega}\Big|_{mean} = 0 \tag{3.28b}$$

Table 3.2 Initial Orbital Element Differences for a Relative Orbit of Radius ρ and Phase Angle α_0 with J_2 Perturbations

δa	$\frac{1}{2}J_2\left(\frac{R_e^2}{a_C}\right)\frac{(3\eta+4)}{\eta^4}\left[-(1-3\cos^2 i_C)\frac{e_C}{\eta^2}\delta e - \sin 2i_C\delta i\right]$
δe	$-\frac{\rho}{2a_C}\left[\sin(\omega_C+\alpha_0) + 2e_C\sin(M_{C_0}+\omega_C+\alpha_0)\right]$
δi	$\frac{\rho}{a_C}\cos\alpha_0$
$\delta\Omega$	$-\frac{\rho}{a_C}\frac{\sin\alpha_0}{\sin i_C}$
$\delta\omega$	$-\frac{\rho}{2a_Ce_C}\cos(\omega_C+\alpha_0) + \frac{\rho}{a_C}\frac{\cos i_C\sin\alpha_0}{\sin i_C}$
δM	$\frac{\rho}{2a_Ce_C}\cos(\omega_C+\alpha_0)$

Equation (3.28a) is the period-matching condition derived in Ref. 11. From Eq. (3.28b), a non-zero δa is obtained that is of order J_2. The modified elemental differences for PCOs are given in Table 3.2.

Both the conditions in Eqs. (3.28) cannot be satisfied simultaneously, since the desired elements of the Deputy also need to satisfy the six HCW PCO conditions. The condition on $\dot{y}_0$, specified in Eq. (3.13), is dropped and the rate-matching constraint

Eq. (3.28a) is used. Since Eq. (3.28b) is no longer satisfied,

$$\delta\dot{\Omega}\Big|_{\text{mean}} = \frac{\partial\dot{\Omega}_C}{\partial a_C}\delta a + \frac{\partial\dot{\Omega}_C}{\partial e_C}\delta e + \frac{\partial\dot{\Omega}_C}{\partial i_C}\delta i\Big|_{\text{mean}} \tag{3.29}$$

Since δa is of the order of J_2, the contribution of a to $\delta\dot{\Omega}$ is of the order of J_2^2. Correct to first order, and for low eccentricities, the expression for z using mean elements is

$$\frac{z}{r}\Big|_{\text{mean}} = \frac{\rho}{a_C}\left[\sin(\theta_C + \alpha_0) + 1.5J_2\left(\frac{R_e}{a_C}\right)^2 n_C \sin^2 i_C \cos\theta_C \cos\alpha_0 t\right]\Bigg|_{\text{mean}} \tag{3.30}$$

The mean value of z is zero. The growth in error amplitude as a function of time can be obtained from above as

$$\frac{z}{r}\Big|_{\text{secular}} = \frac{\rho}{a_C}1.5J_2\left(\frac{R_e}{a_C}\right)^2 n_C \sin^2 i_C \ \cos\alpha_0 t$$

The growth of z is maximum for $\alpha_0 = 0°$ and minimum for $\alpha_0 = 90°$. It should be noted that the drift is not zero as predicted by Eq. (3.30), since there are contributions from δa and e_C that have been ignored in the equation.

3.5 The Unit Sphere Representation of Relative Motion

The relative motion of a Deputy with respect to a Chief satellite can also be studied by using the unit sphere representation.[15] The relative motion between two satellites can be analytically obtained by projecting the positions of the Chief and Deputy onto a sphere of unit radius. This projection is performed by normalizing the positions of the Chief and the Deputy with respect to their radial distances from the center of the Earth. The projected points on the unit sphere are known as sub-satellite points. Figure 3.2 shows how the normalization leads to the projected orbit.

Let $\mathbf{C}_C$ and $\mathbf{C}_D$ be the direction cosine matrices associated with the LVLH frames

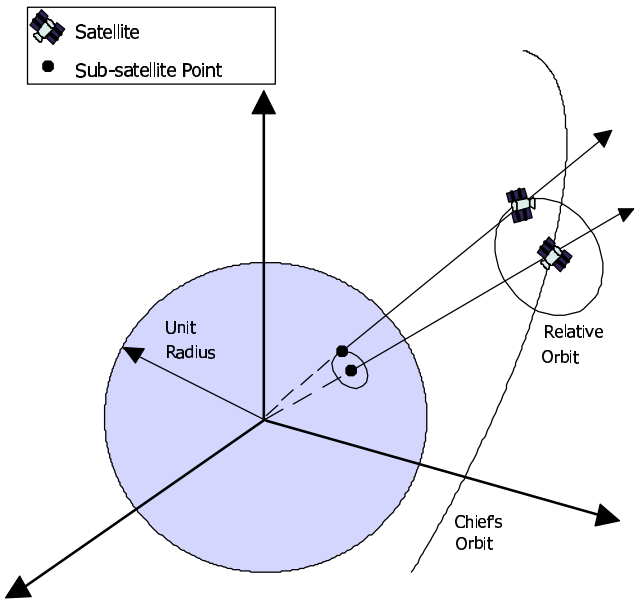

Fig. 3.2 Relative Motion on the Unit Sphere

of the Chief and the Deputy, respectively, characterized by the 3-1-3 Euler angle rotation in Eq. (2.4). The transformation matrix $\mathbf{C}_C\mathbf{C}_D^T$ transforms a vector in the LVLH frame of the Deputy into the LVLH frame of the Chief. On the unit sphere, the position vectors of the Deputy and the Chief in their own LVLH frame are, respectively, $\bar{\mathbf{r}}_D = \{1 \quad 0 \quad 0\}^T$ and $\bar{\mathbf{r}}_C = \{1 \quad 0 \quad 0\}^T$. The quantities with bars over them are used to distinguish the position on the unit sphere from the true position vectors. Then, the relative position on the unit sphere, is given by

$$\left\{ \begin{array}{c} \bar{x} \\ \bar{y} \\ \bar{z} \end{array} \right\} = \mathbf{C}_C\mathbf{C}_D^T\bar{\mathbf{r}}_D - \bar{\mathbf{r}}_C = \left[\mathbf{C}_C\mathbf{C}_D^T - \mathbf{I}\right] \left\{ \begin{array}{c} 1 \\ 0 \\ 0 \end{array} \right\} \tag{3.31}$$

From Eq. (2.4), $\mathbf{C}_C \equiv \mathbf{C}_C(\Omega_C, i_C, \theta_C)$ and $\mathbf{C}_D \equiv \mathbf{C}_D(\Omega_D, i_D, \theta_D)$. Thus by determining the 3-1-3 Euler angles of the Chief and Deputy, the relative position on the unit sphere can be determined. The true relative position in the LVLH frame of the Chief

is then given by the inverse relations

$$x = r_D(1+\bar{x}) - r_C \tag{3.32a}$$

$$y = r_D\bar{y} \tag{3.32b}$$

$$z = r_D\bar{z} \tag{3.32c}$$

The position of the Deputy in the Chief's LVLH frame, projected on the unit sphere is given by

$$\bar{\mathbf{r}}_D^C = (1+\bar{x})\mathbf{i}_r + \bar{y}\mathbf{i}_\theta + \bar{z}\mathbf{i}_h \tag{3.33}$$

Since the motion on the unit sphere is constrained to lie on it, it can be stated that

$$(1+\bar{x})^2 + \bar{y}^2 + \bar{z}^2 = 1 \tag{3.34}$$

and $\bar{x}^2 + \bar{y}^2 + \bar{z}^2 \geq 0$, $\bar{x} \leq 0$.

Let $\bar{\mathbf{v}}_D$ and $\bar{\mathbf{v}}_D^C$ be the inertial velocity vectors of the Deputy expressed its own LVLH frame and the Chief's LVLH frame, respectively. The velocity of the Deputy on the unit sphere cannot have a radial component when expressed in its own LVLH frame. Then,

$$\bar{\mathbf{v}}_D = \boldsymbol{\omega}_D^B \times \mathbf{i}_{r_D} \tag{3.35a}$$

$$\bar{\mathbf{v}}_D^C = (\dot{\bar{x}}\mathbf{i}_r + \dot{\bar{y}}\mathbf{i}_\theta + \dot{\bar{z}}\mathbf{i}_h) + \boldsymbol{\omega}_D^C \times \bar{\mathbf{r}}_D^C \tag{3.35b}$$

From Ref. 15, Eqs. (3.31) can be written explicitly in terms of the orbital angles of

the Chief and Deputy.

$$\begin{aligned}
\bar{x} &= -1 + c_{i_C/2}^2 c_{i_D/2}^2 c_{(\Delta\theta+\Delta\Omega)} + s_{i_C/2}^2 s_{i_D/2}^2 c_{(\Delta\theta-\Delta\Omega)} \\
&\quad + s_{i_C/2}^2 c_{i_D/2}^2 c_{(2\theta_C+\Delta\theta+\Delta\Omega)} + c_{i_C/2}^2 s_{i_D/2}^2 c_{(2\theta_C+\Delta\theta-\Delta\Omega)} \\
&\quad + 1/2 s_{i_C} s_{i_D} \left[c_{\Delta\theta} - c_{(2\theta_C+\Delta\theta)} \right] \qquad (3.36a) \\
\bar{y} &= c_{i_C/2}^2 c_{i_D/2}^2 s_{(\Delta\theta+\Delta\Omega)} + s_{i_C/2}^2 s_{i_D/2}^2 s_{(\Delta\theta-\Delta\Omega)} \\
&\quad - s_{i_C/2}^2 c_{i_D/2}^2 s_{(2\theta_C+\Delta\theta+\Delta\Omega)} - c_{i_C/2}^2 s_{i_D/2}^2 c_{(2\theta_C+\Delta\theta-\Delta\Omega)} \\
&\quad + 1/2 s_{i_C} s_{i_D} \left[s_{\Delta\theta} + s_{(2\theta_C+\Delta\theta)} \right] \qquad (3.36b) \\
\bar{z} &= -s_{i_C} s_{\Delta\Omega} c_{\theta_D} - \left[s_{i_C} c_{i_D} c_{\Delta\Omega} - c_{i_C} s_{i_D} \right] s_{\theta_D} \qquad (3.36c)
\end{aligned}$$

where s and c with the corresponding subscripts, denote the sine and cosine functions with the subscripts as arguments, respectively. Equations (3.36) depend on two angles of the Chief - i_C and θ_C, and the angle differences between the Deputy and Chief - $\Delta\Omega$, Δi and $\Delta\theta$. Since the J_2 potential is symmetric about the Z axis of the Earth, Ω_C does not appear in the solutions for the relative motion variables.

Equations (3.31) and (3.32) provide an exact description of relative motion, even in the presence of perturbations. assuming the use of osculating elements. The use of mean elements for the angles can considerably simplify the model without introducing excessive error.[15] This requires the use of mean rates for the angles Ω, ω, and M for both the Chief and Deputy, from Eqs. (2.15). The angles of inclination are assumed constant.

The relative motion on the unit sphere can alternatively be described using relative Euler parameters.[16] It has been shown in the previous chapter that the motion of a single satellite can be modeled using Euler parameters. The theory in Ref. 5 can be

extended to model relative motion.

Let $\boldsymbol{\beta}_C$ and $\boldsymbol{\beta}_D$ denote the Euler parameters that characterize the LVLH frames of the Chief and Deputy, with respect to the ECI frame. From a control point of view, it is convenient to obtain the Euler parameters that provide the relative orientation of the Chief's LVLH frame with respect to that of the Deputy, which are given by[18]

$$\begin{Bmatrix} \Delta\beta_0 \\ \Delta\beta_1 \\ \Delta\beta_2 \\ \Delta\beta_3 \end{Bmatrix} = \begin{bmatrix} \beta_{C_0} & \beta_{C_1} & \beta_{C_2} & \beta_{C_3} \\ \beta_{C_1} & -\beta_{C_0} & -\beta_{C_3} & \beta_{C_2} \\ \beta_{C_2} & \beta_{C_3} & -\beta_{C_0} & -\beta_{C_1} \\ \beta_{C_3} & -\beta_{C_2} & \beta_{C_1} & -\beta_{C_0} \end{bmatrix} \begin{Bmatrix} \beta_{D_0} \\ \beta_{D_1} \\ \beta_{D_2} \\ \beta_{D_3} \end{Bmatrix} \tag{3.37}$$

The relative EP set $\boldsymbol{\Delta\beta}$, characterizes the relative direction cosine matrix $\mathbf{C}_C\mathbf{C}_D^T$. That is, $\mathbf{C}_C\mathbf{C}_D^T = \mathbf{C}_{rel} \equiv \mathbf{C}_{rel}(\boldsymbol{\Delta\beta})$. From Eq. (3.31), the relative position on the unit sphere is thus given by

$$\begin{Bmatrix} \bar{x} \\ \bar{y} \\ \bar{z} \end{Bmatrix} = \begin{Bmatrix} C_{rel_{11}} - 1 \\ C_{rel_{21}} \\ C_{rel_{31}} \end{Bmatrix} = \begin{Bmatrix} -2\left(\Delta\beta_2^2 + \Delta\beta_3^2\right) \\ 2\left(\Delta\beta_1\Delta\beta_2 - \Delta\beta_0\Delta\beta_3\right) \\ 2\left(\Delta\beta_1\Delta\beta_3 + \Delta\beta_0\Delta\beta_2\right) \end{Bmatrix} \tag{3.38}$$

The relative Euler parameters can be explicitly obtained from the angular differences, as shown below:

$$\Delta\beta_0 = \cos\frac{i_c}{2}\cos\frac{i_D}{2}\cos\left(\frac{\Delta\theta + \Delta\Omega}{2}\right) + \sin\frac{i_C}{2}\sin\frac{i_D}{2}\cos\left(\frac{\Delta\theta - \Delta\Omega}{2}\right) \tag{3.39a}$$

$$\begin{aligned}\Delta\beta_1 = {} & \sin\frac{i_c}{2}\cos\frac{i_D}{2}\cos\left(\frac{\Delta\theta + \Delta\Omega}{2} + \theta_C\right) \\ & - \cos\frac{i_C}{2}\sin\frac{i_D}{2}\cos\left(\frac{\Delta\theta - \Delta\Omega}{2} + \theta_C\right)\end{aligned} \tag{3.39b}$$

$$\begin{aligned}
\Delta\beta_2 &= -\sin\frac{i_c}{2}\cos\frac{i_D}{2}\sin\left(\frac{\Delta\theta+\Delta\Omega}{2}+\theta_C\right) \\
&\quad +\cos\frac{i_C}{2}\sin\frac{i_D}{2}\sin\left(\frac{\Delta\theta-\Delta\Omega}{2}+\theta_C\right) \qquad (3.39c)\\
\Delta\beta_3 &= -\cos\frac{i_c}{2}\cos\frac{i_D}{2}\sin\left(\frac{\Delta\theta+\Delta\Omega}{2}\right) \\
&\quad -\sin\frac{i_C}{2}\sin\frac{i_D}{2}\sin\left(\frac{\Delta\theta-\Delta\Omega}{2}\right) \qquad (3.39d)
\end{aligned}$$

The kinematic relationship governing the propagation of the Chief's LVLH frame with respect to that of the Deputy, is given by

$$\begin{Bmatrix} \Delta\dot{\beta}_0 \\ \Delta\dot{\beta}_1 \\ \Delta\dot{\beta}_2 \\ \Delta\dot{\beta}_3 \end{Bmatrix} = \frac{1}{2}\begin{bmatrix} 0 & -\Delta\omega_1 & -\Delta\omega_2 & -\Delta\omega_3 \\ \Delta\omega_1 & 0 & \Delta\omega_3 & -\Delta\omega_2 \\ \Delta\omega_2 & -\Delta\omega_3 & 0 & \Delta\omega_1 \\ \Delta\omega_3 & \Delta\omega_2 & -\Delta\omega_1 & 0 \end{bmatrix}\begin{Bmatrix} \Delta\beta_0 \\ \Delta\beta_1 \\ \Delta\beta_2 \\ \Delta\beta_3 \end{Bmatrix} \qquad (3.40)$$

where $\boldsymbol{\Delta\omega}$ is the angular velocity vector of the Chief's LVLH frame with respect to that of the Deputy. To complete the kinematic description of Eqs. (3.40), equations for $\boldsymbol{\Delta\omega}$ have to be specified. Equation (2.5b) gives the angular velocity vector of the LVLH frame expressed in LVLH coordinates. The rate of change of i in Eq. (2.5b) can be set to zero for propagating the relative Euler parameters for a mean element description. The relative angular velocity required in Eq. (3.40) is given by

$$\boldsymbol{\Delta}\omega = \omega_{C_{LVLH}} - \mathbf{C}_C\mathbf{C}_D^T\omega_{D_{LVLH}} \qquad (3.41)$$

Either the Euler angle description, with the angles propagated using the mean rates, or the Euler parameter description with "mean" $\boldsymbol{\Delta}\omega$, can be used to find the relative position on the unit sphere. To find the true relative position, r and θ have to be determined. For low eccentricities, it is sufficient to expand Eqs. (2.3c) and (2.3a) to

the second order in eccentricity to obtain results with reasonable accuracy.

$$r \approx a\left[1 - e\cos M - 0.5e^2(\cos 2M - 1)\right] \tag{3.42a}$$

$$\theta \approx \omega + M + 2e\sin M + 1.25e^2 \sin 2M \tag{3.42b}$$

For the computation of the relative velocity, the angular rates are required. These are obtained from Eq. (2.15). Additionally, the following expressions are also useful:

$$\dot{r} = a\left(e\sin M + e^2 \sin M\right)\dot{M} \tag{3.43a}$$

$$\dot{\theta} = \dot{\omega} + \left(1 + 2e\cos M + 2.5e^2\cos 2M\right)\dot{M} \tag{3.43b}$$

3.6 Numerical Comparison of Different Models

Consider a Chief satellite orbit with the following elements:

$$\begin{aligned} a_C &= 7100\text{km} \\ e_C &= 0.005 \\ i_C &= 70^\circ \\ \Omega_{C_0} &= \omega_{C_0} = M_{C_0} = 0^\circ \end{aligned}$$

Two cases are considered. The first case is a relative orbit of radius $\rho = 1$km and phase angle $\alpha_0 = 0^\circ$. The second case has $\rho = 1$km and $\alpha_0 = 90^\circ$. Table 3.3 shows the orbit elements of the Chief and orbital element differences for both cases, in the presence of J_2.

Figures 3.3a and 3.3b show the relative orbits projected on the θ-h plane, for $\alpha_0 = 0^\circ$ and $\alpha_0 = 90^\circ$, respectively. Figures 3.4a, 3.5a, and 3.6a show the errors in the radial, tangential and orbit normal directions for the $\alpha_0 = 0^\circ$ case. The results from the unit

Table 3.3 Mean Elemental Differences, $\rho = 1\text{km}$, without the J_2 Perturbation

$\mathbf{e}_C$		$\rho = 1\text{km}, \alpha_0 = 0^\circ$ $\delta\mathbf{e}$	$\rho = 1\text{km}, \alpha_0 = 90^\circ$ $\delta\mathbf{e}$
a	7100km	-1.965×10^{-3}km	5.011×10^{-6}km
e	0.005	0.000	-7.0423×10^{-5}
i	1.22173rad	1.408×10^{-4}rad	0.000
Ω_0	0	0.000	-1.499×10^{-4}rad
ω_0	0	-1.408×10^{-2}rad	5.126×10^{-5}rad
M_0	0	1.408×10^{-2}rad	0.000

sphere model using mean elements are compared with the integration of the truth model. The errors are of the order of a few meters, for the relative orbit radius of 1km. Figures 3.4b, 3.5b and 3.6b show the errors from the unit sphere model corresponding to the $\alpha_0 = 90^\circ$ case. The errors in this case are lower than those in the $\alpha_0 = 0^\circ$ case. The out-of-plane drift caused by J_2, given by Eq. (3.30), is minimum for $\alpha_0 = 90^\circ$. The errors will be considerably less if osculating elements are used.

Next, a 20km relative orbit is considered, for the same Chief's orbit. The elemental differences for both the $\alpha_0 = 0^\circ$ and $\alpha_0 = 90^\circ$ are given in Table 3.4.

The geometric approach in Eqs. (3.17) gives errors very similar to the unit sphere method for low relative radii. Since the expressions for the relative position are obtained from a linearization of the direction cosine matrix of the Deputy with respect to the Chief, it is expected that the errors will be more significant for large relative

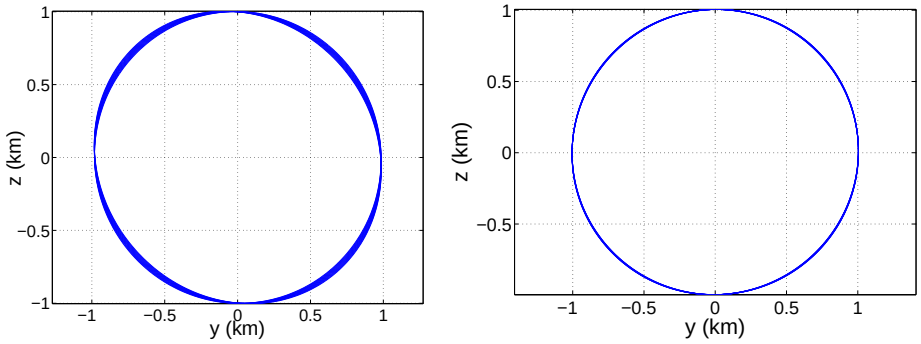

(a) $\alpha_0 = 0°$ (b) $\alpha_0 = 90°$

Fig. 3.3 Relative Orbits Projected on θ-h Plane

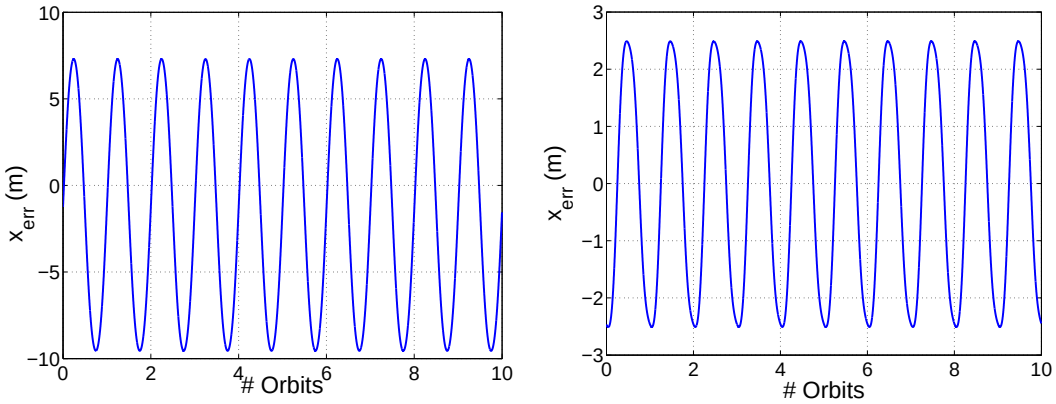

(a) $\rho = 1\text{km}, \alpha_0 = 0°$ (b) $\rho = 1\text{km}, \alpha_0 = 90°$

Fig. 3.4 Error in LVLH x Between Unit Sphere Model with Mean Elements and Truth Model

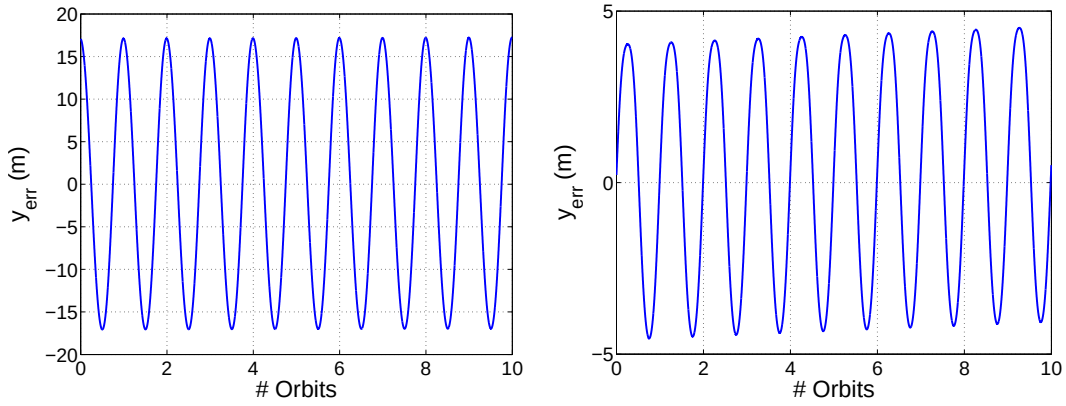

(a) $\rho = 1\text{km}, \alpha_0 = 0°$ (b) $\rho = 1\text{km}, \alpha_0 = 90°$

Fig. 3.5 Error in LVLH y Between Unit Sphere Model with Mean Elements and Truth Model

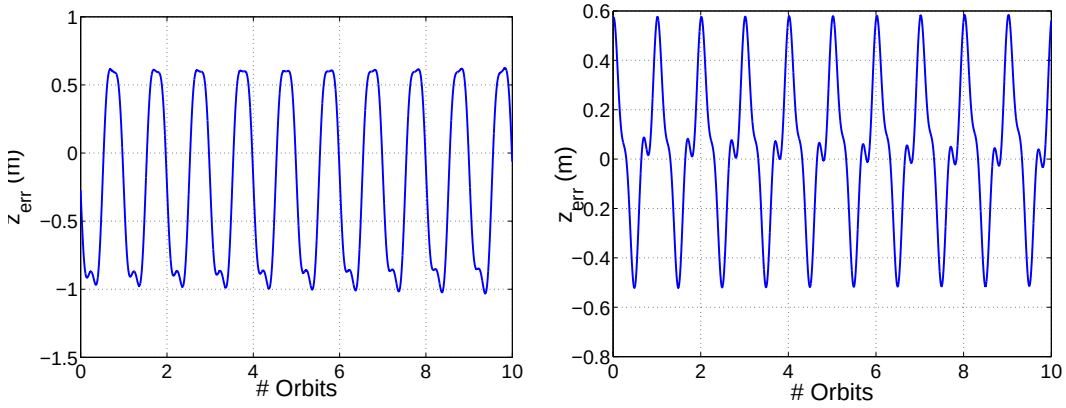

(a) $\rho = 1\text{km}, \alpha_0 = 0°$ (b) $\rho = 1\text{km}, \alpha_0 = 90°$

Fig. 3.6 Error in LVLH z Between Unit Sphere Model with Mean Elements and Truth Model

Table 3.4 Mean Elemental Differences, $\rho = 20\text{km}$ with the J_2 Perturbation

$\mathbf{e}_C$		$\rho = 20\text{km}, \alpha_0 = 0°$ $\delta\mathbf{e}$	$\rho = 20\text{km}, \alpha_0 = 90°$ $\delta\mathbf{e}$
a	7100km	-3.931×10^{-2}km	1.002×10^{-4}km
e	0.005	0.000	-1.423×10^{-3}
i	1.22173rad	2.817×10^{-3}rad	0.000
Ω_0	0	0.000	-2.998 $\times 10^{-3}$rad
ω_0	0	-0.282rad	1.025×10^{-3}rad
M_0	0	0.282rad	0.000

radii. The unit sphere approach does not require linearization, therefore it is expected to be more accurate than the geometric method for such cases. Figures 3.7-3.9 show the errors from the unit sphere and geometric methods for both cases of α_0. The blue solid line corresponds to the unit sphere errors and the red dashed line corresponds to the linearized, geometric model. As can be seen from Fig. 3.8, the errors from the unit sphere and the linearize model are almost the same in the y direction even for the high relative radius. However, the errors in the orbit normal direction are much larger with the linearized model. The errors are also no longer of zero mean. This is also observed in the errors in the radial direction, as shown in Fig. 3.7. The unit sphere method thus shows lower errors in propagation when compared with the linearized, geometric model, as the relative radius increases.

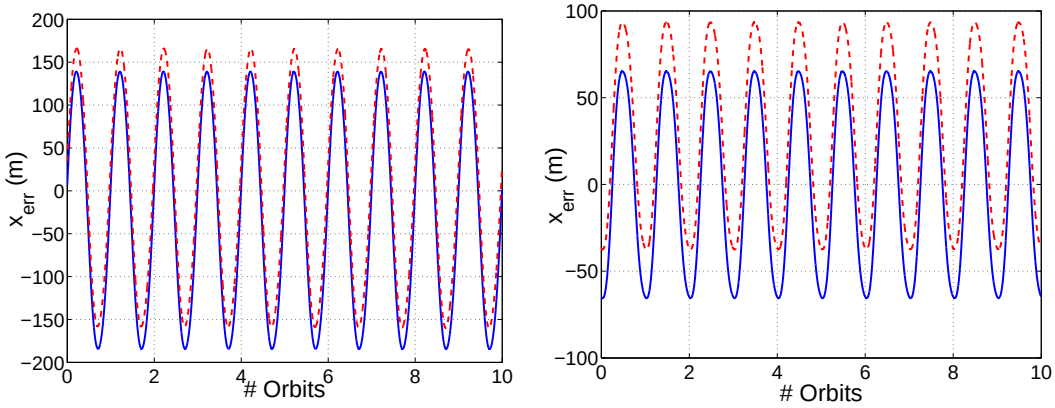

(a) $\rho = 20\text{km}, \alpha_0 = 0°$ (b) $\rho = 20\text{km}, \alpha_0 = 90°$

Fig. 3.7 Comparison of LVLH x Errors from Linearized Geometric Model and Unit Sphere Approach

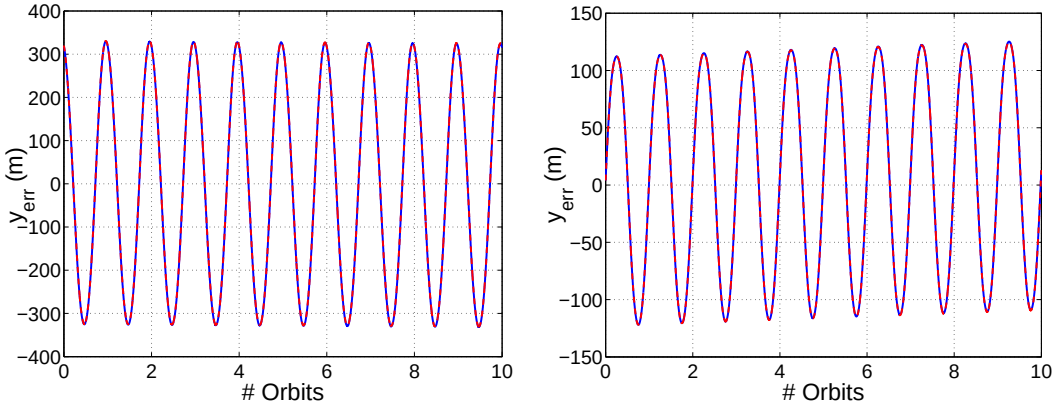

(a) $\rho = 20\text{km}, \alpha_0 = 0°$ (b) $\rho = 20\text{km}, \alpha_0 = 90°$

Fig. 3.8 Comparison of LVLH y Errors from Linearized Geometric Model and Unit Sphere Approach

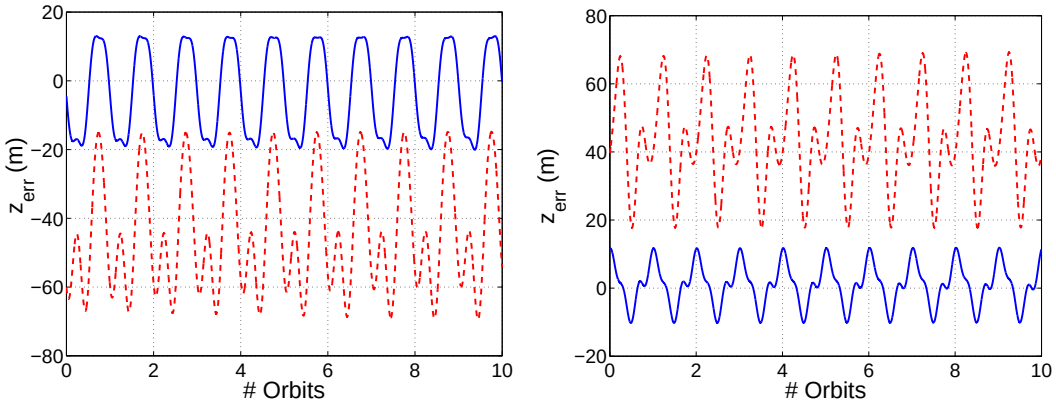

(a) $\rho = 20\text{km}, \alpha_0 = 0°$ (b) $\rho = 20\text{km}, \alpha_0 = 90°$

Fig. 3.9 Comparison of LVLH z Errors from Geometric Method and Unit Sphere Approach

3.7 Summary

Various system models that are used for relative motion analysis, both in the absence and presence of the J_2 perturbation have been studied. The deviation of the HCW equations in the presence of nonlinearities, eccentricity and J_2 perturbations have been explained, and some of the methods used to obtain bounded relative motion have been introduced. The unit sphere model, which has been shown to be a kinematically exact model with osculating elements, can be used to model relative motion by the use of mean elements; in which case the errors when compared to the truth model are very low. This has been demonstrated for a variety of cases. The unit sphere model is also compared with the geometric method, and shows lower errors for relative orbits of high radii.

CHAPTER IV

MODELING RELATIVE MOTION FOR HIGH-ECCENTRICITY REFERENCE ORBITS

4.1 Introduction

The unit sphere approach outlined in the previous chapter has been shown to work very well for reference orbits of low eccentricity. Certain missions require reference orbits to have very high eccentricities. This chapter studies the problems associated with the modeling of relative motion, in particular, the problems with series expansion solutions to Kepler's equation, Eq. (2.1).

4.2 Failure of Series Expansions for High Eccentricities

The relation between the true anomaly f and mean anomaly E is straightforward:

$$\tan\frac{f}{2} = \left(\frac{1+e}{1-e}\right)\tan\frac{E}{2} \tag{4.1}$$

The mean anomaly M can be obtained from E from Kepler's equation directly.

Figure 4.1a is a graphical representation of the relation between E and M. Figure 4.1b shows the errors between an analytical calculation of E from M, through a second-order expansion in eccentricity, and E calculated iteratively by a Newton-Raphson method with a tolerance of 10^{-12}. The second-order expansion for E is sufficient for very low eccentricities; for $e = 0.05$, the errors are of the order of 10^{-5}. However, for $e = 0.2$, the order is two magnitudes higher. For $e = 0.8$, the errors are very high.

It is possible to improve the accuracy of the series solution by including higher order

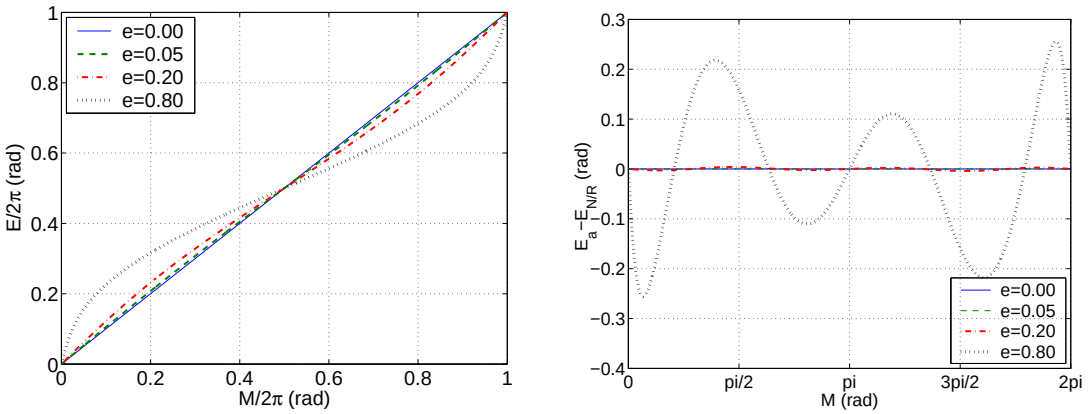

(a) Relation Between E and M

(b) Errors From Eccentricity Expansions

Fig. 4.1 Errors from Analytical Series Expansion in Eccentricity

terms. Battin,[3] for example, provides expansions up to the sixth order of eccentricity. Sabol et al.[14] use a Fourier-Bessel expansion that can be taken to higher orders. For cases where $e < 0.1$, the expansion provided is easily realizable and used readily. However, for cases with larger eccentricities, the expansion in Ref. 14 also shows errors, and additional terms need to be generated in the series.

The problem herein is two-fold:

1. The number of terms required in the series for E, to obtain values within the desired tolerance, is not known *a priori*.

2. It will be shown that beyond a certain eccentricity, the series solutions in Eqs. (2.3) do not converge for some values of the mean anomaly.

Reference 3 tests the convergence of E in a circular region in the complex plane around the point defined by M. The maximum value of eccentricity for which the expansion converges is given by the root of $\cosh\rho = \rho\sinh\rho$. A numerical solution of

this equation yields:

$$e < 0.6627434194... \tag{4.2}$$

for convergence of the series.

4.3 Modified Method for Orbits of High-Eccentricity

For the cases where the eccentricity is low, the usual method is to step through time, obtain the mean angles Ω, ω and M from the secular rates, and substitute these in Eqs. (3.36). M and $\dot{M}$ are also used in Eqs. (3.42) and (3.43) to find r and θ. However, for high eccentricities, it has been shown that Eqs. (3.42) and (3.43) are no longer reliable and for some cases, can no longer be used. Since $\theta = \omega + f$, and $r = a(1 - e\cos E)$, Eq. (2.1) has to be solved iteratively to obtain E from M, and f needs to be obtained from M. It should be noted that this process needs to be performed twice - once each, for the Chief and Deputy.

In order to avoid solving Kepler's equation iteratively for each satellite, the true anomaly of the Chief f_C is used as the independent variable. Since M_C can be obtained directly from f_C, the time corresponding to the mean anomaly can also be obtained by

$$t = t_0 + \frac{M(t) - M(t_0)}{\dot{M}} \tag{4.3}$$

With the availability of the current time, Eqs. (2.15) can be used to find Ω_C and ω_C (for the Chief), Ω_D, ω_D and M_D (for the Deputy). Kepler's equation will have to be solved iteratively to obtain f_D from M_D.

The use of the true anomaly as the independent variable instead of time has been discussed in Ref. 13. The relative motion is described using elemental differences. Mean rates are used to find the elements at any time. To transform the equations such that true anomaly is the independent variable, the following identity is used:

$$\frac{dt}{df} = \frac{r^2}{h} = \frac{\eta^3}{n(1+e\cos f)^2}$$

However, the equations of relative motion are derived from a linearization similar to the geometric model described in the previous chapter.

The advantage of stepping through true anomaly of the Chief, over stepping through time, is immediately apparent when the region near the perigee of highly eccentric orbits is considered. Quantities near the perigee change very fast, and the time step required during integration in this region is much smaller than that near the apogee. This is automatically taken care of by stepping through f_C. Additionally, it will be shown that if the formation is established near the perigee ($M_{C_0} = 0°$), small errors in initial conditions can cause significant errors between the analytical expression and the solution of the truth model, when compared to an orbit established near the apogee ($M_{C_0} = 180°$).

4.4 Breakdown of PCO Conditions for High-Eccentricity Reference Orbits

The initial conditions that have been presented in Table 3.2 ensure a relative orbit of radius ρ and phase angle α_0, for reference orbits of low eccentricities. For high-eccentricity reference orbits, the first order expansion in Eqs. (3.21) and (3.22) are no longer sufficient to ensure accuracy. Even though the period-matching condition in

Eq. (3.28) still ensures boundedness of the relative orbit, as eccentricity increases, the projected orbit no longer remains circular. A characterization of the relative orbit for highly eccentric reference orbits is not available at this time. Hence, for convenience, in this thesis, the relative orbit continues to be characterized by its radius ρ and phase angle α_0.

4.5 Numerical Results

4.5.1 Comparison of the Results from the Modified Unit Sphere Approach with the True Solution

In the previous chapter, and Ref. 15, the accuracy of the unit sphere model has already been demonstrated for the cases where eccentricity is low. Here, a high-eccentricity case is considered for a reference orbit that has an apogee of $12R_e$ and perigee distance of $1.2R_e$. Inclination is selected to be 50°. The initial conditions for the Chief are

$$\begin{aligned} a_C &= 42095.70\text{km} \\ e_C &= 0.8182 \\ i_C &= 50^\circ \\ \Omega_{C_0} &= \omega_{C_0} = 0^\circ \\ M_{C_0} &= 180^\circ \end{aligned}$$

The initial M_C signifies the establishment of the orbit at apogee. The relative orbit selected is one of radius 20km. The mean elemental differences that yield the orbital elements of the Deputy, given the elements of the Chief, are shown in Table 4.1

Figures 4.2a and 4.2b show the errors between the analytical solutions and the corre-

Table 4.1 Mean Elemental Differences with Highly Eccentric Chief's Orbit, $\rho = 20\text{km}$

$\mathbf{e}_C$		$\rho = 20\text{km}, \alpha_0 = 0°$ $\delta\mathbf{e}$	$\rho = 20\text{km}, \alpha_0 = 90°$ $\delta\mathbf{e}$
a	42095.7km	-1.282×10^{-2}km	2.457×10^{-3}km
e	0.8182	0.000	1.512×10^{-4}
i	0.87266rad	4.751×10^{-4}rad	0.000
Ω_0	0	0.000	-6.202×10^{-4}rad
ω_0	0	-2.903×10^{-4}rad	3.987×10^{-4}rad
M_0	3.14159rad	2.903×10^{-4}rad	0.000

sponding results of integration of the 12th order ECI differential equations, for $\alpha_0 = 0°$ and $\alpha_0 = 90°$, respectively, without the J_2 perturbation. These figures establish the accuracy of the method in the absence of J_2. As can be seen, the errors, though very small, show sudden jumps near perigee. These appear due to errors in numerical integration in the region of the perigee. In the absence of J_2, the sixth-order ECI model for a single satellite is given by

$$\ddot{\mathbf{r}} = -\frac{\mu}{r^3}\mathbf{r} \tag{4.4}$$

By changing the independent variable to the true anomaly of the satellite, f, the equations of motion may be regularized to yield

$$\mathbf{r}'' = \frac{1}{1 + e\cos f}\left\{-\mathbf{r} + 2e\sin f\mathbf{r}'\right\} \tag{4.5}$$

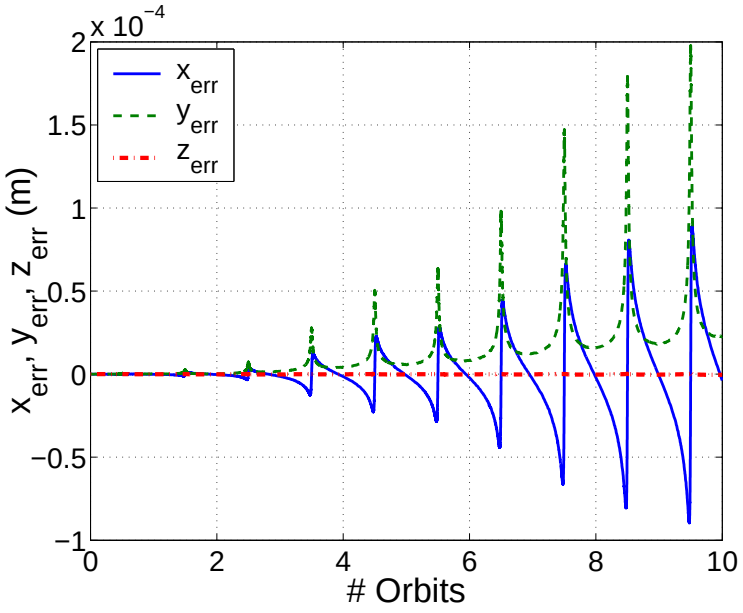

(a) $\rho = 20\text{km}, \alpha_0 = 0°$

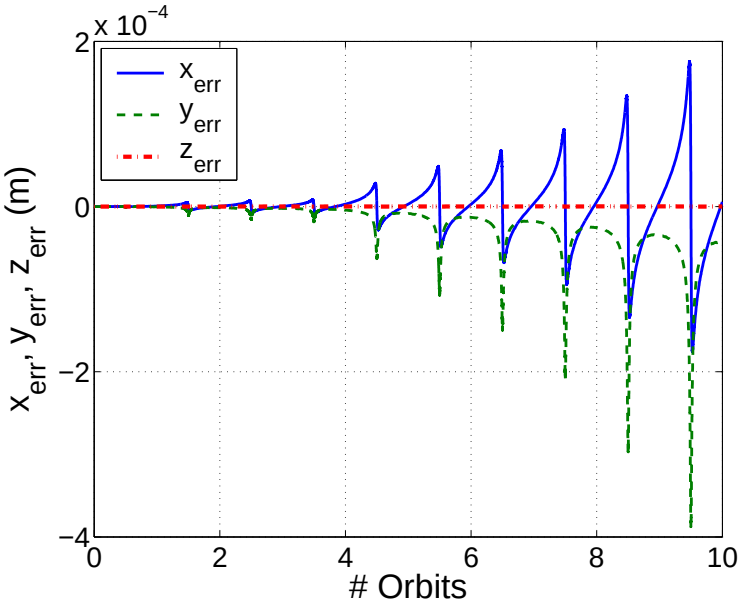

(b) $\rho = 20\text{km}, \alpha_0 = 90°$

Fig. 4.2 Errors in Relative Position for High Eccentricity Chief's Orbit, without J_2

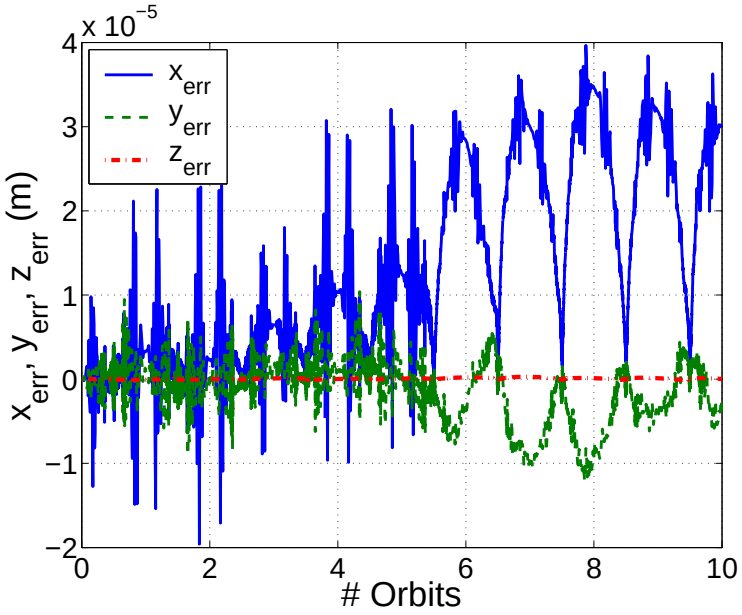

(a) $\rho = 20\text{km}, \alpha_0 = 0°$

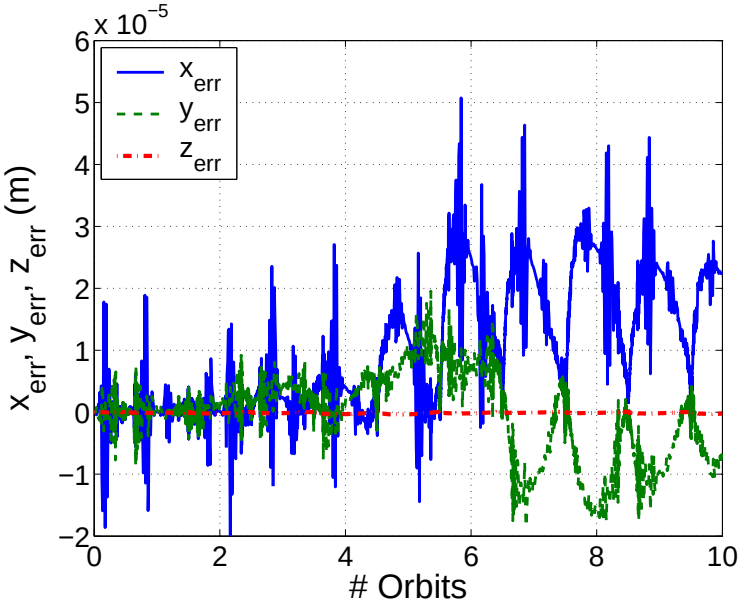

(b) $\rho = 20\text{km}, \alpha_0 = 90°$

Fig. 4.3 Errors in Relative Position for High Eccentricity Chief's Orbit, without J_2, Using Regularized ECI Model

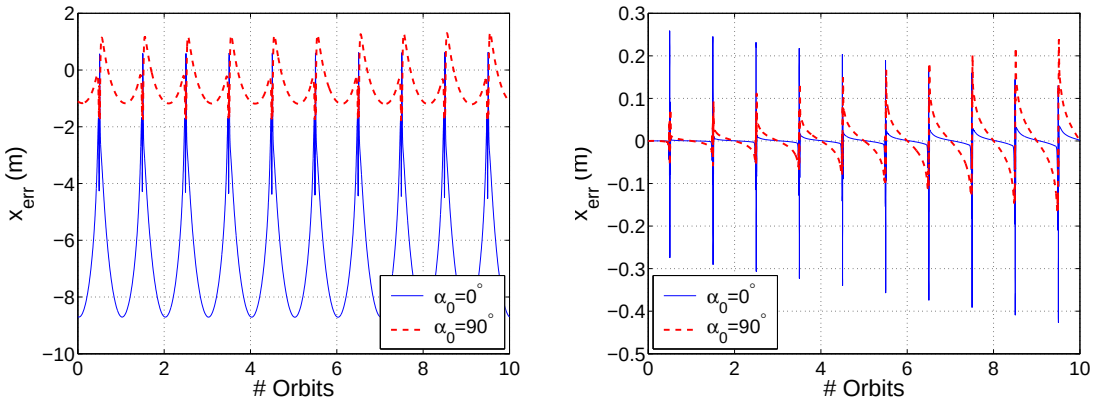

(a) Mean Elements (b) Osculating Elements

Fig. 4.4 Errors in LVLH x Using Mean and Osculating Elements for the Very High Eccentricity Case; $\rho = 20\text{km}, \alpha_0 = \{0° \quad 90°\}$

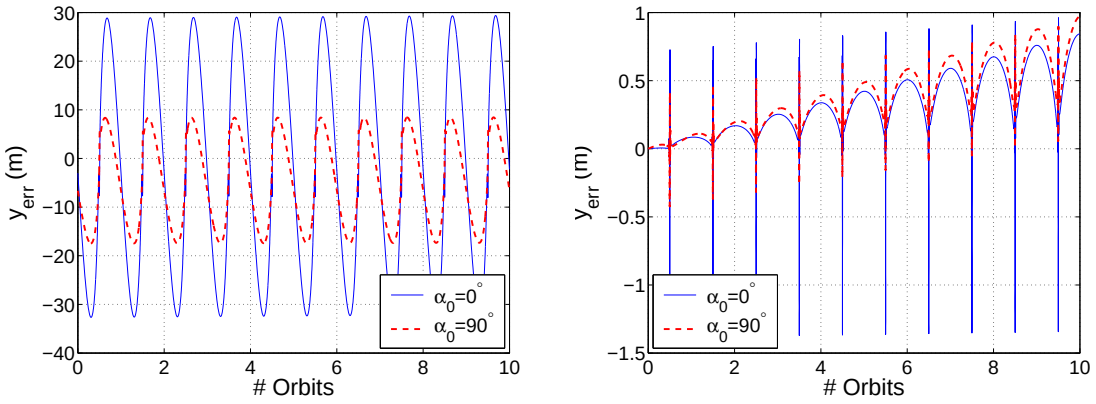

(a) Mean Elements (b) Osculating Elements

Fig. 4.5 Errors in LVLH y Using Mean and Osculating Elements for the Very High Eccentricity Case; $\rho = 20\text{km}, \alpha_0 = \{0° \quad 90°\}$

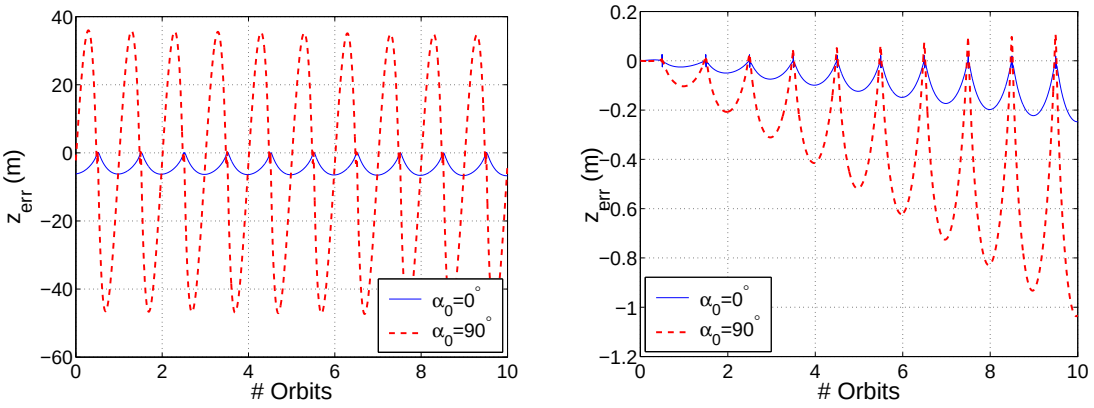

(a) Mean Elements (b) Osculating Elements

Fig. 4.6 Errors in LVLH z Using Mean and Osculating Elements for the Very High Eccentricity Case; $\rho = 20\text{km}, \alpha_0 = \{0° \quad 90°\}$

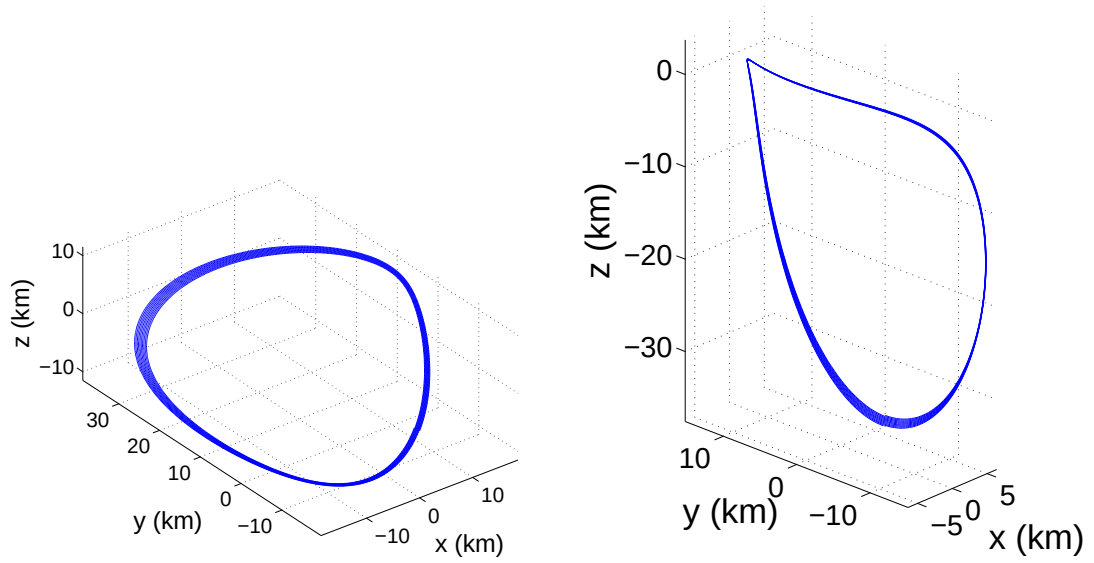

(a) $\alpha_0 = 0°$ (b) $\alpha_0 = 90°$

Fig. 4.7 Relative Orbits for the Very High Eccentricity Case; $\rho = 20\text{km}, \alpha_0 = \{0° \quad 90°\}$

The use of Eq. (4.5) instead of Eq. (4.4) as the truth model for the high-eccentricity case, reduces relative position errors in the x and y by almost one order of magnitude, but causes little improvement in the z errors. This is seen in Figs. 4.3a and 4.3b. The jumps in the errors as the satellites cross their respective perigees, are also not seen. However, since the contribution of error from numerical integration is very low when compared with the error due to the use of mean elements, this thesis uses the ECI model with time as the independent variable as the truth model, even for the high eccentricity cases.

Figures 4.4, 4.5, and 4.6, show the x, y, and z errors respectively, in the presence of the J_2 perturbation. The figures on the left indicate the results obtained from the use of mean elements, for both cases of α_0. The figures on the right use osculating elements. These results show that the unit sphere method in conjunction with osculating elements is highly accurate. The errors obtained using the mean elements remain bounded over the period of 10 orbits. Figures 4.7a and 4.7b show the relative orbits for $\alpha_0 = 0^\circ$ and $\alpha_0 = 90^\circ$, respectively, using the truth model.

4.5.2 Errors for Orbit Establishment at Apogee and Perigee

To study the errors associated with orbit establishment at the apogee and perigee, a large relative orbit with $\rho = 100$km is considered, with the elements of the Chief being

$$\begin{aligned} a_C &= 12000\text{km} \\ e_C &= 0.4 \\ i_C &= 50^\circ \\ \Omega_{C_0} &= \omega_{C_0} = 0^\circ \\ M_{C_0} &= 0^\circ, 180^\circ \end{aligned}$$

The set of Figs. 4.8-4.13 demonstrate the reduction of errors if the orbit is established at apogee instead of perigee. Figures 4.8, 4.10, 4.12 show the error in x, y and z if the orbit is established at perigee, for both cases of α_0 as indicated by the solid and dashed lines. The figures on the left use mean elements in the unit sphere approach, and the figures on the right use Brouwer's theory to obtain the osculating elements from the mean elements. These are compared with the errors if the orbit is established at apogee, given by Figs. 4.9, 4.11 and 4.13.

Comparing Figs. 4.8 with 4.9, the error in x using mean elements for $\alpha_0 = 90^\circ$ shows no secular growth if the orbit is established at apogee, and the magnitude of the error is less. No perceptible difference is seen for $\alpha_0 = 0^\circ$. In this case, an initial error is expressed in the form of a bias over ten orbits. The use of osculating elements removes the bias in x errors (Fig. 4.8b) but does not reduce the magnitude of errors. If however the orbit is established at apogee, Fig. 4.9b shows the errors are less than 1m, which is very accurate, given that the orbit has a relative radius of 1km.

The errors in y are presented in Figs. 4.10 and 4.11. Established at perigee, y shows a growth in the amplitude of the errors. By using osculating elements, the secular nature of the error remains unchanged (Fig. 4.10b). If the orbit is established at the apogee, the errors in y are bounded and show no growth (Fig. 4.11a). The use of osculating elements with apogee establishment shows errors that are of the order of a few meters.

Finally, the errors in z are presented in Figs. 4.12 and 4.13. The magnitude of the errors is reduced by approximately half if the orbit is established at perigee, when using mean elements (Figs. 4.12a and 4.13a). The use of osculating elements, with orbit establishment at perigee, reduces the order of errors to that of meters, but the errors show growth. The errors are reduced further by the use of osculating elements if the orbit is established at apogee (4.13b). Thus establishing the orbit at apogee shows lower errors in simulation for high-eccentricity reference orbits, compared to establishment at perigee.

4.6 Summary

The failure of eccentricity expansions, for reference orbits of very high eccentricity has been shown. When time is used as the independent variable and eccentricity expansions are not used, it becomes necessary to solve Kepler's equation to obtain the true anomaly from the mean anomaly, for both the Chief and the Deputy, at every time instant to obtain the relative motion. It has been shown that by using the true anomaly of the Chief as the independent variable, Kepler's equation needs to be solved only once. Formations with high-eccentricity reference orbits, as well as formation

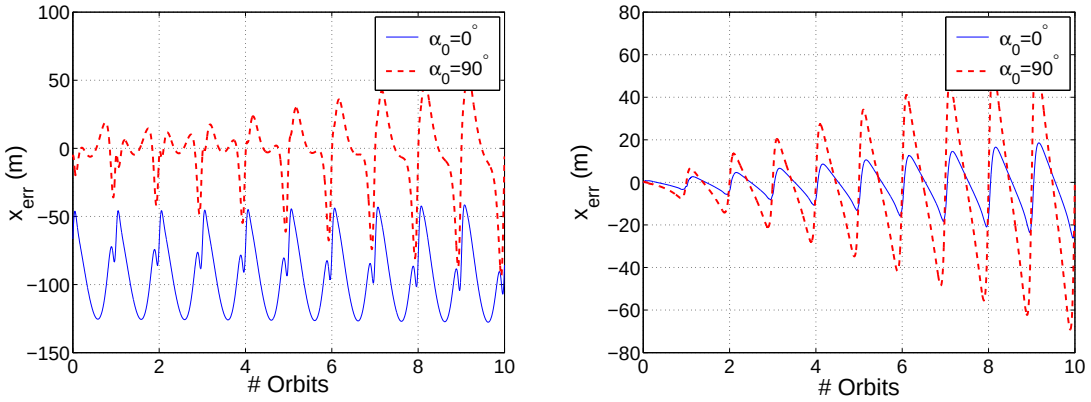

(a) Mean Elements (b) Osculating Elements

Fig. 4.8 Errors in LVLH x Using Mean and Osculating Elements with Orbit Established at Perigee; $\rho = 100\text{km}, \alpha_0 = \{0° \quad 90°\}$

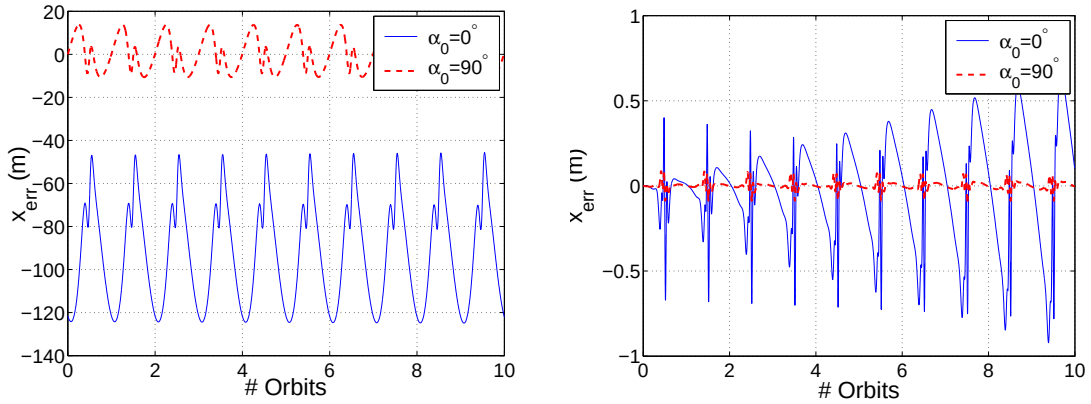

(a) Mean Elements (b) Osculating Elements

Fig. 4.9 Errors in LVLH x Using Mean and Osculating Elements with Orbit Established at Apogee; $\rho = 100\text{km}, \alpha_0 = \{0° \quad 90°\}$

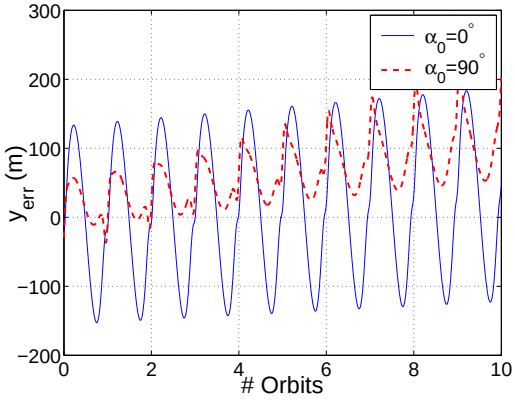

(a) Mean Elements

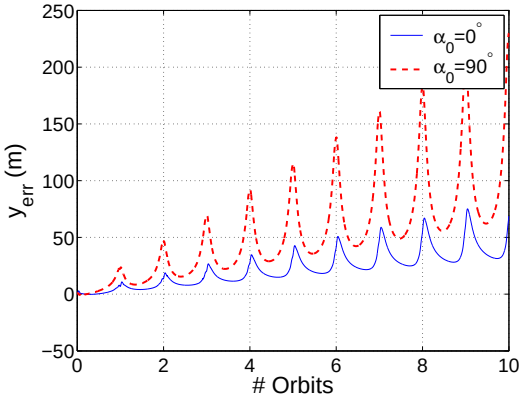

(b) Osculating Elements

Fig. 4.10 Errors in LVLH y Using Mean and Osculating Elements with Orbit Established at Perigee; $\rho = 100\text{km}, \alpha_0 = \{0° \quad 90°\}$

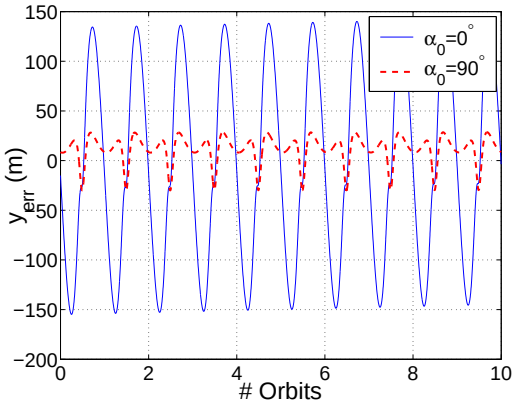

(a) Mean Elements

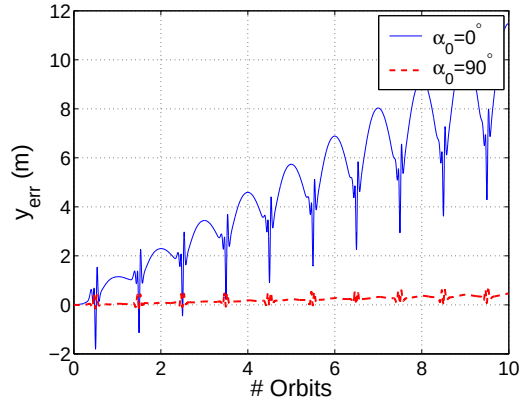

(b) Osculating Elements

Fig. 4.11 Errors in LVLH y Using Mean and Osculating Elements with Orbit Established at Apogee; $\rho = 100\text{km}, \alpha_0 = \{0° \quad 90°\}$

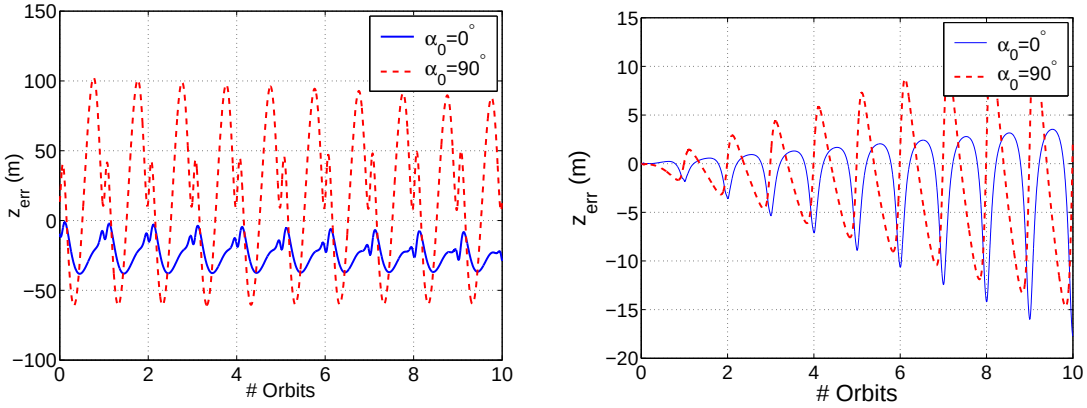

(a) Mean Elements (b) Osculating Elements

Fig. 4.12 Errors in LVLH z Using Mean and Osculating Elements with Orbit Established at Perigee; $\rho = 100\text{km}, \alpha_0 = \{0° \quad 90°\}$

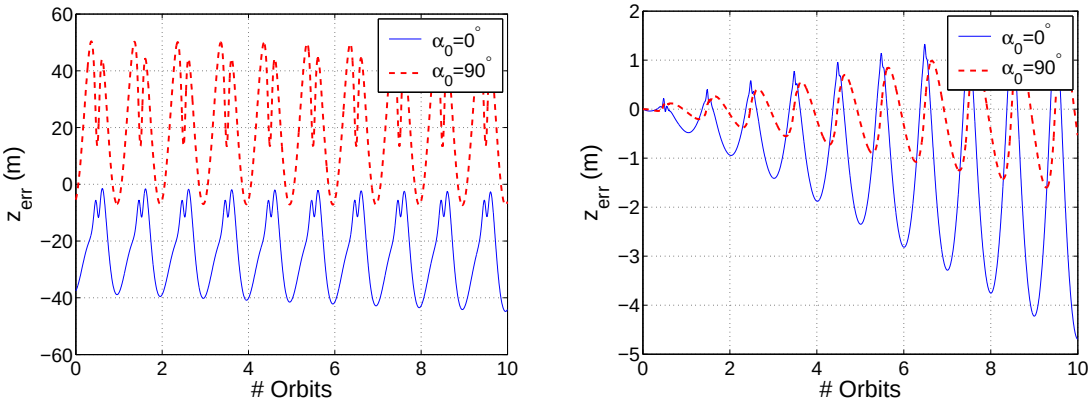

(a) Mean Elements (b) Osculating Elements

Fig. 4.13 Errors in LVLH z Using Mean and Osculating Elements with Orbit Established at Apogee; $\rho = 100\text{km}, \alpha_0 = \{0° \quad 90°\}$

of large relative radii, can thus be accurately represented by the unit sphere model. Furthermore, it has been shown that establishing the formation when the Chief is at its apogee shows less error in simulation, if the eccentricity of the reference orbit is high. This method will be used in the next chapter for reconfiguration of formations involving highly eccentric reference orbits.

CHAPTER V

FORMATION RECONFIGURATION THROUGH IMPULSIVE AND CONTINUOUS CONTROL

5.1 Introduction

Different systems have been explored to model relative motion in the previous chapters. However, not all are amenable for control design. From Eq. (2.22), it can be seen that the control in Kechichian's equations appears at various levels, including $\dot{\Omega}$ and $\ddot{\Omega}$. These equations require the time derivative of control. While the unit sphere model[15] provides a very good representation for relative motion, in the presence of control, osculating elements have to be used, which increases the complexity of the equations. The controls appear in their simplest form in the ECI model and Gauss' equations. Reference 24 discusses the effect of applying impulsive control on the orbital elements, perturbed by the J_2 effect. Control laws for formation establishment and maintenance are also presented in in Ref. 16. Reference 25 presents Lyapunov, LQR, and period-matching control schemes that generate circular projected orbits.

The problem of relative orbit reconfiguration is discussed in this chapter. Reconfiguration can be performed by using either impulsive control through velocity increments or by a continuous control that globally and asymptotically stabilizes the system with the desired trajectory as a reference. Additionally, a kinematic approach to the reconfiguration will also be discussed.

5.2 Impulsive Control

In this section optimal two-impulse maneuvers are considered for reconfiguring a formation characterized by relative radius ρ_i and initial phase angle α_{0_i}, to one characterized by their respective final values, ρ_f and α_{0_f}. In Vaddi,[26] sub-optimal velocity impulses were obtained to establish and reconfigure a formation. Reference 26 obtains these sub-optimal solutions in the absence of the J_2 perturbation. Further, a priori assumptions are made regarding the spacing of the impulses. In this chapter, optimal two-impulse maneuvers for reconfiguration of large formations, in the presence of J_2 and high eccentricity of the Chief, are obtained using numerical optimization.

5.2.1 Gauss' Equations with Velocity Impulses

It has been shown through Eqs. (2.20) that the control accelerations are related to the corresponding changes in orbital elements through the $\mathbf{G}$ matrix. If the controls are applied in the form of velocity impulses then $\mathbf{u}dt \approx \Delta\mathbf{v} = \{v_r \quad v_\theta \quad v_h\}^T$. The infinitesimal change in the values of the orbital elements due to the application of an impulse is then approximately also the total change in their respective values; that is, $\dot{\mathbf{e}}dt = d\mathbf{e} \approx \Delta\mathbf{e}$. In such cases, the changes in the orbital elements are given by the following relationship:

$$\Delta\mathbf{e} \;=\; \mathbf{G}(\mathbf{e})\Delta\mathbf{v}$$

5.2.2 Formulation of an Optimal Control Problem

Since there are three components of the velocity impulse and $\mathbf{G} \equiv \mathbf{G}(f)$, at least two impulses are required to obtain the 6 desired orbital element changes. Considering the general case of N impulses, the number of variables to be optimized are $3N+N = 4N$, which correspond to the velocity impulse components and optimal positions for

impulse application. A terminal coast phase is also allowed; thus bringing the total number of variables to optimize to $4N + 1$. Keeping in mind the problems associated with formations where the Chief's orbit has high eccentricity, the true anomaly of the Chief is used as the independent variable, instead of time. The cost function used is the sum of the magnitudes of the velocity increments, given by

$$J = \sum_{i=1}^{N} W_i ||\Delta \mathbf{v}_i|| \tag{5.1}$$

where W_i is the positive weight associated with the ith impulse. In general, $W_i = 1$.

5.2.3 Algorithm

Initial guesses are made for the components of the the N velocity impulses and N true anomalies at which they are applied, as well as the true anomaly where the coast phase ends. Initial guesses for the N true anomalies can be obtained by selecting equally-spaced values from 0 to 2π. Any non-zero value can be used as initial guesses for the velocity impulse components. The initial conditions provided are the relative orbit parameters (ρ_i, α_{0_i}). Since the initial conditions of the Chief are known, the initial conditions for the Deputy are obtained from Table 3.2. The motions of both the satellites (Chief and Deputy) are propagated using the mean element formulation with the rates given by Eq. (2.15). Steps are taken in f_C until the first true anomaly value for thrust application is reached. The elements are updated using the $\mathbf{G}$ matrix in Eq. (2.21). The process is repeated until all the N impulses are applied, and the mean rates are used for the coast phase. Let the elements of the Deputy after the last impulse be $\mathbf{e}_D(f_N)$. Since the final conditions are specified in the form of (ρ_f, α_{0_f}), the desired final values of the elements of the Deputy are

$$\mathbf{e}_{D_f} = \mathbf{e}_C(f_N) + \delta\mathbf{e}(\rho_f, \alpha_{0_f})$$

Thus, six nonlinear constraints to the Optimal Control Problem (OCP) are obtained as follows:

$$|\mathbf{e}_D(f_N) - \mathbf{e}_C(f_N) - \delta\mathbf{e}(\rho_f, \alpha_{0_f})| = \mathbf{0} \tag{5.2}$$

Equations (5.1) and (5.2) are used with the FORTRAN package NPOPT[27] to solve the OCP numerically.

Though the velocity impulses are obtained from a mean element technique, they are simulated by integrating the twelfth-order nonlinear ECI system of equations. The validity of this scheme for high eccentricity reference orbits will be investigated subsequently. The equations for inertial position $\mathbf{r}_D$ and velocity $\mathbf{v}_D$ are propagated until an impulse time t_i. At this point, the orbital elements $\mathbf{e}_D(t_i)$ are obtained from $\mathbf{r}_D(t_i)$ and $\mathbf{v}_D(t_i)$. Since these are osculating elements, they are converted to mean elements for consistency with the method used to obtain the impulses. Then, the inertial position and velocity corresponding to the mean elements are obtained, and the velocity increment $\mathbf{\Delta v}_i$ is added to the mean inertial velocity. Inertial position does not change on application of a velocity impulse. The mean position and velocity after the impulse, are converted to mean orbital elements and subsequently to osculating orbital elements. The osculating inertial position and velocity obtained from these orbital elements are used as initial conditions for the next stage of propagation, from t_i to t_{i+1}. The process is repeated for each impulse.

5.2.4 Using the Kinematic Description for the Reconfiguration Problem

The kinematic description for relative motion described in Ref. (16) provides an alternative method for studying and visualizing the reconfiguration problem. This description will be used subsequently to provide insight in the continuous-control

reconfiguration problem. The mean elements of the Chief at any time t are given by Eqs. (2.15), with a_C, e_C, and i_C held constant. The desired mean orbital elements for the Deputy at any given time are given by the relations in Table 3.2. Let the Euler parameter set $\boldsymbol{\beta}_{D_{des}}$ denote the desired orientation of the LVLH frame with respect to the ECI frame, which can be obtained from the corresponding 3-1-3 Euler angles, $\Omega_{D_{des}}$, $i_{D_{des}}$, and $\theta_{D_{des}}$ at t. Similarly the desired angular velocity in the LVLH frame, $\boldsymbol{\omega}_{D_{des_{LVLH}}}$, can be obtained from Eq. (2.5a). The current orientation of the Deputy is denoted by $\boldsymbol{\beta}_D$. Then the error Euler parameter set $\boldsymbol{\Delta\beta}$, which is also the relative Euler parameter set that characterizes the current orientation of the LVLH frame of the Deputy with respect to its desired orientation, can be obtained from an expression analogous to Eq. (3.37):

$$\begin{Bmatrix} \Delta\beta_0 \\ \Delta\beta_1 \\ \Delta\beta_2 \\ \Delta\beta_3 \end{Bmatrix} = \begin{bmatrix} \beta_{D_0} & \beta_{D_1} & \beta_{D_2} & \beta_{D_3} \\ \beta_{D_1} & -\beta_{D_0} & -\beta_{D_3} & \beta_{D_2} \\ \beta_{D_2} & \beta_{D_3} & -\beta_{D_0} & -\beta_{D_1} \\ \beta_{D_3} & -\beta_{D_2} & \beta_{D_1} & -\beta_{D_0} \end{bmatrix} \begin{Bmatrix} \beta_{D_{des_0}} \\ \beta_{D_{des_1}} \\ \beta_{D_{des_2}} \\ \beta_{D_{des_3}} \end{Bmatrix} \tag{5.3}$$

The error in angular velocity in the LVLH frame, for small angular deviations, is

$$\boldsymbol{\Delta\omega} = \boldsymbol{\omega}_{D_{LVLH}} - \boldsymbol{\omega}_{D_{des_{LVLH}}} \tag{5.4}$$

where $\boldsymbol{\omega}_{D_{LVLH}}$ is the current angular velocity vector of the Deputy. If the current and desired LVLH frames coincide, $\boldsymbol{\Delta\beta} = \{1 \quad 0 \quad 0 \quad 0\}^T$.

5.3 Lyapunov Approach for Continuous-Control Reconfiguration

In this section, a continuous control law for reconfiguration is discussed. It is assumed that the Chief is not controlled, and the Deputy has to be reconfigured to a new orbit characterized by a desired orbital element set. Schaub et al.[17] present a

Lyapunov-based control law for reconfiguration that uses mean elements. Though mean elements can be used for orbits of low eccentricity, their use in highly eccentric cases needs to be explored. Another feature in the analysis presented in Ref. 17 is the use of time-dependent feedback gains that encourage orbital element corrections to occur at particular ideal positions along the orbit. The effectiveness of a control vector on the change of a particular orbital element can be studied from Eq. (2.20). However, it was found for the high eccentricity cases considered in this thesis, using time-dependent gains had no particular advantage, if the formation is established at apogee. Analysis in Ref. 17 also does not rigorously prove the stability of the orbital element-based control law due to the nature of the control influence matrix $\mathbf{G}$ in Eq. (2.20).

The Lyapunov-based controller presented in this thesis is proven to globally and asymptotically stabilize the error dynamics. Instead of using orbital element errors, the candidate Lyapunov function presented here uses the kinematic description for satellite motion.

5.3.1 Kinematic Basis

Let the orbital elements of the Chief at any time be $\mathbf{e}_C(t)$. Then, from Table 3.2, the desired orbital elements of the Deputy at any given time are

$$\mathbf{e}_{D_{des}}(t) = \mathbf{e}_C(t) + \delta\mathbf{e}(t) \tag{5.5}$$

It should be noted that the desired orbit of the Deputy can be arbitrary. Let the desired Euler parameters corresponding to Eq. (5.5) be $\boldsymbol{\beta}_{D_{des}}$.

Let the current elements of the Deputy be $\mathbf{e}_D(t)$ and the Euler parameters corre-

sponding to the current elements be $\boldsymbol{\beta}_D$. The position and velocity of the Deputy in its LVLH frame are given by Eqs. (2.23) and (2.24). The acceleration of the Deputy in the LVLH frame is given by Eq. (2.25):

$$\mathbf{a}_D = \left\{ \begin{array}{c} \ddot{r}_D - \left(\omega_{D_h}^2 + \omega_{D_\theta}^2\right) r_D \\ \dot{\omega}_{D_h} r_D + 2\omega_{D_h}\dot{r}_D + \omega_{D_r}\omega_{D_\theta} r_D \\ -\dot{\omega}_{D_\theta} r_D - 2\omega_{D_\theta}\dot{r}_D + \omega_{D_r}\omega_{D_h} r_D \end{array} \right\} = \left\{ \begin{array}{c} u_r + u_{J2_r} - \frac{\mu}{r_D^2} \\ u_\theta + u_{J2_\theta} \\ u_h + u_{J2_h} \end{array} \right\} \tag{5.6}$$

where $\mathbf{u} = \left\{ u_r \quad u_\theta \quad u_h \right\}^T$ is the control acceleration. The components of the disturbing acceleration to J_2 are given by Eqs. (2.12). The angular velocity vector $\boldsymbol{\omega}_D$ is the angular velocity of the Deputy expressed in its LVLH frame as shown in Eq. (2.5b). Since the instantaneous osculating $\omega_\theta = 0$, the following relations hold:

$$\omega_{D_h} = \frac{h_D}{r_D^2} \tag{5.7}$$

$$\omega_{D_r} = \frac{u_h + u_{J2_h}}{\omega_{D_h} r_D} \tag{5.8}$$

The error Euler parameters define the orientation of the current LVLH frame with respect to the desired orientation frame and are given by Eq. (5.3). The kinematic equations that relate the $\boldsymbol{\Delta\beta}$ to the relative angular velocity are

$$\left\{ \begin{array}{c} \Delta\dot{\beta}_0 \\ \Delta\dot{\beta}_1 \\ \Delta\dot{\beta}_2 \\ \Delta\dot{\beta}_3 \end{array} \right\} = \frac{1}{2} \left[\begin{array}{cccc} 0 & -\Delta\omega_r & -\Delta\omega_\theta & -\Delta\omega_h \\ \Delta\omega_r & 0 & \Delta\omega_h & -\Delta\omega_\theta \\ \Delta\omega_\theta & -\Delta\omega_h & 0 & \Delta\omega_r \\ \Delta\omega_h & \Delta\omega_\theta & -\Delta\omega_r & 0 \end{array} \right] \left\{ \begin{array}{c} \Delta\beta_0 \\ \Delta\beta_1 \\ \Delta\beta_2 \\ \Delta\beta_3 \end{array} \right\} \tag{5.9}$$

where $\boldsymbol{\Delta\omega}$ is the inertial angular velocity of the current LVLH frame with respect to the desired LVLH frame, expressed in the current LVLH frame. That is,

$$\boldsymbol{\Delta\omega} = \boldsymbol{\omega}_{D_{LVLH}} - \mathbf{C}_{rel}\boldsymbol{\omega}_{D_{des_{LVLH}}} \tag{5.10}$$

with,

$$\mathbf{C}_{rel} \;=\; \mathbf{C}_D\mathbf{C}_{D_{des}}^T \equiv \mathbf{C}_{rel}(\boldsymbol{\Delta\beta})$$

5.3.2 The Lyapunov Function

If the desired states are those that correspond to the thrust-free solutions of the motion of the Deputy, then no control action is required to maintain the desired states after the orbit has been established. On the other hand, if the desired states do not correspond to the natural motion of the Deputy, thrust will be required to maintain the required motion.

The following Lyapunov function is defined to accomplish the desired objective of globally and asymptotically stabilize the error dynamics:

$$\begin{aligned} V \;=\; & K_1\left[(1-\Delta\beta_0)^2 + \widetilde{\boldsymbol{\Delta\beta}}^T\widetilde{\boldsymbol{\Delta\beta}}\right] + \frac{K_2}{2}\Delta'\omega_h^2 \\ & + \frac{K_3}{2}\left(r_D - r_{D_{des}}\right)^2 + \frac{K_4}{2}\left(\dot{r}_D - \dot{r}_{D_{des}}\right)^2 \end{aligned} \tag{5.11}$$

where $K_i > 0$. $\widetilde{\boldsymbol{\Delta\beta}} = \{\Delta\beta_1 \quad \Delta\beta_2 \quad \Delta\beta_3\}^T$ is the reduced error Euler parameter vector. $\boldsymbol{\Delta'\omega}$ is the direct angular velocity error, defined as

$$\boldsymbol{\Delta'\omega} = \boldsymbol{\omega}_{D_{LVLH}} - \boldsymbol{\omega}_{D_{des_{LVLH}}} \tag{5.12}$$

By comparing Eqs. (5.10) and (5.12), it is evident that in general $\boldsymbol{\Delta'\omega} \neq \boldsymbol{\Delta\omega}$.

When the current LVLH frame and desired LVLH frame align with each other, $\boldsymbol{\Delta\beta} = \{1 \quad 0 \quad 0 \quad 0\}^T$. When the desired orbit for the Deputy is obtained, $\boldsymbol{\Delta'\omega} = 0$, $r_D - r_{D_{des}} = 0$ and $\dot{r}_D - \dot{r}_{D_{des}} = 0$. Thus, V is zero at the origin and positive definite everywhere else.

A control law that asymptotically stabilizes the current orbit with respect to the desired orbit can be obtained by taking the time derivative of the Lyapunov function:

$$\begin{aligned}\dot{V} &= -2K_1\Delta\dot{\beta}_0 + K_2\Delta'\omega_h\Delta'\dot{\omega}_h + K_3\left(r_D - r_{D_{des}}\right)\left(\dot{r}_D - \dot{r}_{D_{des}}\right) \\ &\quad + K_4\left(\dot{r}_D - \dot{r}_{D_{des}}\right)\left(\ddot{r}_D - \ddot{r}_{D_{des}}\right) \end{aligned} \tag{5.13}$$

An interesting property of the relative direction cosine matrix $\mathbf{C}_{rel}$, is made use of in the following analysis:

$$\begin{aligned} & \mathbf{C}_{rel}(\boldsymbol{\Delta\beta})\widetilde{\boldsymbol{\Delta\beta}} = \mathbf{C}_{rel}^T(\boldsymbol{\Delta\beta})\widetilde{\boldsymbol{\Delta\beta}} = \widetilde{\boldsymbol{\Delta\beta}} \\ \therefore \quad & \boldsymbol{\Delta\omega}^T\widetilde{\boldsymbol{\Delta\beta}} = \boldsymbol{\Delta'\omega}^T\widetilde{\boldsymbol{\Delta\beta}} \end{aligned} \tag{5.14}$$

Using Eq. (5.14) in Eq. (5.13), the following equation is obtained:

$$\dot{V} = K_1\Delta'\omega_r\Delta\beta_1 + \Delta'\omega_h\left(K_1\Delta\beta_3 + K_2\Delta'\dot{\omega}_h\right) + \Delta\dot{r}\left(K_3\Delta r + K_4\Delta\ddot{r}\right) \tag{5.15}$$

where $\Delta r = r_D - r_{D_{des}}$, $\Delta\dot{r} = \dot{r}_D - \dot{r}_{D_{des}}$, and $\Delta\ddot{r} = \ddot{r}_D - \ddot{r}_{D_{des}}$.

Control laws to render $\dot{V}$ negative definite can be derived by making the following choices:

$$\Delta'\omega_r = \omega_{D_r} - \omega_{D_{des_r}} = -K_5K_1\Delta\beta_1 \tag{5.16a}$$

$$K_2\Delta'\dot{\omega}_h = K_2\left(\dot{\omega}_{D_h} - \dot{\omega}_{D_{des_h}}\right) = -K_6\Delta'\omega_h - K_1\Delta\beta_3 \tag{5.16b}$$

$$K_4\Delta\ddot{r} = -K_3\Delta\dot{r} - K_7\Delta r \tag{5.16c}$$

where K_5, K_6, and K_7 are positive constants. The desired values $\ddot{r}_{D_{des}}$, $\dot{\omega}_{D_{des_h}}$ and $\omega_{D_{des_r}}$ can be obtained by substituting the desired elements of the Deputy from Eq. (5.5) in Eqs. (5.6)-(5.8). The number of gains can be reduced by using the

following definitions:

$$c_1 = \frac{K_3}{K_4}, \quad c_2 = \frac{K_7}{K_4}, \quad c_3 = \frac{K_6}{K_2}, \quad c_4 = \frac{K_1}{K_2}, \quad c_5 = K_5 K_1$$

Equations (5.16), along with Eqs. (5.6)-(5.8), lead to the following control laws stabilize the system about the origin:

$$\begin{aligned} u_r &= -c_1 \Delta\dot{r} - c_2 \Delta r - \left(\omega_{D_h}^2 r_D - \omega_{D_{des_h}}^2 r_{D_{des}}\right) \\ &\quad - \left(u_{J2_r} - u_{J2_{des_r}}\right) + \left(\frac{\mu}{r_D^2} - \frac{\mu}{r_{D_{des}}^2}\right) \qquad (5.17a) \\ u_\theta &= -c_3 \Delta' \omega_h r_D - c_4 \Delta\beta_3 r_D \\ &\quad - \left[u_{J2_\theta} - \left(\frac{r_D}{r_{D_{des}}}\right) u_{J2_{des_\theta}}\right] + 2\left[\omega_{D_h}\dot{r}_D - \left(\frac{r_D}{r_{D_{des}}}\right)\dot{r}_{D_{des}}\omega_{D_{des_h}}\right] \qquad (5.17b) \\ u_h &= -c_5 \Delta\beta_1 \omega_{D_h} r_D + \left[\left(\frac{\omega_{D_h} r_D}{\omega_{D_{des_h}} r_{D_{des}}}\right) u_{J2_{des_h}} - u_{J2_h}\right] \qquad (5.17c) \end{aligned}$$

By substituting Eqs. (5.17) in Eq. (5.15), the time derivative of the Lyapunov reduces to

$$\dot{V} = -K_1 K_5 \Delta\beta_1^2 - K_6 \Delta' \omega_h^2 - K_7 \left(\dot{r}_D - \dot{r}_{D_{des}}\right)^2 \qquad (5.18)$$

It is observed that $\dot{V}$ is only negative semi-definite since some of the other states may be non-zero even when $\Delta\beta_1 = \Delta'\omega_h = (\dot{r}_D - \dot{r}_{D_{des}}) = 0$. Asymptotic stability cannot be concluded in the sense of Lyapunov. Hence, LaSalle's Invariant Principle will be used to conclude asymptotic stability.

5.3.3 Concluding Asymptotic Stability

LaSalle's Theorem is stated in Appendix B. A full proof can be found in Ref. 28. If $\mathbf{x}$ are the states corresponding to the error dynamics given by the Euler parameter errors, angular velocity errors, radial distance error and radial velocity error, the region in consideration is $D = \{\mathbf{x} \in \Re^7\}$. It has already been shown in Eqs. (5.11)

and (5.18), that $V(\mathbf{x})$ is positive definite and $\dot{V}(\mathbf{x})$ is negative semi-definite in D. $E = \left\{\mathbf{x} \in D | \dot{V}(\mathbf{x}) = 0\right\}$ is the set that contains the points where $\Delta\beta_1 = 0$, $\Delta'\omega_h = 0$, and $\dot{r}_D = \dot{r}_{D_{des}}$. It needs to be shown that the region M contains only the origin, i.e., when $\Delta\beta_1 = \Delta\omega_h = \dot{r}_D - \dot{r}_{D_{des}} = 0$, all other error variables are zero.

Since,

$$\begin{aligned} \Delta'\omega_h &= 0 \\ \Rightarrow \omega_{D_h} &= \omega_{D_{des_h}} \end{aligned}$$

From Eqs. (5.8) and (5.17c)

$$\begin{aligned} \omega_{D_r} &= \frac{u_h + u_{J2_h}}{\omega_{D_h} r_D} \\ &= \frac{-c_5 \Delta\beta_1 \omega_{D_h} r_D + \omega_{D_h}\omega_{D_{des_r}} r_D - u_{J2_h} + u_{J2_h}}{\omega_{D_h} r_D} \\ &= \frac{\omega_{D_h}\omega_{D_{des_r}} r_D}{\omega_{D_h} r_D} \\ \therefore \omega_{D_r} &= \omega_{D_{des_r}} \end{aligned} \tag{5.19}$$

From the kinematic constraint, $\omega_{D_\theta} = \omega_{D_{des_\theta}} = 0$, and hence

$$\boldsymbol{\Delta'\omega} = \mathbf{0} \tag{5.20}$$

Next, consider the first of Eqs. (5.6). Since $\dot{r}_D = \dot{r}_{D_{des}}$ it follows that

$$\ddot{r}_D = \ddot{r}_{D_{des}}$$

Then,

$$u_r + u_{J2_r} - \frac{\mu}{r_D^2} + \omega_{D_h}^2 r_D = u_{J2_{des_r}} - \frac{\mu}{r_{D_{des}}^2} + \omega_{D_{des_h}}^2 r_{D_{des}}$$

From Eq. (5.17a)

$$-c_1\left(\dot{r}_D - \dot{r}_{D_{des}}\right) - c_2\left(r_D - r_{D_{des}}\right) - \left(\omega_{D_h}^2 r_D - \omega_{D_{des_h}}^2 r_{D_{des}}\right) =$$
$$\left(u_{J2_r} - u_{J2_{des_r}}\right) - \left(\frac{\mu}{r_D^2} - \frac{\mu}{r_{D_{des}}^2}\right) - u_{J2_r} + \frac{\mu}{r_D^2} - \omega_{D_h}^2 r_D + u_{J2_{des_r}}$$
$$-\frac{\mu}{r_{D_{des}}^2} + \omega_{D_{des_h}}^2 r_{D_{des}}$$

The following results are obtained after simplifying the above equations:

$$\begin{aligned} -c_2\left(r_D - r_{D_{des}}\right) &= 0 \\ \therefore r_D &= r_{D_{des}} \end{aligned} \tag{5.21}$$

Similarly, since $\Delta\omega_h = 0$, $\dot{\omega}_{D_h} = \dot{\omega}_{D_{des_h}}$. Equation (5.17b) can be substituted in the second of Eq. (5.6) to obtain

$$\Delta\beta_3 = 0 \tag{5.22}$$

Since $\Delta\beta_1 = \Delta\beta_3 = 0$, it is clear that $\Delta\dot{\beta}_1 = \Delta\dot{\beta}_3 = 0$. The following results are obtained from the right hand side of Eq. (5.9):

$$\boldsymbol{\Delta\dot{\beta}} = \mathbf{0} \tag{5.23}$$

Only one of $\Delta\beta_0$ and $\Delta\beta_2$ needs to be determined; the value of the other is fixed by the Euler parameter constraint:

$$\boldsymbol{\Delta\beta}^T\boldsymbol{\Delta\beta} = \Delta\beta_0^2 + \Delta\beta_2^2 = 1 \tag{5.24}$$

Consider again, Eq. (5.10):

$$\begin{aligned}\boldsymbol{\Delta\omega} &= \boldsymbol{\omega}_D - \mathbf{C}_{rel}\boldsymbol{\omega}_{D_{des}} \\ &= \left\{ \begin{array}{c} \omega_{D_r} \\ 0 \\ \omega_{D_h} \end{array} \right\} - \left\{ \begin{array}{c} (\Delta\beta_0^2 - \Delta\beta_2^2)\omega_{D_{des_r}} - \Delta\beta_0\Delta\beta_2\omega_{D_{des_h}} \\ 0 \\ \Delta\beta_0\Delta\beta_2\omega_{D_{des_r}} + (\Delta\beta_0^2 - \Delta\beta_2^2)\omega_{D_{des_h}} \end{array} \right\} \end{aligned} \tag{5.25}$$

Since $\boldsymbol{\omega}_{D_{des}} = \boldsymbol{\omega}_D$,from Eq. (5.23),

$$\begin{aligned} & \Delta\dot{\beta}_1 = \frac{1}{2}\left[\Delta\omega_r\Delta\beta_0 + \Delta\omega_h\Delta\beta_2\right] = 0 \\ \Rightarrow \quad & \left[(1 - \Delta\beta_0^2 + \Delta\beta_2^2)\omega_{D_r} + \Delta\beta_0\Delta\beta_2\omega_{D_h}\right]\Delta\beta_0 \\ & + \left[-\Delta\beta_0\Delta\beta_2\omega_{D_r} + (1 - \Delta\beta_0^2 + \Delta\beta_2^2)\omega_{D_h}\right]\Delta\beta_2 = 0 \\ \therefore \quad & \Delta\beta_2^2\Delta\beta_0\omega_{D_r} + \Delta\beta_2(1 + \Delta\beta_2^2)\omega_{D_h} = 0 \end{aligned} \tag{5.26}$$

Similarly,

$$\begin{aligned} & \Delta\dot{\beta}_3 = 0 \\ \Rightarrow \quad & \left[-\Delta\beta_0\Delta\beta_2\omega_{D_r} + (1 - \Delta\beta_0^2 + \Delta\beta_2^2)\omega_{D_h}\right]\Delta\beta_0 \\ & - \left[(1 - \Delta\beta_0^2 + \Delta\beta_2^2)\omega_{D_r} + \Delta\beta_0\Delta\beta_2\omega_{D_h}\right]\Delta\beta_2 = 0 \\ \therefore \quad & -\Delta\beta_2(1 + \Delta\beta_2^2)\omega_{D_r} + \Delta\beta_2^2\Delta\beta_0\omega_{D_h} = 0 \end{aligned} \tag{5.27}$$

From Eqs. (5.26) and (5.27),

$$\left[\begin{array}{cc} \omega_{D_r} & \omega_{D_h} \\ \omega_{D_h} & -\omega_{D_r} \end{array} \right] \left\{ \begin{array}{c} \Delta\beta_2^2\Delta\beta_0 \\ \Delta\beta_2(1 + \Delta\beta_2^2) \end{array} \right\} = \mathbf{0}$$

Since, for orbital motion,

$$-\omega_{D_r}^2 - \omega_{D_h}^2 \neq 0$$

$$
\begin{aligned}
\Rightarrow \quad & \begin{cases} \Delta\beta_2^2 \Delta\beta_0 = 0 \\ \Delta\beta_2(1 + \Delta\beta_2^2) = 0 \end{cases} \\
\therefore \quad & \begin{cases} \boldsymbol{\Delta\beta_2 = 0 = \Delta\beta_1 = \Delta\beta_3} \\ \boldsymbol{\Delta\beta_0 = 1} \end{cases}
\end{aligned} \tag{5.28}
$$

From Eqs. (5.20), (5.21), and (5.28), it is clear that the set M contains only the origin. Hence any trajectory starting in Ω, will asymptotically approach M, i.e, the origin as $t \to \infty$. The equilibrium is thus proven to be asymptotically stable and the controller drives the current trajectory to the desired trajectory asymptotically. Further, since $V \to \infty$ as $||\mathbf{x}|| \to \infty$, the controller globally, asymptotically, stabilizes the desired trajectory.

5.3.4 Gain Selection

The value of the gains have to be selected such that the total control requirement (TCR) is minimized as much as possible. For a nonlinear, coupled set of equations such as the case in consideration, an estimate of the suitable gains can be obtained from a linearization of the closed-loop system. With an initial guess obtained from such an estimate, the gains need to be adjusted so that TCR is reduced as much as possible.

It is observed that upon closing the loop by replacing the controls from Eqs. (5.17) in Eq. (5.6), the differential equation in translation error, Eq. (5.16c), is decoupled from the attitude error equations Eqs. (5.16a) and Eqs. (5.16b). Furthermore, it can also be seen that the second-order equation for translation error does not require

linearization. For small angle differences,

$$\begin{aligned}\Delta\beta_0 &\approx 1\\ \Delta\beta_1 &\approx \frac{\delta i}{2}\\ \Delta\beta_2 &\approx 0\\ \Delta\beta_3 &\approx \frac{\delta\Omega + \delta\theta}{2}\end{aligned}$$

and,

$$\begin{aligned}\Delta\omega_r &\approx \Delta'\omega_r\\ \Delta\omega_h &\approx \Delta'\omega_h\end{aligned}$$

It can be shown that by linearizing the $\Delta\dot{\omega}_h$ and $\Delta\omega_r$ equations in Eqs. (5.6), the following equations are obtained:

$$\Delta\ddot{r} + c_1\Delta\dot{r} + c_2\Delta r = 0 \tag{5.29a}$$

$$\Delta\ddot{\beta}_3 + c_3\Delta\dot{\beta}_3 + \frac{c_4}{2}\Delta\beta_3 = 0 \tag{5.29b}$$

$$\Delta\dot{\beta}_1 + \frac{c_5}{2}\Delta\beta_1 = 0 \tag{5.29c}$$

The gains c_2, c_4, and c_5 are a measure of the natural frequency of the system. If it is desired that the reconfiguration be performed within one orbit, then a reasonable choice for the gains are:

$$c_2 = \frac{c_4}{2} = \frac{c_5}{2} = O(n_C^2) \tag{5.30}$$

Further, from the condition of critical damping, it follows that:

$$\begin{aligned}c_1 &= 2\,(c_2)^{\frac{1}{2}}\\ c_3 &= (2c_4)^{\frac{1}{2}}\end{aligned} \tag{5.31}$$

Equations (5.30) and (5.31) provide excellent initial guesses for the gains to be used in

the control law. Further tuning of the gains is necessary for each individual example under consideration.

5.3.5 Implementation

The orbital elements of the Chief and Deputy can be obtained at any time instant by integrating two sixth-order Gauss' equation sets in Eqs. (2.20). The orbital elements can be used to obtain all the quantities required by the control laws Eqs. (5.17). However, this is really a brute-force approach. For cases where the reference orbit has low eccentricity, the control law can be simplified by the use of mean elements. The control that is obtained is then applied to the truth model for the Deputy.

The desired elements of the Deputy are obtained from Table 3.2. However, it is observed that the eccentricity difference has a term dependent on the mean anomaly of the Chief. This term causes the desired relative orbit to constantly change even in the absence of J_2, and the radial and tangential controls do not reach zero asymptotically. From a practical point of view, this is now a problem of relative orbit maintenance. To implement the control, the desired elements are specified at a particular number of orbits from the initiation of the control action. If the initial elements of the Chief are $\mathbf{e}_C(0)$, the elements of the Chief after, say N desired orbits, are $\mathbf{e}_C(NT)$ where T is the time period of the orbit. For mean elements, $\mathbf{e}_C(NT)$ can be determined analytically by using the mean rates. Using the PCO requirements and rate-matching condition, the elements of the Deputy can be found by:

$$\mathbf{e}_{D_{des}}(NT) = \mathbf{e}_C(NT) + \delta\mathbf{e}(\rho_{des}, \alpha_{0_{des}}, NT)$$

The mean rates for this desired orbit are calculated from Eqs. (2.15). The initial orbital elements of the desired trajectory of the Deputy, $\mathbf{e}_{D_{des}}(0)$ are then found by

subtracting the contribution of these mean rates over N orbits from $\mathbf{e}_{D_{des}}(NT)$.

5.4 Numerical Results

In this section the results obtained in the analysis in the chapter will be studied.

5.4.1 Impulsive Reconfiguration

Consider a Chief satellite in an orbit with the following elements:

$$\mathbf{e}_C = \{7100\text{km} \quad 0.005 \quad 70^\circ \quad 0^\circ \quad 0^\circ \quad 0^\circ\}^T$$

The reconfiguration from an initial formation of relative radius 1km to one of radius 2km is considered, for two initial phase angles, $\alpha_0 = 0^\circ$ and $\alpha_0 = 90^\circ$. The variation of fuel cost with final phase angle is studied. Figure 5.1 shows the total impulse required (sum of magnitudes of velocity increments) using two impulses. It is shown in Ref. (26) that the total velocity increment requirement for reconfiguring the Deputy's orbit is minimum if the initial and final phase angles are the same, i.e, $\alpha_{0_i} = \alpha_{0_f}$. The positions (true anomaly of Chief) and times of impulse application are obtained from the numerical optimization and are presented in Table 5.1. The results for $\alpha_{0_i} = 90^\circ$ are almost exactly symmetrical to those for $\alpha_{0_i} = 0^\circ$.

It is observed that the tangential components of the impulses are negligible when compared with the radial and out-of-plane components. This is because there is negligible change in semi-major axis involved and radial impulses are used to change the eccentricity. Additionally, the two impulses are separated by nearly 180° of true anomaly.

Table 5.1 Velocity Increments for Reconfiguration with Chief in a Low-Eccentricity Orbit, $\alpha_{0_i} = 0^\circ$

α_{0_f}	Impulse 1				Impulse 2			
(deg)	f_{C_1}	$\Delta\mathbf{v}_1$ (m/s)			f_{C_2}	$\Delta\mathbf{v}_2$ (m/s)		
	(deg)	Δv_{1_r}	Δv_{1_θ}	Δv_{1_h}	(deg)	Δv_{2_r}	Δv_{2_θ}	Δv_{2_h}
0	0.00	0.265	-0.001	0.543	179.52	-0.263	0.001	-0.512
10	160.05	-0.274	0.001	-0.560	339.96	0.270	-0.001	0.530
20	142.08	-0.296	0.002	-0.606	321.80	0.290	-0.001	0.575
30	126.33	-0.331	0.003	-0.673	305.94	0.322	-0.001	0.641
40	112.73	-0.372	0.004	-0.754	292.28	0.361	-0.001	0.721
50	100.87	-0.418	0.004	-0.842	280.40	0.404	-0.001	0.809
60	90.34	-0.464	0.005	-0.932	269.88	0.449	-0.001	0.902
70	80.81	-0.510	0.006	-0.102	260.36	0.495	-0.000	0.996
80	72.02	-0.554	0.006	-0.111	251.59	0.540	0.000	1.088
90	63.77	-0.595	0.006	-1.186	243.36	0.582	0.001	1.177

Figures 5.2a and 5.2b show the projection of the relative motion in the $\theta - h$ plane, for the formation in transit, for two different cases with the Chief in the low eccentricity orbit specified above. The first case is a reconfiguration from $\alpha_0 = 0^\circ$ to $\alpha_0 = 90^\circ$, and the second is the other way round. In both the cases, the initial formation has a relative radius of 1km and a final relative radius of 2km. The reconfiguration from $\alpha_0 = 0^\circ$ to $\alpha_0 = 90^\circ$ has characteristics similar to the Hohmann transfer for a single satellite. It should be noted that out-of-plane motion also exists, and there is no possibility of collision between the Deputy and the Chief.

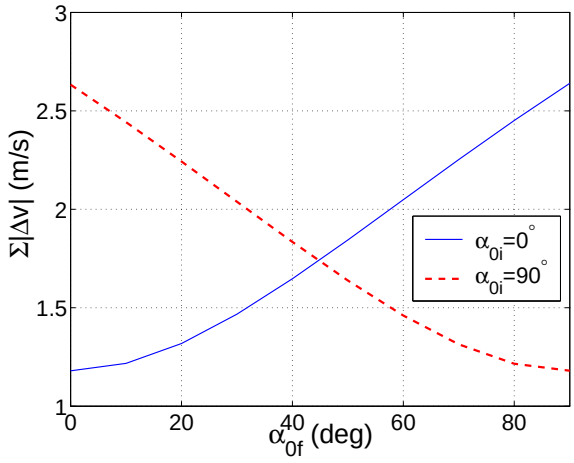

Fig. 5.1 Total Velocity Impulse Requirement for Reconfiguration, Low-Eccentricity Reference Orbit

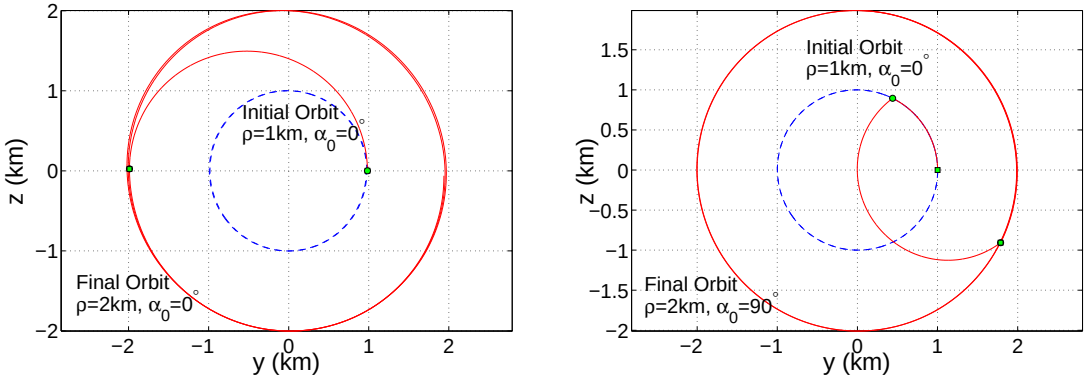

Fig. 5.2 Relative Orbit Reconfiguration, Low-Eccentricity Reference Orbit (2-Impulse Maneuver)

To study the reconfiguration of a formation with the Chief in a highly eccentric orbit, the following orbital elements of the Chief are selected:

$$\mathbf{e}_C = \{42095.70\text{km} \quad 0.8182 \quad 50^\circ \quad 0^\circ \quad 0^\circ \quad 11.76^\circ\}$$

Table 5.2 Velocity Increments for Reconfiguration with Chief in a Highly Eccentric Orbit, $\alpha_{0_i} = 0^\circ$

α_{0_f}	Impulse 1				Impulse 2			
(deg)	f_{C_1}	$\Delta\mathbf{v}_1$ (m/s)			f_{C_2}	$\Delta\mathbf{v}_2$ (m/s)		
	(deg)	Δv_{1_r}	Δv_{1_θ}	Δv_{1_h}	(deg)	Δv_{2_r}	Δv_{2_θ}	Δv_{2_h}
0	156.17	0.102	-0.240	-0.260	200.42	0.021	0.140	-0.171
10	155.71	0.130	-0.268	-0.310	206.08	-0.004	0.086	-0.036
20	146.32	0.135	-0.246	-0.462	217.78	-0.006	0.041	0.039
30	144.58	0.091	-0.172	-0.568	212.81	0.012	0.063	0.167
40	144.26	0.053	-0.108	-0.665	207.23	0.019	0.065	0.286
50	143.52	0.013	-0.038	-0.770	202.97	0.025	0.060	0.388
60	142.65	-0.033	0.042	-0.865	199.67	0.037	0.054	0.480
70	141.77	-0.087	0.131	-0.942	197.07	0.055	0.049	0.564
80	140.96	-0.146	0.225	-0.995	194.96	0.078	0.046	0.640
90	140.20	-0.206	0.321	-1.017	193.21	0.104	0.041	0.705

In the high eccentricity case, $M_{C_0} = 11.76^\circ$ corresponds to $f_{C_0} = 105^\circ$. This value of the true anomaly is chosen arbitrarily and ensures that the formation is established far enough from the perigee so that the errors from the analytical model are of the same order as those for the formation established at apogee. This choice of M_{C_0} also allows enough "room" for the first impulse to occur before the apogee is reached.

Table 5.3 Velocity Increments for Reconfiguration with Chief in a Highly Eccentric Orbit, $\alpha_{0_i} = 90^\circ$

α_{0_f}	Impulse 1				Impulse 2			
(deg)	f_{C_1}	$\Delta\mathbf{v}_1$ (m/s)			f_{C_2}	$\Delta\mathbf{v}_2$ (m/s)		
	(deg)	Δv_{1_r}	Δv_{1_θ}	Δv_{1_h}	(deg)	Δv_{2_r}	Δv_{2_θ}	Δv_{2_h}
0	156.90	0.517	-0.865	0.133	199.14	-0.297	-0.139	-0.730
10	155.74	0.386	-0.697	-0.010	198.67	-0.166	0.016	-0.587
20	154.84	0.256	-0.527	-0.153	198.99	-0.033	0.171	-0.444
30	157.47	0.111	-0.334	-0.297	202.56	0.107	0.328	-0.286
40	156.36	0.169	-0.383	-0.377	201.71	0.021	0.196	-0.147
50	155.00	0.183	-0.366	-0.446	209.48	-0.008	0.097	-0.024
60	147.32	0.151	-0.279	-0.509	210.27	-0.014	0.049	0.035
70	144.03	0.091	-0.169	-0.532	206.97	0.002	0.052	0.123
80	143.62	0.036	-0.072	-0.518	203.89	0.010	0.042	0.215
90	142.95	-0.011	0.014	-0.489	201.11	0.011	0.015	0.286

The reconfiguration from an initial formation characterized by $\rho_i = 10$km, to one characterized by $\rho_i = 20$km, is studied. Similar to the low eccentricity example, the variation of total impulse required with the final phase angle is obtained for two initial phase angles, $\alpha_0 = 0^\circ$ and $\alpha_0 = 90^\circ$. The results are presented in Tables (5.2) and (5.3).

Figure 5.3 shows the total impulse required for reconfiguration in the above cases. Unlike the low eccentricity example, no symmetry is observed between the total velocity

impulses required for $\alpha_{0_i} = 0°$ and $\alpha_{0_i} = 90°$. Furthermore, unlike the previous case where the eccentricity of the Chief's orbit was low, the lowest total velocity increment requirement is not necessarily achieved if the initial and final phase angles are the same. For example, the reconfiguration from $(\rho = 10\text{km}, \alpha_0 = 90°)$ to $\rho = 20\text{km}$ for different final phase angles α_{0_f}, has the lowest velocity increment requirement when $\alpha_{0_f} = 60°$.

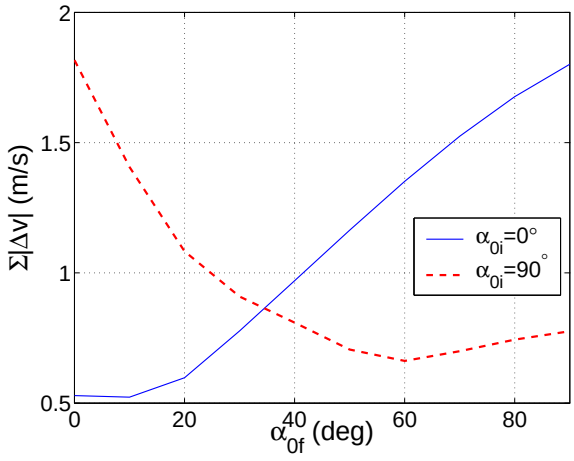

Fig. 5.3 Total Velocity Impulse Requirement for Reconfiguration, High-Eccentricity Reference Orbit

It is also observed that the impulses are placed almost symmetrically in close proximity of the apogee. Since the velocity of a spacecraft is lowest near apogee, lower velocity increments are required for orbit changes in this region. It is also known from Eq. (2.21) that for orbits of low eccentricity, inclination changes are most efficiently obtained at the equator, while right ascension changes are most efficiently obtained at zenith or nadir. However, for highly eccentric orbits, the radius of the orbit influences the result significantly. This results in different positions of impulse application, all approximately in the same region ($f_{C_1} \approx 155°$, $f_{C_2} \approx 205°$). For very high eccentrici-

ties such as the one considered, eccentricity effects will dominate the fuel requirement.

If the formation had been established at the apogee, then the the two impulses can no longer be chosen symmetrically about the apogee without the second impulse occurring almost after one orbit around the Earth. For orbits with high semi-major axes such as the one considered, the time period is almost one day, which results in the two impulses being separated by almost one day.

Figure 5.4a shows the relative motion of the Deputy under the effect of the two impulses for a reconfiguration from ($\rho = 10\text{km}, \alpha_0 = 0^\circ$) to ($\rho = 20\text{km}, \alpha_0 = 0^\circ$). Figure 5.4b shows the reconfiguration from ($\rho = 20\text{km}, \alpha_0 = 90^\circ$) to ($\rho = 10\text{km}, \alpha_0 = 90^\circ$). The squares on the plot indicate the start and the end of the simulation, while the circles indicate points of application of the velocity impulse. The initial relative orbit for the second case does not resemble the relative orbit in Fig. 4.7b, even though five of the orbital elements of the Chief are the same. The mean anomaly of the Chief at epoch time for the present example is not the same as that used to generate Fig. 4.7b. In the previous example, $M_{C_0} = 180^\circ$, while in Fig. 5.4b, $M_{C_0} = 11.76^\circ$. This is a consequence of the fact that the initial eccentricity difference chosen between the Deputy and Chief, depends on M_C, as can be seen from Table 3.2.

5.4.2 Analysis of the Results of the Reconfiguration Problem Using Euler Parameters

The kinematic approach discussed in the previous sections can be used to analyze the reconfiguration problem. In particular, the variations of the error Euler parameters and angular velocity error about the h-axis are studied for both the low eccentricity as well as high eccentricity cases of the previous sections.

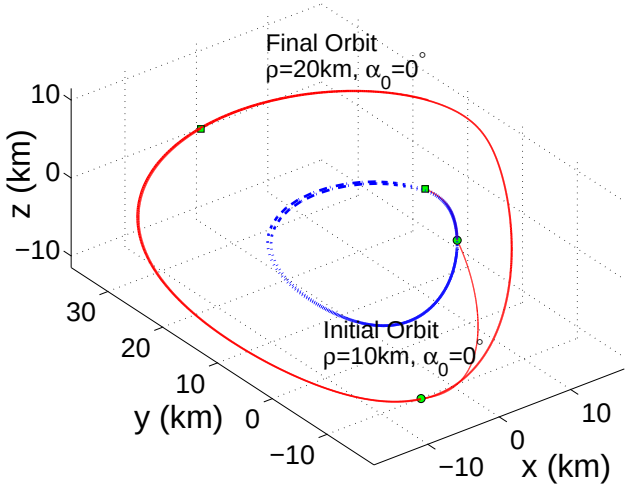

(a) $(\rho = 10\text{km}, \alpha_0 = 0°) \rightarrow (\rho = 20\text{km}, \alpha_0 = 0°)$

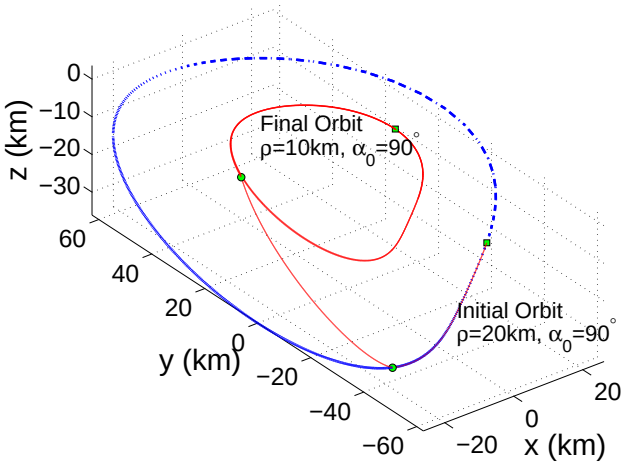

(b) $(\rho = 20\text{km}, \alpha_0 = 90°) \rightarrow (\rho = 10\text{km}, \alpha_0 = 90°)$

Fig. 5.4 Relative Orbit Reconfiguration, High-Eccentricity Reference Orbit

Figure 5.5a shows the error in angular velocity about the orbit normal, $\Delta\omega_h$, for the low eccentricity case. Figure 5.5b shows the angular velocity error for the high eccentricity case. The low eccentricity reconfiguration is from $(\rho = 1\text{km}, \alpha_0 = 0°)$ to $(\rho = 2\text{km}, \alpha_0 = 0°)$ in the absence of the J_2 perturbation. The high eccentricity reconfiguration is from $(\rho = 10\text{km}, \alpha_0 = 0°)$ to $(\rho = 20\text{km}, \alpha_0 = 0°)$, also in the absence of the J_2 perturbation. Figures 5.6a-5.6d present the variations in the relative EPs for the low eccentricity case. Similarly, Figs. 5.7a-5.7d present these variations for the high eccentricity case. It should be noted that the application of an impulse does not cause a jump in the angular velocity error.

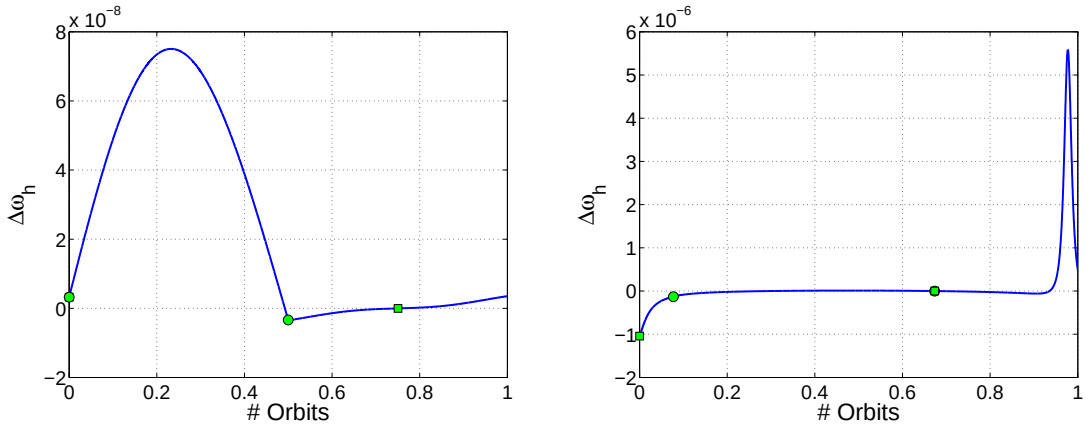

(a) Low Eccentricity (b) High Eccentricity

Fig. 5.5 $\Delta\omega_h$ During Impulsive Reconfiguration, Low-Eccentricity and High-Eccentricity Reference Orbit

The error Euler parameters for the low eccentricity case, in Figs. 5.6a-5.6d, show jumps in the case of $\Delta\beta_1$ and $\Delta\beta_0$. However, $\Delta\beta_2$ and $\Delta\beta_3$ are continuous. Since the position of the satellite does not change on the application of an impulse, neither does the relative position between the Deputy and Chief. A discontinuity in the values of

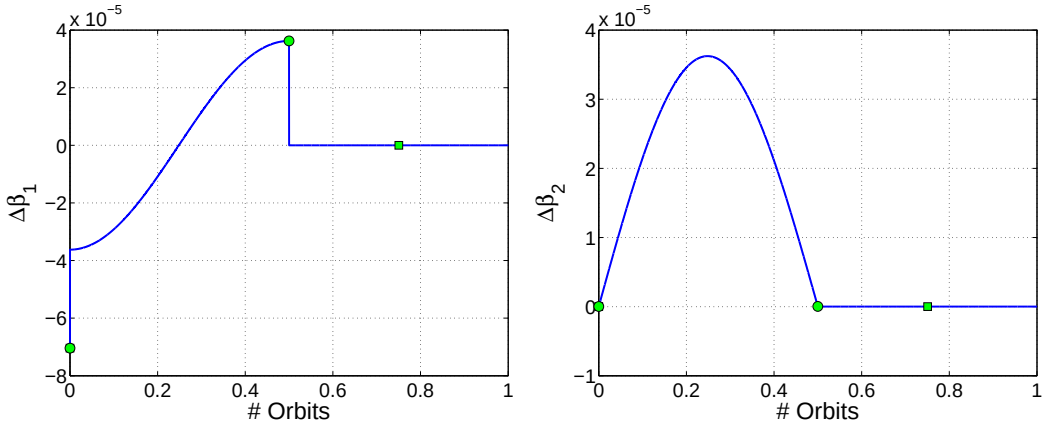

(a) $\Delta\beta_1$ (b) $\Delta\beta_2$

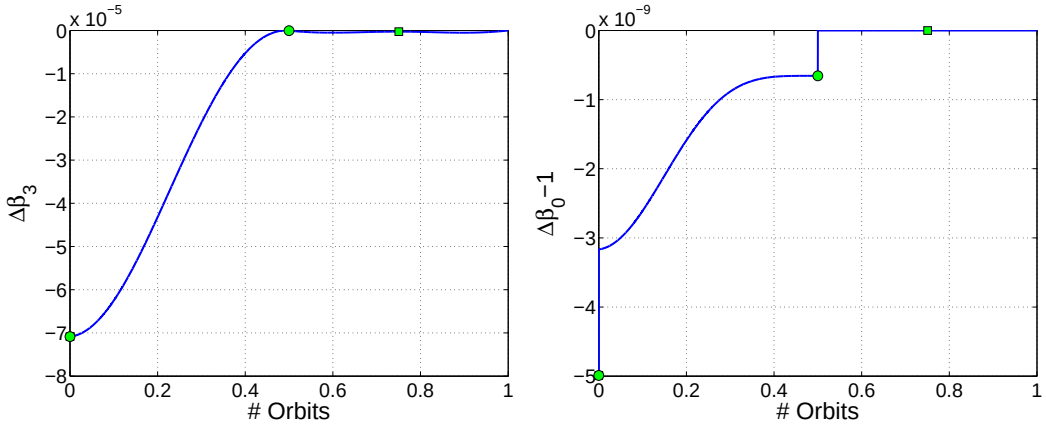

(c) $\Delta\beta_3$ (d) $\Delta\beta_0$

Fig. 5.6 Error Euler Parameters During Impulsive Reconfiguration, Low-Eccentricity Reference Orbit

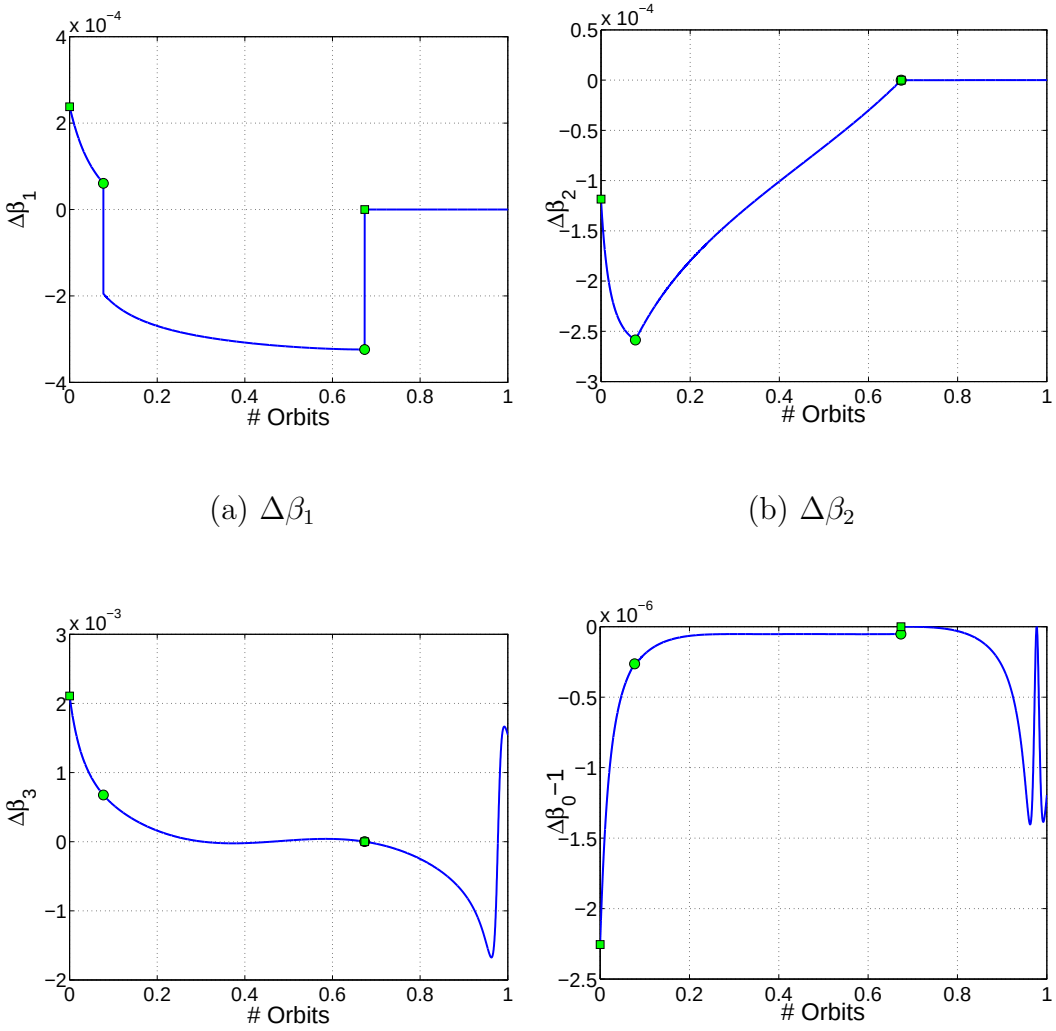

(a) $\Delta\beta_1$ (b) $\Delta\beta_2$

(c) $\Delta\beta_3$ (d) $\Delta\beta_0$

Fig. 5.7 Error Euler Parameters During Impulsive Reconfiguration, High-Eccentricity Reference Orbit

$\Delta\beta_2$ or $\Delta\beta_3$ would cause the relative position to change through Eq. (3.38).

Beyond the end of the final coast phase, the open-loop dynamics of the system govern the relative motion of the satellite. From Table 3.2, it can be seen that the elemental differences are time-varying quantities that depend on the current orbital elements of the Chief. Of these elemental differences, δe is also dependent on the mean anomaly of the Chief, M_C, which results in short-periodic variations in δe. The other elemental differences that are time-varying, δM and $\delta\omega$, also show long-periodic variations. If the eccentricity of the Chief is low, the desired orbital elements of the Deputy show mostly long-periodic behavior since the second term of δe is negligible when compared with the first. This results in only a very slow change in the values of the desired orbital elements, and after the end of the coast phase, the errors between the current orbital elements of the Deputy and the desired elements grow very slowly. For high eccentricity reference orbits, however, the short-periodic variations in δe cause the desired orbital elements to change at the orbital rate of the Chief. As a result, even though the error EPs and the angular velocity error are zero at the end of the coast phase, they no longer remain zero if the simulation is continued beyond the end of the coast phase.

In the presence of the J_2 perturbation, $\mathbf{\Delta}\beta$ reach the desired value of $\{1 \quad 0 \quad 0 \quad 0\}^T$ but drift in the elements due to J_2 causes the error EPs and angular velocity error to deviate from the desired value after the end of the coast phase.

In Figs. 5.6a-5.6d, the first impulse is applied immediately at epoch. This is also evident from Table 5.1. The orbit is established at the equator and the points of equatorial crossing are the optimal positions for inclination changes. However, for

the high eccentricity case, the out-of-plane impulse components, considered using the theory for low eccentricity orbits, seem inefficiently placed. For the low eccentricity reconfiguration problem, the required change in inclination, $\Delta i = -1.408 \times 10^{-4}$rad. From Eqs. (2.20), at the equator, the application of an out-of-plane impulse does not change right ascension. It can be shown that the change in $\Delta\beta_1$ due to an out-of-plane impulse is given by

$$\delta\left(\Delta\beta_1\right) = \frac{\Delta v_h}{2r\omega_h} = \frac{r}{2h}\Delta v_h$$

and from Gauss' equations

$$\Delta v_h = \frac{h}{r}\left(\Delta\Omega \sin\theta \cos i + \Delta i \cos\theta\right)$$

Hence, at the equator,

$$\delta\left(\Delta\beta_1\right) = \frac{h}{r}\Delta i \frac{r}{2h} = \frac{\Delta i}{2}$$

For the optimal two-impulse problem, the change in inclination is performed in equal parts at the equator crossings. Using the value for Δi and the initial angles of the Chief and Deputy, the approximate change in $\Delta\beta_1$ is 3.5×10^{-5} at each impulse. This change is observed in Figs. 5.6a and 5.6c due to both the impulses.

The two-impulse numerical problem yields optimal velocity impulses and true anomaly values for application. While it is difficult to draw any useful information from the high eccentricity case, by studying the error EPs and angular velocity errors for the low eccentricity example, valuable insight can be obtained into the process of selecting gains in the continuous control scheme, to minimize the total control requirement, in the subsequent analysis.

5.4.3 Lyapunov-Based Reconfiguration Control

Consider first, the low-eccentricity reference orbit given by:

$$\mathbf{e}_C = \{7100\text{km} \quad 0.005 \quad 70^\circ \quad 0^\circ \quad 0^\circ \quad 0^\circ\}^T$$

The initial configuration of the relative orbit has $\rho = 1$km and $\alpha_0 = 0^\circ$. Figures 5.8a and 5.8b show the θ-h projection of the reconfiguration to $\rho = 2\text{km}, \alpha_0 = 0^\circ$ and $\rho = 2\text{km}, \alpha_0 = 90^\circ$, respectively.The effects of the J_2 perturbation are included in the model used to generate the results. The gains used are shown in Table 5.4.

Table 5.4 Gains Used in the Lyapunov-Based Controller

Case	ρ_i (km)	α_{0_i} (deg)	ρ_f (km)	α_{0_f} (deg)	c_1	c_2	c_3	c_4	c_5
1	1	0	2	0	$2\sqrt{c_2}$	$0.85n_C^2$	$\sqrt{2c_4}$	$2.3n_C^2$	$2n_C$
	1	0	2	90	$2.1\sqrt{c_2}$	$10n_C^2$	$1.2\sqrt{2c_4}$	$2n_C^2$	$1.5n_C$
2	10	0	20	0	$2\sqrt{c_2}$	$4n_C^2$	$\sqrt{2c_4}$	$2n_C^2$	$4n_C$
	10	0	20	90	$2\sqrt{c_2}$	$5n_C^2$	$\sqrt{2c_4}$	$2n_C^2$	$4n_C$

As an initial guess for the gains, the linearized analysis was used as described previously. The final values of the gains were selected by trying different values for c_2, c_4, and c_5 around those prescribed by the linearized model. The gains corresponding to the damping coefficients in the linearized model, c_1 and c_3, were then selected in a similar manner. It can be seen that c_1 and c_3 are very close to the values required for critical damping in the linearized model, for both, low-eccentricity, as well as high-eccentricity reference orbits. The gain c_4 also is not very different from the desired

value for the linearized model. The selection of the gains c_2 and c_5, however, is not as easily achieved as the other gains.

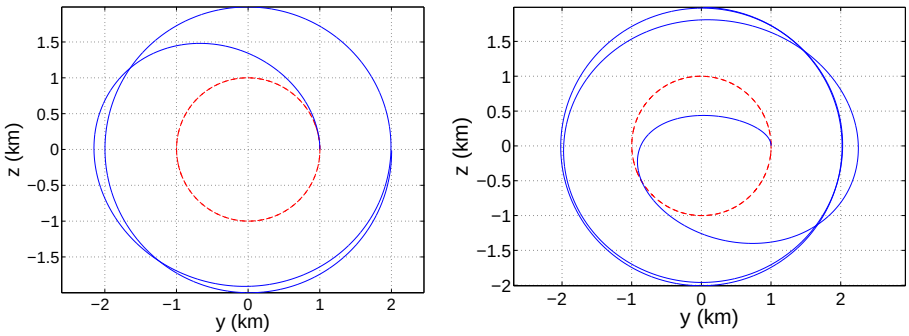

(a) $\alpha_{0_f} = 0°$ (b) $\alpha_{0_f} = 90°$

Fig. 5.8 Lyapunov-based Reconfiguration Control: Projected Orbit for $\alpha_{0_f} = \{0° \quad 90°\}$

The reconfiguration for the $\alpha_{0_f} = 0°$ case is very similar to the impulsive reconfiguration except for the overshoot in the $-y$ direction. Figures 5.9a and 5.9b show the total control requirement (TCR) for both cases of α_0. It is observed that there is very little difference in the TCR for the cases with and without J_2, due to the low differential J_2 acceleration appearing in the control laws in Eqs. (5.17). The TCR for the $\alpha_{0_f} = 90°$ is greater than the TCR for the $\alpha_{0_f} = 0°$, as is expected. The TCR for a reconfiguration from $(\rho = 1\text{km}, \alpha_0 = 90°)$ to $(\rho = 2\text{km}, \alpha_0 = 90°)$ is the same if the initial and final phase angles are 0°, provided the orbit is established at $M = 90°$. If the orbit is not established at 90°, then the TCR is greater since the control is applied at the equator, where the control requirement for a change in right ascension is maximum. Unlike the optimal impulsive control scheme, the positions for the application of control cannot be selected optimally by the Lyapunov analysis

presented in this thesis.

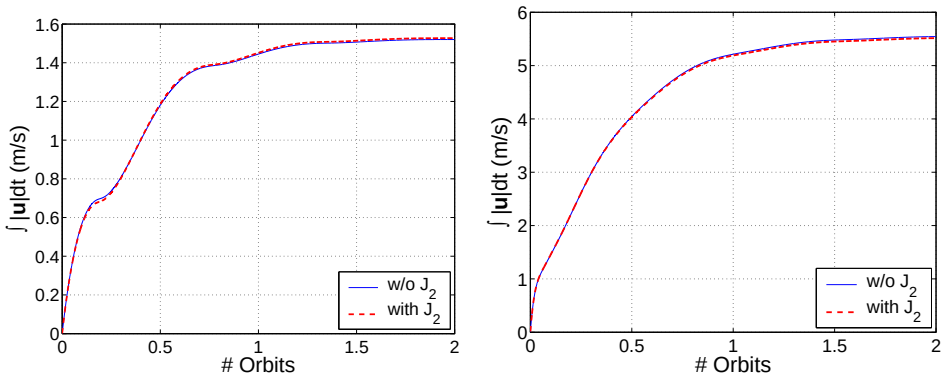

(a) $\alpha_{0_f} = 0°$ (b) $\alpha_{0_f} = 90°$

Fig. 5.9 Total Control Requirement for the Low Eccentricity Case

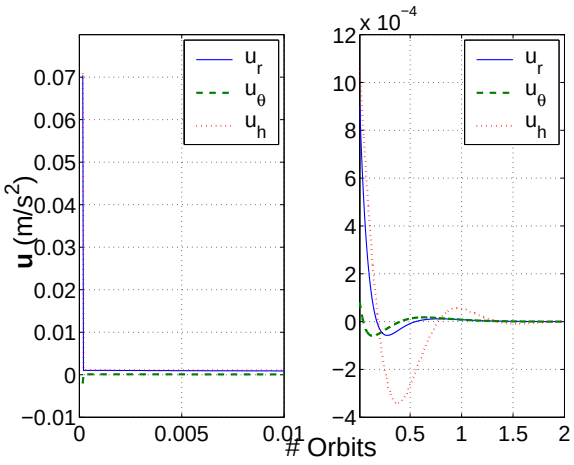

Fig. 5.10 Control Accelerations, $\alpha_0 = 0°$

The time history of the controls along the r, θ and h directions are shown in Fig. 5.10. These are the controls for the $\alpha_0 = 0^\circ$ case. The largest part of the control takes place at the start of the simulation. The control action viewed in the scale of the figure appears similar to an impulse. Further, it can be seen that as time progresses, $\mathbf{u} \to \mathbf{0}$. Figures 5.11a-5.12b show the state errors (difference between current states and desired states) for the reconfiguration to $\alpha_0 = 0^\circ$. The value of $\Delta\beta_0$ is very close to 1, so the difference is very small when compared with the other error EPs. The rate at which the error EPs in Fig. 5.11a go to zero is dependent on the rates at which the angular velocity errors in Fig. 5.11b go to zero. This can be adjusted by selecting appropriate gains.

A comparison of Figs. 5.11a-5.12b with the kinematic approach to impulsive reconfiguration presented in Fig. 5.5a and Figs. 5.6a-5.6d shows the difference between continuous and impulsive control very well. For example, using impulsive control, $\Delta\beta_3$ settles to zero within half an orbit, whereas in the case of continuous control it takes around one orbit. This is related to the overshoot along the y-axis observed in Fig. 5.8a. If gains can be selected such that the error dynamics of the continuous control approach for reconfiguration are made similar to the optimal two-impulse problem the TCR can be reduced further. However, for the case under consideration, it may require the selection of a different Lyapunov function.

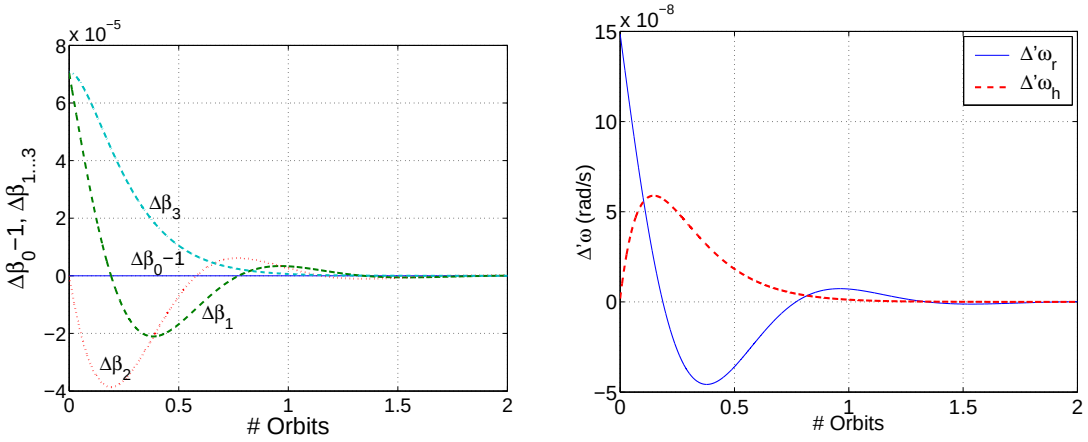

(a) Error Euler Parameters (b) Angular Velocity Error

Fig. 5.11 Error Euler Parameters and Angular Velocity Errors, $\alpha_0 = 0°$

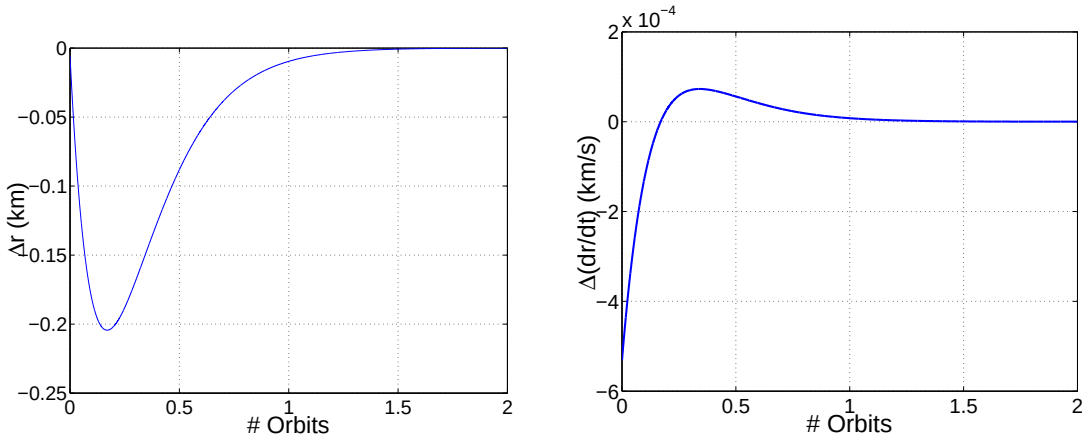

(a) Radial Position Error (b) Radial Velocity Error

Fig. 5.12 Radial Position and Velocity Errors, $\alpha_0 = 0°$

The high-eccentricity reconfiguration example is the same as the one used for the study of impulsive reconfiguration. The following are the elements of the Chief:

$$\mathbf{e}_C = \{42095.70\text{km} \quad 0.8182 \quad 50^\circ \quad 0^\circ \quad 0^\circ \quad 180^\circ\}$$

To minimize control requirement, the orbit is established at apogee. Reconfigurations from $(\rho = 10\text{km}, \alpha_0 = 0^\circ)$ to $(\rho = 20\text{km}, \alpha_0 = 0^\circ)$ and to $(\rho = 20\text{km}, \alpha_0 = 90^\circ)$ are considered. Figures 5.13a and 5.13b show the reconfigurations for each case. While both simulations include the J_2 perturbation, for high eccentricity reconfigurations, mean elements can no longer be used. It is observed that the simplified model tracks the mean desired elements of the Deputy satellite very well, but when the control is applied to the true system, noticeable drift is seen. It thus becomes necessary to use osculating elements for the desired Deputy trajectory, obtained from integration of the truth model.

Figures 5.14a and 5.14b, respectively, show the TCR for $\alpha_{0_f} = 0^\circ$ and $\alpha_{0_f} = 90^\circ$, with and without J_2. Similar to the impulse control problem for the same example, the TCR for these orbits are lower than those where semimajor axis is smaller. The TCR in the presence of J_2 is also lower than the TCR without the J_2 perturbation. This is only possible if the J_2 drift aids the reconfiguration, and is not a general rule.

It can be seen from the control laws in Eqs. (5.17), that the effect of the J_2 perturbation is expressed as the differential J_2 forces. It was observed that the exclusion of these terms simplified the control law significantly, but changed the TCR only marginally. This was found to be true even for the high eccentricity case.

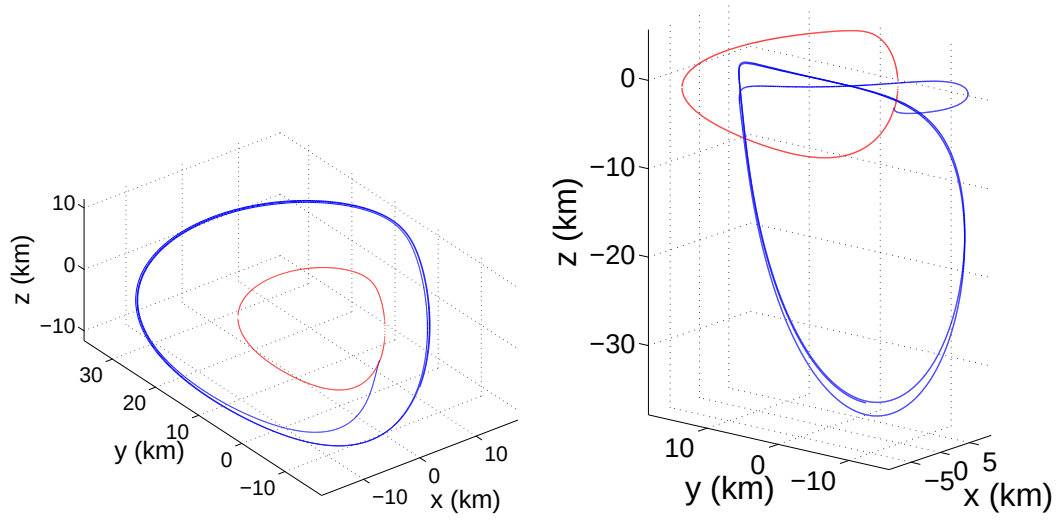

(a) $\alpha_{0_f} = 0°$ (b) $\alpha_{0_f} = 90°$

Fig. 5.13 Continuous Control Reconfiguration for High-Eccentricity Reference, with the J_2 Perturbation, $\alpha_{0_f} = \{0° \quad 90°\}$

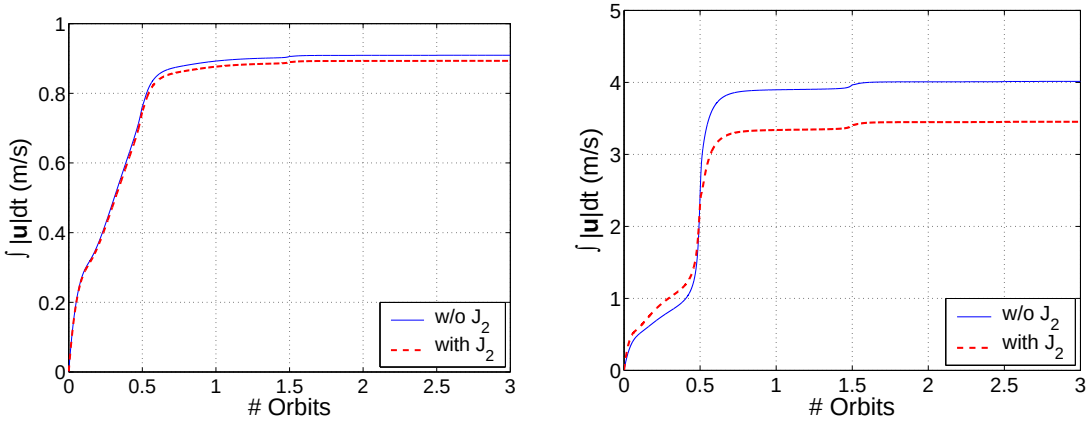

(a) $\alpha_{0_f} = 0°$ (b) $\alpha_{0_f} = 90°$

Fig. 5.14 Total Control Requirement for the High Eccentricity Case

5.5 Summary

In this chapter different approaches to satellite formation reconfiguration have been presented. These approaches have been used to study reconfiguration for reference orbits of both low eccentricity as well as very high eccentricity. Optimal two-impulse maneuvers have been presented, and it has been observed that for high-eccentricity reference orbits, the impulses are preferably placed near the apogee. A kinematic approach has been presented that uses error Euler parameters and angular velocity errors to study the reconfiguration process. The error Euler parameters and error angular velocities are used along with radial position and velocity errors to form a candidate Lyapunov function. A control can be derived from this Lyapunov function that globally and asymptotically stabilizes the Deputy about its desired trajectory. By studying the linearized closed-loop model, estimates for the gains to be used in the control laws can be obtained. The gains need to be selected such that the error dynamics from the continuous control reconfiguration are as close as possible to the error dynamics from the impulsive control case. This will ensure the lowest total control requirement. Numerical examples have been provided to detail the various aspects of the chapter.

CHAPTER VI

SUMMARY AND FUTURE WORK

6.1 Summary

The work in the thesis is summarized as follows. Chapters I and II served as an introduction to the basic concepts involved in satellite motion and satellite relative motion. The origin of the J_2 perturbation was discussed. The different systems of equations that model the motion of a satellite under the effect of the J_2 perturbation were presented. However, the effects of drag, solar radiation pressure, and lunisola perturbations, on the motion of the satellite were not discussed.

In Chapter III, the problem of relative motion was presented in detail, with a description of the different models. The unit sphere model was compared with the geometric method. It was found that since the unit sphere model is not a linearized model like the geometric method, errors are less for large relative orbits. Further, while similar to the analytical solution using mean elements, the unit sphere model gives the relative position directly without requiring the conversion of orbital elements to inertial coordinates.

The problem of highly eccentric reference orbits was discussed in Chapter IV. The unit sphere model was modified to allow simulations of such orbits. While a numerical solution to Kepler's equation was still necessary, it was required to be solved only for the Deputy since the true anomaly of the Chief was used as the independent variable. The results from this chapter show that the modified unit sphere approach is very useful for the simulation of high-eccentricity reference or large formation orbits.

Chapter V dealt with the reconfiguration problem. Two approaches were discussed - impulsive control and continuous control. The optimal impulsive controls were obtained from a numerical scheme that included J_2 effects. This method was also used on the high-eccentricity reference case. The continuous control law was derived from a candidate Lyapunov function whose asymptotic stability was proven. The results from both schemes were compared. It was also shown that mean elements can be used in the control law for the low eccentricity case with no significant error. However, the high eccentricity cases require the use of osculating elements.

6.2 Future Work

The initial conditions that yield circular projected orbits are valid only for low-eccentricity reference orbits. For high eccentricities, while the relative orbit is still characterized by the the relative radius ρ and the phase angle α_0, the projected orbits are no longer circular. A complete characterization of the relative orbits for high-eccentricity reference orbits is required to determine the effect of the various orbital element differences on their shape, size, and orientation.

It is intended that the work in this thesis be extended by using the continuous control approach with equations where the true anomaly is the independent variable instead of time. This will require Gauss' equations in the nonsingular form which can easily be derived. The work in the thesis used the Lyapunov-based controller to track an orbit whose orbital elements were derived from the rate-matching condition and circular orbit requirements. Since it is known that the mentioned conditions no longer yield circular orbits when projected for higher eccentricities, the controller could be extended to track such orbits.

REFERENCES

[1] Kozai, Y., "The Motion of a Close Earth Satellite," *The Astronomical Journal*, Vol. 64, November 1959, pp. 367–377.

[2] Brouwer, D., "Solution of the Problem of Artificial Satellite Theory Without Drag," *The Astronomical Journal*, Vol. 64, November 1959, pp. 378–397.

[3] Battin, R. H., *An Introduction to the Mathematics and Methods of Astrodynamics*, AIAA Education Series, Reston, VA, revised ed., 1999.

[4] Kechichian, J. A., "Motion in General Elliptic Orbit with Respect to a Dragging and Precessing Coordinate Frame," *The Journal of Astronautical Sciences*, Vol. 46, No. 1, January-March 1998, pp. 25–46.

[5] Junkins, J. L. and Turner, J. D., "On the Analogy Between Orbital Dynamics and Rigid Body Dynamics," *The Journal of the Astronautical Sciences*, Vol. 27, No. 4, Oct-Dec 1979, pp. 345–358.

[6] Born, G. H., Goldstein, D. B., and Thompson, B., "An Analytical Theory for Orbit Determination," *The Journal of Astronautical Sciences*, Vol. 49, No. 2, April-June 2001, pp. 345–361.

[7] Clohessy, W. H. and Wiltshire, R. S., "Terminal Guidance System for Satellite Rendezvous," *Journal of Aerospace Sciences*, Vol. 27, September 1960, pp. 653–658, 674.

[8] Vaddi, S. S., Vadali, S. R., and Alfriend, K. T., "Formation Flying: Accommodating Nonlinearity and Eccentricity Perturbations," *Journal of Guidance, Control, and Dynamics*, Vol. 26, No. 2, March-April 2003, pp. 214–223.

[9] Schweigart, S. A. and Sedwick, R. J., "High-Fidelity Linearized J2 Model for Satellite Formation Flight," *Journal of Guidance, Control, and Dynamics*, Vol. 25, No. 6, November-December 2002, pp. 1073–1080.

[10] Schaub, H. and Alfriend, K. T., "J_2 Invariant Relative Orbits for Formation Flying," *International Journal of Celestial Mechanics and Dynamical Astronomy*, Vol. 79, 2001, pp. 77–95.

[11] Vadali, S. R., Vaddi, S. S., and Alfriend, K. T., "A New Concept for Controlling Formation Flying Satellite Constellations," *Proceedings of the AAS/AIAA Space Flight Mechanics Meeting*, No. AAS 01-218, AAS Publications, Santa Barbara, CA, February 2001.

[12] Gim, D.-W. and Alfriend, K. T., "The State Transition Matrix of Relative Motion for the Perturbed Non-Circular Reference Orbit," *Proceedings of the AAS/AIAA Space Flight Mechanics Meeting*, No. AAS 01-222, AAS Publications, Santa Barbara, CA, February 2001.

[13] Schaub, H., "Incorporating Secular Drifts into the Orbit Element Difference Description of Relative Orbits," *Proceedings of the AAS/AIAA Space Flight Mechanics Meeting*, No. AAS 03-115, AAS Publications, Ponce, Puerto Rico, February 2003.

[14] Sabol, C., McLaughlin, C. A., and Luu, K. K., "Meet the Cluster Orbits with Perturbations of Keplerian Elements (COWPOKE) Equations," *Proceedings of the 13th AAS/AIAA Space Flight Mechanics Conference*, No. AAS 03-138, AAS Publications, Ponce, Puerto Rico, February 2003.

[15] Vadali, S. R., "An Analytical Solution for Relative Motion of Satellites," *Proceedings of the DCSSS Conference*, Cranfield University, Cranfield, UK, July 2002.

[16] Vadali, S. R. and Vaddi, S. S., "Large-Angle Kinematics for the Control of Satellite Relative Motion," *Proceedings of the AIAA/AAS Astrodynamics Conference*, No. AAS 02-258, AIAA, Monterey, CA, August 2002.

[17] Schaub, H., Vadali, S. R., Junkins, J. L., and Alfriend, K. T., "Spacecraft Formation Flying Using Mean Orbital Elements," *The Journal of Astronautical Sciences*, Vol. 48, No. 1, January-March 2000, pp. 69–87.

[18] Junkins, J. L. and Turner, J. D., *Optimal Spacecraft Rotational Maneuvers*, Elsevier, Amsterdam, The Netherlands, 1986.

[19] Vallado, D. A., *Fundamentals of Astrodynamics and Applications*, Microcosm Press, El Segundo, CA, 2nd ed., 2001.

[20] Junkins, J. L. and Singla, P., "How Nonlinear Is It?" *Proceedings of the John L. Junkins Astrodynamics Symposium*, No. AAS 03-286, AAS Publications, College Station, TX, May 2003.

[21] Vadali, S. R., Vaddi, S. S., and Alfriend, K. T., "An Intelligent Control Concept for Formation Flying Satellites," *International Journal of Robust and Nonlinear Control*, Vol. 12, 2002, pp. 97–115.

[22] Melton, R. G., "Time Explicit Representation of Relative Motion Between Elliptical Orbits," *Journal of Guidance, Control, and Dynamics*, Vol. 23, No. 4, July-August 2000, pp. 604–610.

[23] Alfriend, K. T., Schaub, H., and Gim, D.-W., "Gravitational Perturbations, Nonlinearity and Circular Orbit Assumption Effects on Formation Flying Control Strategies," *Proceedings of the 23rd Annual AAS Guidance and Control Conference*, No. AAS 00-012, AAS Publications, Breckenridge, CO, February 2000.

[24] Schaub, H. and Alfriend, K. T., "Impulse Feedback Control to Establish Specific Mean Orbit Elements of Spacecraft Formations," *Journal of Guidance, Control, and Dynamics*, Vol. 24, No. 4, July-August 2001, pp. 739–745.

[25] Vaddi, S. S. and Vadali, S. R., "Linear and Nonlinear Control Laws for Formation Flying," *Proceedings of the 13th AAS/AIAA Space Flight Mechanics Conference*, No. AAS 03-109, AAS Publications, Ponce, Puerto Rico, February 2003.

[26] Vaddi, S. S., *Modeling and Control of Satellite Formations*, Ph.D. Dissertation, Texas A&M University, College Station, TX, 2003.

[27] Gill, P. E., Murray, W., and Saunders, M. A., *Users Guide for SNOPT Version 6, A FORTRAN Package for Large-Scale Nonlinear Programming*, Department of Mathematics, UC San Diego/Systems Optimization Laboratory, Stanford University, La Jolla, CA/Stanford, CA, December 2002.

[28] Khalil, H. K., *Nonlinear Systems*, Prentice Hall, Upper Saddle River, NJ, 3rd ed., 2002.

APPENDIX A

LYAPUNOV STABILITY THEORY

Consider an autonomous (time-invariant) system governed by the following differential equation:

$$\dot{\mathbf{x}} = \mathbf{f}(\mathbf{x}) \tag{A.1}$$

Definition. *(Equilibrium)* $\overline{\mathbf{x}}$ *is an equilibrium of point of (A.1) if it is a "constant" or stationary solution of (A.1), i.e. if* $\mathbf{x}(0) = \overline{\mathbf{x}}$ *then* $\mathbf{x}(t) = \overline{\mathbf{x}}$.

A consequence of this is that at any equilibrium point, $\mathbf{f}(\bar{\mathbf{x}}) = \mathbf{0}$. For convenience, it is assumed that the equilibrium is alwasy at the origin of $\Re^n$, i.e $\bar{\mathbf{x}} = \mathbf{0}$. There is no loss of generality in doing so because any equilibrium can be shifted to the origin through a change of variables. Suppose $\bar{\mathbf{x}} \neq \mathbf{0}$ then consider the change of variables $\mathbf{y} = \mathbf{x} - \bar{\mathbf{x}}$. Then,

$$\dot{\mathbf{y}} = \dot{\mathbf{x}} = \mathbf{f}(\bar{\mathbf{x}}) = \mathbf{f}(\mathbf{y} + \bar{\mathbf{x}}) \equiv \mathbf{g}(\mathbf{y})$$

where, $\mathbf{g}(\mathbf{0}) = \mathbf{0}$. In the new variable, the system has an equilibrium at the origin.

Definition. *(Stability) The equilibrium point* $\mathbf{x} = \mathbf{0}$ *of (A.1) is*

- *stable if, for each* $\varepsilon > 0$*, there is* $\delta = \delta(\varepsilon) > 0$ *such that*

$$||\mathbf{x}(0)|| < \delta \Rightarrow ||\mathbf{x}(t)|| < \varepsilon, \quad \forall t \geq 0$$

- *unstable if it is not stable*
- *asymptotically stable if it stable and* δ *can be chosen such that*

$$||\mathbf{x}(0)|| < \delta \Rightarrow \lim_{t \to \infty} \mathbf{x}(t) = \mathbf{0}$$

Lyapunov's Stability Theorem. *Let* $\mathbf{x} = \mathbf{0}$ *be an equilibrium point for (A.1) and* $D \subset \Re^n$ *be a domain containing* $\mathbf{x} = \mathbf{0}$. *Let* $V : D \to \Re$ *be a continuously differentiable function such that*

$$V(0) = 0 \quad \text{and} \quad V(\mathbf{x}) > 0 \quad \text{in} \quad D - \{\mathbf{0}\}$$

$$\dot{V}(\mathbf{x}) \leq 0 \quad \text{in} \quad D$$

Then, $\mathbf{x} = \mathbf{0}$ *is stable. Moreover, if*

$$\dot{V}(\mathbf{x}) < 0 \quad \text{in} \quad D - \{\mathbf{0}\}$$

then $\mathbf{x} = \mathbf{0}$ *is asymptotically stable.*

Proof. Refer to Khalil.[28] □

Definition. *(Radial Unboundedness) If there exists a scalar function* $V(\mathbf{x})$ *that has the following property:*

$$V(\mathbf{x}) \to \infty \quad \text{as} \quad ||\mathbf{x}|| \to \infty$$

then the the function is said to be radially unbounded.

Barbashin-Krasovskii Global Stability Theorem. *Let* $\mathbf{x} = \mathbf{0}$ *be an equilibrium point for (A.1). Let* $V : \Re^n \to \Re$ *be a continuously differentiable function such that*

$$V(\mathbf{0}) = 0 \quad \text{and} \quad V(\mathbf{x}) > 0, \quad \forall \mathbf{x} \neq \mathbf{0}$$

$$||\mathbf{x}|| \to \infty \Rightarrow V(\mathbf{x}) \to \infty$$

$$\dot{V}(\mathbf{x}) < 0, \quad \forall \mathbf{x} \neq \mathbf{0}$$

then $\mathbf{x} = \mathbf{0}$ *is globally asymptotically stable.*

Proof. Refer to Khalil.[28] □

APPENDIX B

LASALLE'S THEOREM

Lyapunov's Stability Theory only provides sufficient conditions for stability of an equilibrium. It is possible that an equilibrium is stable even if the candidate Lyapunov function does not satisfy the requirements of the theorem. A control law derived from the candidate Lyapunov that is designed to stabilize the system must do so asymptotically. Often, asymptotic stability cannot be concluded because $\dot{V}(\mathbf{x} \neq \mathbf{0}) \leq 0$ does not necessarily hold.

Definition. *(Positive Limit Point) Let* $\mathbf{x}(t)$ *be a solution of (A.1). A point* p *is said to be a positive limit point of* $\mathbf{x}(t)$ *if there is a sequence* $\{t_n\}$*, with* $t_n \to \infty$ *as* $n \to \infty$*, such that* $\mathbf{x}(t_n) \to p$ *as* $n \to \infty$*. The set of all positive limit points of* $\mathbf{x}(t)$ *is call the positive limit set of* $\mathbf{x}(t)$*.*

Definition. *(Invariant Set) A set* M *is said to be an invariant set with respect to (A.1) if*

$$\mathbf{x}(0) \in M \Rightarrow \mathbf{x}(t) \in M, \quad \forall t \in \Re$$

LaSalle's Theorem. *Let* $\Omega \subset D$ *be a compact set that is positively invariant with respect to (A.1). Let* $V : D \to \Re$ *be a continuously differentiable function such that* $\dot{V}(x) \leq 0$ *in* Ω*. Let* E *be the set of all points in* Ω *where* $\dot{V}(x) = 0$*. Let* M *be the largest invariant set in* E*. Then every solution starting in* Ω *approaches* M *as* $t \to \infty$*.*

Proof. Refer to Khalil.[28] □

Corollary 1. [1] *Let* $\mathbf{x} = \mathbf{0}$ *be an equilibrium point for (A.1). Let* $V : D \to \Re$ *be a continuously differentiable positive definite function on a domain* D *containing the origin* $\mathbf{x} = \mathbf{0}$*, such that* $\dot{V}(\mathbf{x}) \leq 0$ *in* D*. Let* $S = \{\mathbf{x} \in D | \dot{V}(\mathbf{x}) = 0\}$ *and suppose that no solution can stay identically in* S*, other than the trivial solution* $\mathbf{x}(t) \equiv \mathbf{0}$*. Then, the origin is asymptotically stable.*

Corollary 2. *Let* $\mathbf{x} = \mathbf{0}$ *be an equilibrium point for (A.1). Let* $V : \Re^n \to \Re$ *be a continuously differentiable, radially unbounded, positive definite function such that* $\dot{V}(\mathbf{x}) \leq 0 \quad \forall \mathbf{x} \in \Re^n$*. Let* $S = \{\mathbf{x} \in \Re^n | \dot{V}(\mathbf{x}) = 0\}$ *and suppose that no solution can stay identically in* S*, other than the trivial solution* $\mathbf{x}(t) \equiv \mathbf{0}$*. Then, the origin is globally asymptotically stable.*

[1] *The two corollaries are known as the theorems of Barbashin and Krasovskii*

VITA

Prasenjit Sengupta was born in New Delhi, India in November, 1979. He received his baccalaureate degree in aerospace engineering, with honors, from the Indian Institute of Technology, Kharagpur, India in July, 2001. After his master's degree he will continue doctoral studies in aerospace engineering at Texas A&M University.

He can be reached at the Department of Aerospace Engineering, Texas A&M University, College Station, TX 77843.

This document was typeset in LaTeX by Prasenjit Sengupta.